NTNU
Norwegian University of Science and Technology
Department of Marine Technology

M.Sc.THESIS

Title:	Delivered:
Wave Energy Driven Desalination of Seawater – Experimental investigation of the hydrodynamic performance	14.06.2011
	Availability: Open
Student: Andreas Palmstrøm and Rolf Anders Brandsvoll	**Number of pages:** 184

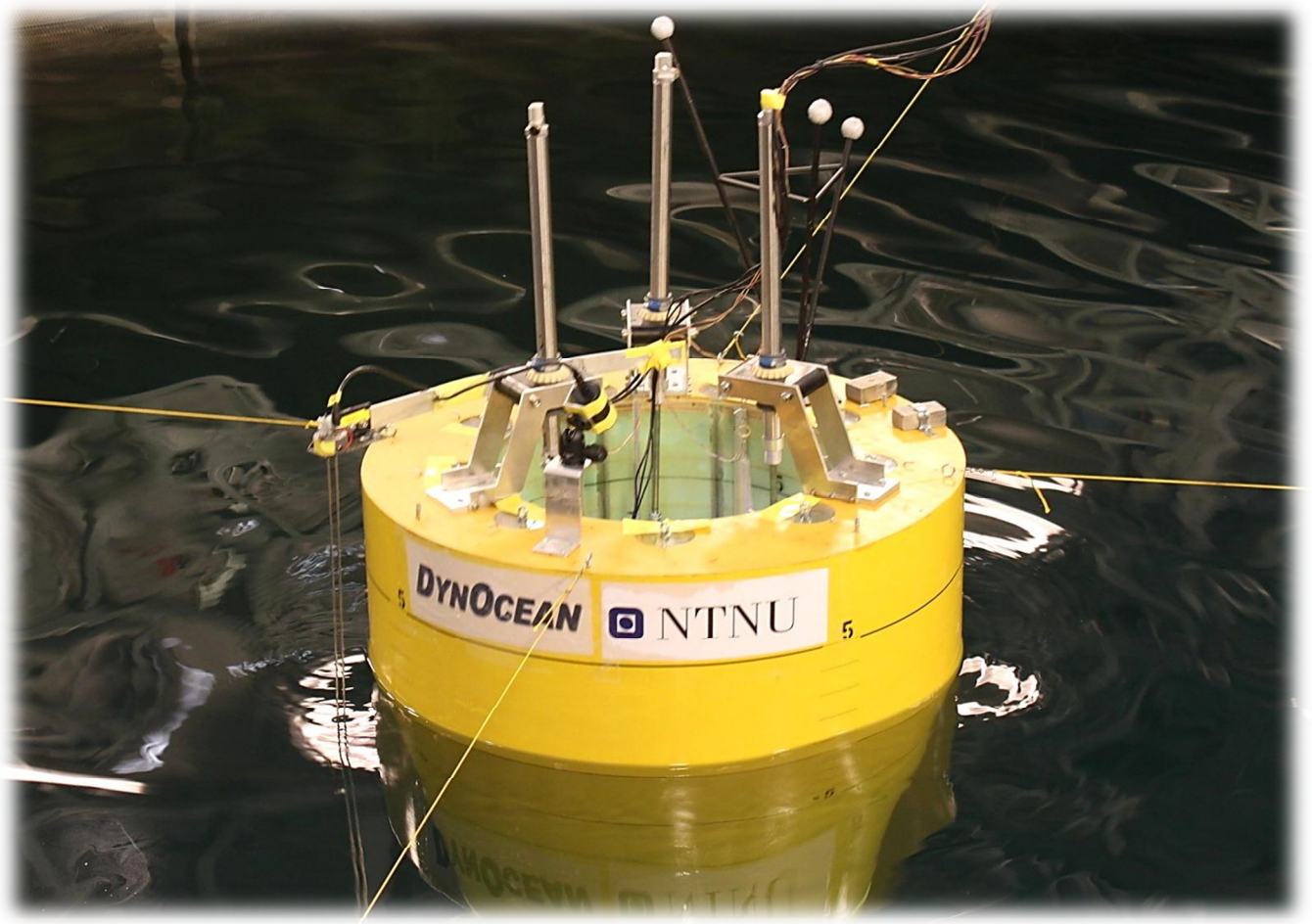

Keyword:

Wave Power, Desalination, Model Testing, Model Concept Design, Numerical Analysis, SIMO

Advisor:

Sverre Steen and Thomas B. Johannessen

Address:
NTNU
Department of Marine Technology
N-7491 Trondheim

Location
Marinteknisk Senter
O. Nielsens vei 10

Tel. +47 73 595501
Fax +47 73 595697

MASTER THESIS IN MARINE TECHNOLOGY
SPRING 2011
FOR
STUD. TECHN. Andreas Palmstrøm

And

STUD. TECHN. Rolf Anders Brandsvoll

Wave Energy Driven Desalination of Seawater – Experimental investigation of the hydrodynamic performance

There is an increasing scarcity of fresh water worldwide. A fair number of the locations with current or prospective shortages of water are located close to coastlines with wave conditions that might be suitable for wave power extraction. The idea to be explored in this project is to generate fresh water using reverse osmosis, where the high water pressure required is produced by pumps driven directly by wave power. In this manner one avoids the costly and complicated process of making electricity from the wave power. Also, one avoids the costs and emissions related to diesel-driven reverse osmosis plants.8
This idea was proposed as a topic for project and master theses by Thomas B. Johannessen, and the project will be performed with him as co-supervisor. The idea described above will be explored by the two students working as a team, delivering a common thesis and receiving the same grade.
Co-operation might be sought with Stud. Techn. Sindre Sole, who is working on the modeling and optimization of the pump system.

The idea was patented 22nd of September 2008, and is now under revision.

Overall aim and focus
The overall aim of the MSc project is to suggest optimum design and validate the hydrodynamic performance of the design.

The tentative work for the master thesis will focus on the following:

- Plan the model test
    a. Make a design for the model and energy extraction system
    b. Cooperate with the technicians in the production of the model and instrumentation set-up
- Do numerical simulations of the tests to be performed in model scale
- Perform the model test
- Analyse the model test results to determine motions and energy extraction potential
    a. Compare with numerical simulations, and draw conclusions towards the reliability of the numerical simulations
- Suggest improvements to the design
    a. If possible, alternative designs should be tested
- Give recommendations and conclusions regarding the future development of the system

The candidates should in their report give a personal contribution to the solution of the problem formulated in this text. All assumptions and conclusions must be supported by mathematical models and/or references to physical effects in a logical manner.

The candidates should apply all available sources to find relevant literature and information on the actual problem.

In the thesis the candidates shall present their personal contribution to the resolution of problem within the scope of the thesis work.

Theories and conclusions should be based on mathematical derivations and/or logic reasoning identifying the various steps in the deduction.

The candidates should utilize the existing possibilities for obtaining relevant literature.

The thesis should be organized in a rational manner to give a clear exposition of results, assessments, and conclusions. The text should be brief and to the point, with a clear language. Telegraphic language should be avoided.

The thesis shall contain the following elements: A text defining the scope, preface, list of contents, summary, main body of thesis, conclusions with recommendations for further work, list of symbols and acronyms, reference and (optional) appendices. All figures, tables and equations shall be numerated. Furthermore, proper documentation of the model tests and their results shall be given. This shall include, but is not limited to, photographic and other documentation of the model and the test set-up, a list of all relevant measurement channels, a test index (list of run numbers and the particulars of each run), and summaries of the results of all runs. Time series of the tests shall be included in electronic form (CD, DVD, or other suitable medium)

The original contribution of the candidate and material taken from other sources shall be clearly defined. Work from other sources shall be properly referenced using an acknowledged referencing system.

The thesis shall be submitted in two copies:

- Signed by the candidate
- The text defining the scope included
- In bound volume(s)
- Drawings and/or computer prints that cannot be bound should be organized in a separate folder.
- The bound volume shall be accompanied by a CD or DVD containing the written thesis in Word or PDF format. In case computer programs have been made as part of the thesis work, the source code shall be included. In case of experimental work, the experimental results shall be included in a suitable electronic format.

Supervisor : Sverre Steen
Advisor : Thomas B. Johannesen
Start : 17th of January 2011
Deadline : 14 June, 2011

Trondheim
Supervisor

Preface

This is the master thesis of Andreas Palmstrøm and Rolf Anders Brandsvoll in their final semester of their Master of Science education at NTNU, the spring of 2011. The work presented is the continuation of the project thesis work of both authors.

Working with the subject has been of great value for the authors. Both of us have during the last semester developed a better and profound understanding of hydrodynamics governing wave power devices and mechanical coupled systems. Valuable experience from model making, model testing, project control and numerical simulations has been attained. The scope of work has been of great relevance in relation to our line of study at NTNU and out interests.

The weeks prior to the model test and the actual test week were very work intensive. We were rewarded with a very successful model test and good data. Regular wave tests were performed, but due to lack of time, not used in the post analysis.

The concept studied is an idea of Thomas B. Johannessen. We would like to give him a great thank you for providing us such an interesting and exciting Master Thesis which has involved so many practical and theoretical challenges. Throughout the entire year Thomas B. Johannessen have devoted us time and given us great guidance.

We would like to thank our institute supervisor, Professor Sverre Steen that always kept us in the right direction. The many constructive discussions with Professor Steen helped us with the understanding of the subject and making the right decisions regarding the model test.

Great help were given in the construction of the rig used in the pendulum test by Trond Innseth. Erik Lehn at Marintek helped us with theory regarding this concept. Our two contact persons at the test facility, Terje Rosten and Knut Arne Hegstad contributed with constructive discussions in the model concept phase. We would like to thank the above persons as well as all workshop employees involved.

Trondheim, 14.06.2011

Andreas Palmstrøm	Rolf Anders Brandsvoll

Summary

Water scarcity is a growing problem today. With an increasing world population as well as an increase in temperature due to global warming, the need for fresh water in the future will be more important. The originator of this concept, Thomas B. Johannessen has the last years been working on the design of a device that produces freshwater by wave driven desalination of seawater. The system is called Dynocean Buoy.

The Dynocean Buoy is a two body WEC (wave energy converter) that extracts energy from the relative motion in heave, pitch and roll between the two bodies. It consists of an inner disc inside a moonpool of an outer buoy. The relative motions are produced by incoming waves and this energy is extracted by piston pumps. Unlike most conventional WEC`s the Dynocean Buoy does not convert the wave energy to electricity. It directly produces fresh water from seawater by a reverse osmosis process. The challenges associated with electricity production are eliminated.

This thesis is written to investigate the performance and feasibility of the Dynocean buoy. The main purpose of this thesis is to analyze the feasibility of the system by carrying out a model test. The second purpose is to construct a numerical model of the device that reproduces the results from the model test in the time domain. This numerical model can then be used for further design of the device. Both processes have been performed in parallel throughout the project.

Model test process:

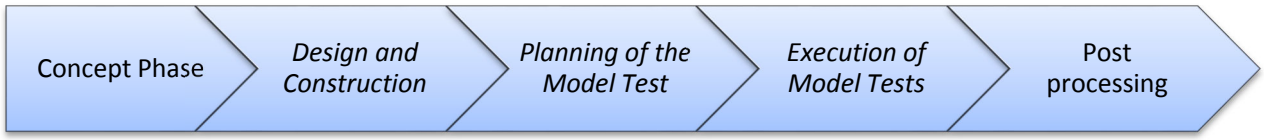

Concept phase

Many considerations and compromises need to be addressed when performing a model test. Scale of the model, manufacturing method, structural issues, materials, building costs and most importantly how to simulate the power extraction were natural considerations in the early concepts phase. In addition to investigate the feasibility of the device, it was decided to vary different input parameters in order to check the effect of different setups on the power output of the system. The impact of three main input parameters was decided to be studied during this stage:

- Hull design
- Vertical center of gravity (VCG)
- Characteristics of the power extraction units

Design and Construction

- **Adjustable ballast system**

Nine cylindrical steel weights were used to vary the VCG by raising and lowering them inside the hull (b).

- **Power extraction unit characteristics**

To simulate the water pumps in full-scale, three double acting pneumatic cylinders were chosen. Blind plugs with different bores were used as chokes on the cylinders. With this configuration the damping level could be varied.

- **Interchangeable bottom section**

One edged and one rounded bottom section was constructed to analyze the impact of the different damping level on the power output.

- **Hydrostatic analysis**

A hydrostatic stability analysis of the system has been performed. This was done to get the desired variation range of the VCG.

- **Natural periods**

Natural periods for different VCGs were calculated prior to the model test to get these in the same area as the spectral peak period (Tp) of the most occurring sea state of the designated operating area.

- **Guide system**

The challenge was to minimize relative yaw motion in order for the system to extract energy. A smart guide system that allowed relative pitch and roll motion was designed (c). The guide system was constructed to be applicable also for the full-scale version, not only the one-directional waves in the model test. Significant effort was put down to make a system that prevented jamming.

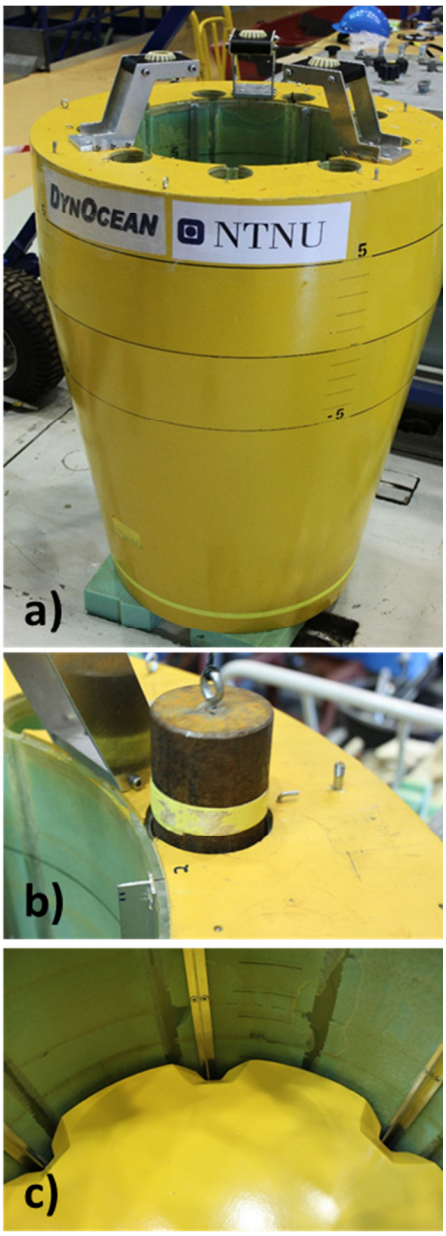

Planning of the model test

It is important to have a clear purpose with a model test. In this case it was to check the feasibility of the Dynocean Buoy mode of operation and design as well as the impact the different input parameters had on the efficiency.

The best way to check the feasibility is to test the device in real sea states. For this reason it was focused on running a large quantity of tests in irregular seas. Another key parameter of feasibility is how the device responds in survival conditions of the operating area.

Important parameters of this device are the natural periods and damping of the motions in different DOFs. For this reason several decay tests were planned and later executed.

Execution of Model Test

A pendulum test was performed to calculate the mass moment of inertia of the buoy. Once the buoy was launched into the water inclination tests was performed to obtain accurate GM values for the different VCG conditions. To prevent interference from natural periods of the moorings a simple test was performed to check the natural period in yaw and surge motion.

Skilled staff at Marintek instructed the authors how to use the wave maker and the test recording equipment needed to perform irregular sea- and decay tests.

Post processing

Post processing tools were made in MATLAB. Before interpretation of the results all high frequency noise from the different channels were removed by a low-pass filter. The same analyzing tools used on the model test results have also been applied to the results from the numerical analysis.

Numerical analyze process:

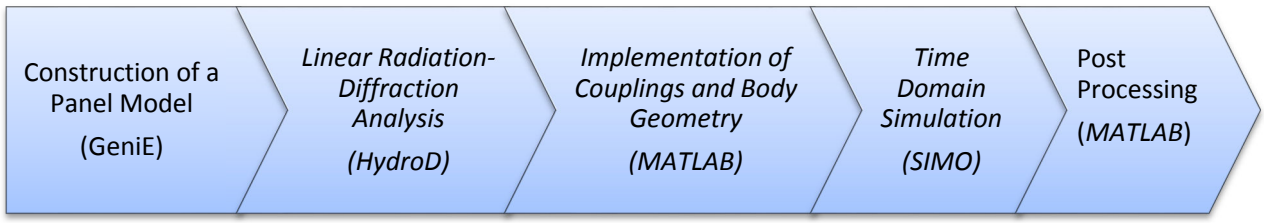

The model test results indicate that the Dynocean Buoy concept is viable. Power calculations for the typical sea states in the designated operating area of the buoy are highly satisfactory. With the most typical sea state with a spectral peak period (Tp) of 9.0 seconds and significant wave height (Hs) of 2.2 m the power output is estimated to 180 kW for the best buoy configuration.

Small deviations in the power output were observed by use of different damping levels on the power extractions units. The same also applied for different bottom sections. However, by applying low VCG the buoy had a 36 % increase in power output compared to high VCG. This increase is explained by the change in the pitch Eigen period from approximately 16 to 9 seconds – almost exactly at the spectral peak period of the sea state. This proves that the device is able to extract energy from relative rotation.

It is important for the viability of the system to adjust the VCG to the current sea condition and to avoid excessive pitch motion in survival conditions. An active adjustable ballast system has been suggested in order to achieve this.

Only one complete run for a one year survival condition with high VCG condition were performed. Tp for this survival condition was measured to approximately 11 s and the Hs to 7.7 m. The wave spectrum contains significant energy at the frequencies around the Eigen period in pitch and heave motion. This is together with the inertia forces from the waves the reasons for very large pitch motions of the buoy. Max pitch angle was measured to 44 degrees. Green water flushing over the topside from the inner disc was observed several times as illustrated in the figure.

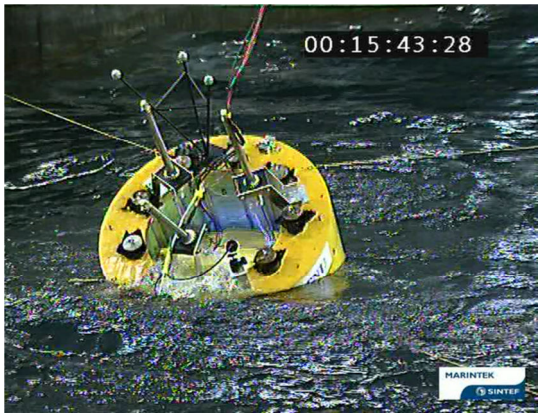

This is a critical challenge that must be addressed before full-scale development of the buoy can be carried out. It is advised to move the natural period in pitch outside the Tp during storms in order to prevent extreme pitch motions. The proposed active ballast system can be used for this purpose.

The numerical analyses reproduced the results for low sea states with good accuracy. For higher sea states the numerical model gave significantly larger power output than measured in the model test. Two decay tests, heave of the buoy alone and heave of the disc inside a stationary buoy, were tuned and reproduced with good results.

Implementation of more realistic power take off cylinder characteristics must be done, especially regarding static friction. Friction in the guide rails must also be modeled more complete to improve results.

Although the numerical model has shortcomings it describes the desirable motion good enough to conclude that SIMO is a good tool in the further design of the Dynocean Buoy.

Table of Contents

List of Figures

List of Tables

Abbreviation List

COB	Center of buoyancy
COG	Center of gravity
Hs	Significant wave height
MWL	Mean water line
PTO	Power take off
SD	Standard deviation
Tp	Spectral peak period
VCG	Vertical Center of Gravity
WEC	Wave Energy Converter

Symbol List

Constants:

g	acceleration of gravity;
$\rho_{tankwater}$	density of tank water;
$\rho_{seawater}$	density of sea water;

Ch.4 - Scaling

$_F$	full-scale index
$_M$	model scale index
λ	scale ratio
D	dimension
F_N	Froude number
U	velocity
L	length of a structure
A	area
t	time
f	frequency
a	acceleration
p	pressure
m	mass
F	force
M	moment

Ch.5 - Environmental conditions

H_s	significant wave height
p_{H_s}	probability for occurrence of a given H_s
p_i	probability
N_{T_p}	total number of each T_p in the given H_s class
$p_{T_{p,i}}$	probability for occurrence of the ith T_p
$T_{p,ave}(H_s)$	average peak period for the ith peak period in each H_s class
$T_{p,i}$	peak period for the ith peak period in each H_s class.
N	Number of sea states
$p_{survival}$	probability of occurrence of survival condition

Ch.6 - Power extraction system

$F_{average}$	average force when extracting the piston rod
$V_{average}$	average velocity when extracting the piston rod
B_{linear}	linear damping of the power extraction units

Ch.7 - Model

x	displacement
F	exerted force on a spring
k	spring stiffness

Ch.8 - Stability analysis

$\overline{GM}$	distance from center of gravity to metacenter
$\overline{KB}$	distance from keel to center of buoyancy
$\overline{BM}$	distance from keel to metacenter
$\overline{KG}$	distance from keel to center of buoyancy
∇	volume displacement
I_{xx}	mass moment of inertia about the x-axis
I_{zz}	mass moment of inertia about the z-axis
r_{xx}	radius of gyration of horizontal x-axis
r_{zz}	radius of gyration of the vertical z-axis
m_i	sub-mass
y_i	distance from keel to the point of gravity in each sub mass
I_{mass}	moment of inertia
$I_{cm,i}$	mass moment of inertia for a given sub mass, i .
h_i	distance from keel to the point of gravity
$r_{gyration}$	radius of gyration
r_{outer}	Outer radius of buoy
r_{inner}	Inner radius of buoy

I	area moment of inertia
M	total mass
r	mean radius of a shell
l	length of shell

Ch.10 - Pendulum test

T_0	first oscillation period when oscillation around point 0
T_1	second oscillation period when oscillation around point 0
I_O	mass moment of inertia about point 0
h	distance between the point 0 and VCG
M	mass of the model
m	additional mass
a	horizontal distance from COG to the placing of m
I_m	mass moment of inertia about VCG

Ch.9 - Natural periods

M	mass
A_{33}	added mass in heave
C_{33}	water plane stiffness
$F_3(t)$	force in heave
D	diameter of disc
T_n	Natural period
ω_n	natural frequency
A_w	water plane area
T_{55}	natural period in pitch
T_{33}	natural period in heave
h	draught of moonpool
I_{55}	mass m
r_{55}	radius of gyration about the sway-axis
A_{55}	Added mass in pitch
C_{55}	stiffness in pitch
V	volume

Ch.10 - Inclination test

ϕ	angle between GM and BM
a	distance from VGC to the placing of m_1
m_1	mass placed the a distance from VCG

Ch.10 - Mooring lines setup

T_{11}	surge natural period
A_{11}	added mass in heave
k_{surge}	system surge stiffness
k_{yaw}	system yaw stiffness
k_{sl}	stiffness of a single spring
P_0	pre-tensioning
$r_{fairlead}$	fairlead radius

Ch.13 - Wave calibration

η	surface elevation
a_n	amplitude
ω_n	wave circular frequency
t	time
ε_n	phase angle
m_n	moment
ω^n	circular frequency
$S(\omega)$	wave spectrum
m_0	0^{th} moment
γ	gamma value of the spectrum

Ch.14 - Decay test

M	total body mass and added mass
B_1	linear damping term
B_2	quadratic damping term
x	position
$\dot{x}$	velocity
$\lvert\dot{x}\rvert$	Equivalent linearization
$\ddot{x}$	acceleration
C	restoring stiffness
p_{EQ}	equivalent damping
p_1	damping term 1
p_2	damping term 2
p_3	damping term 3
δ	logarithmic decrement
ρ_{xy}	correlation coefficient
σ_y	standard deviation of the random variable x
σ_x	standard deviation of the random variable y

Ch.15 - Irregular waves

$P(t)$	time dependent power
$\vec{F}(t)$	time dependent force
$\vec{v}(t)$	time dependent velocity

Ch.16 - Survivability

λ	wave length
D	diameter
T	Period

Ch.17 - Numerical simulation

K_{hydro}	stiffness matrix

1. Introduction

Water scarcity is a growing problem in areas of the world. With an increasing world population as well as a global increase of temperature due to global warming, the need of fresh water in the future will be more important. Our supervisor, Thomas B. Johannessen has during the last couple of years been working on the design of a device that produces freshwater by the means of wave driven desalination of seawater. The system is called Dynocean Buoy.

The Dynocean Buoy device is based on simple principles. This can be constructed by cheap and "low-tech" technology. The device is robust and can easily be towed out to shore in order to produce fresh water by desalination of seawater.

In this thesis a model test of the buoy in a scale 1:28.7 has been performed. The main goal for the model test is to verify the feasibility of the design of the buoy, as well as to identify improvements to the design. A calculation of the power output of the system is the key parameter when studying the feasibility of the system.

A numerical analysis has been performed of the system. A SIMO time domain analysis of coupled bodies subjected to a large variety of loads were modeled in order to reproduce the same results as from the model-test. The numerical SIMO model can be used for further analytical design analysis if is in good agreement with the experimental model test.

Much effort towards building a prototype of 1:4 scale to be placed in real sea are undertaken by Thomas B. Johannessen.

The work done in the master thesis is a follow up from the project thesis in Brandsvoll (2010) and Palmstrøm (2010). This work contains literature studies of the subject, simple dynamic analysis as well as preparations for the model test. The main working principles of the device are explained in this master thesis; however the reader is referred to project thesis`s above for more background information of the device.

All figures are created in Microsoft PowerPoint if not referred to any source. The calculations are mostly performed in MATLAB, while some are done in Excel.

Scope of Work

A summary of the scope of work is presented below. For a full description of the work scope the reader is advised to read the facsimile in the beginning of the thesis. The main object was to plan and execute a model test of the Dynocean Buoy. Numerical analysis of the system should be done in parallel. The focus of the model test and the numerical analysis was to investigate the feasibility of the device. Energy extraction potential should be the main basis of evaluation. Alternative design should be tested.

2. Dynocean Buoy Design

The Dynocean Buoy is still in the concept phase. However, the main dimensions for the main buoy are determined and these are used as a basis in this thesis. A full description of the system is given in Palmstrøm (2010) and Brandsvoll (2010), therefore only a brief summary of the working principles with main dimensions will be presented here.

The Dynocean Buoy is a two body WEC (wave energy converter) that extracts energy from the relative motion between the two bodies. The relative motions are produced by incoming waves. The energy is extracted from the relative movement between the two bodies by piston pumps. The key feature of this The Dynocean Buoy compared to most other WEC`s is that it is used produce fresh water and not electrical energy. This limits the marked, but at the same time it cuts the losses in converting the energy to electricity.

The system desalinates seawater to produce fresh water of a reverse osmosis process. The energy required in this technique goes into pressurizing sea water. This is obtained by piston pumps between the two bodies. The fresh water is then transported to shore with a hose. The position of the pistons pumps are out from the center, thereby extracting energy in relative pitch and roll motion in addition to heave motion between the two bodies. The device should be only to keep it in a mean horizontal position.

The system is to be completely manufactured in a fabrication site. Minimum work is to be done offshore to keep the costs down.

In figure 2.1 a principle sketch of the cross section of the device is given. It consists of a large outer buoy with a hollow cylindrical shape. Inside the buoy an inner disc is placed in the moonpool. The three pistons pumps extracting the energy are also illustrated.

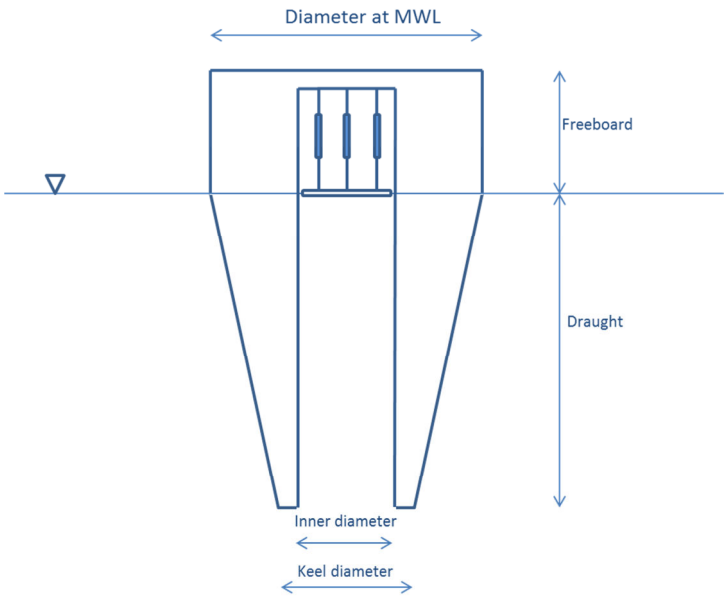

Figure 2.1, Cross-section of the Dynocean Buoy

Throughout the thesis, the Dynocean Buoy is divided in following parts:

- **Buoy:** The large outer buoy surrounding a cylindrical moonpool.
- **Disc:** inner body floating in the moonpool inside the buoy.
- **Power extraction system:** The power extraction units which extracts energy from the relative motion between the two floating bodies
- **Cylinder:** One of the three power extraction units in the power extraction system.

The table below presents the main dimension of the device.

Buoy	Model scale	Full-scale	Unit
Outer diameter at MWL	0,84	24,00	[m]
Inner diameter	0,49	14,00	[m]
Outer diameter at keel	0,59	17,00	[m]
Draught	0,78	22,50	[m]
Freeboard	0,30	8,60	[m]

Table 2.1, Main buoy dimensions in model-scale and full-scale

Figure 2.2, The Dynocean Buoy Model

4. Scaling

In order to ensure similar behavior in model-scale and full-scale scaling laws are needed. Scaling laws described in Steen (2010) is applied when analyzing the model-test results. Geometric-, kinematic- and dynamic similarity is necessary in order to obtain similarity in forces between model-scale and full-scale results.

4.1 Geometric Similarity

Geometric similarity is necessary to ensure that the shape of the structure is the same in model-scale as in full-scale. This implies that it is a constant ratio between dimensions that is represented by a scaling factor:

$$\lambda = \frac{D_F}{D_M} \tag{4.1}$$

Where D_F and D_M represents the dimensions of the full-scale and model-scale respectively. Geometric similarity requirements also apply on the surrounding environment like waves and water depth.

A scale ratio of 1:28.7 has been used in this model-test. A balance between cost and unwanted scale effects have to be considered when performing a model-test. A too small model can give problems with scale effects and measuring accuracy, whilst large models are generally more expensive to build. A too large model will in addition introduce more unwanted tank wall reflections.

Another limiting factor on the size of the model is the testing facility. Scale effects include small scale viscous effects that occur in different magnitude in laboratory scale and full-scale. Nonlinear wave effects, vortex shedding and turbulence are examples of this. Restrictions of tank facility, materials and equipment as well as cost have been taken into account when deciding the applied model scale.

For the behavior of WECs it is recommended a minimum scale of 1:50 (Cruz 2008). For validation of numerical models, a scale ratio between 1:20 and 1:33 is recommended. This model is within both the suggested scale ratios.

4.2 Kinematic Similarity

Kinematic similarity requires that the ratios between velocities in model scale have to be equal to corresponding ratios in full scale.

4.3 Dynamic Similarity

Dynamic similarity ensures similarity in force contributions. For a rigid model like the Dynocean Buoy, six components are of importance:

- Inertia forces
- Viscous forces
- Gravitational forces
- Pressure forces
- Elastic forces on the fluid
- Surface forces

4.3.1 Froude Number

The Dynocean Buoy is defined as a large volume structure according to Faltinsen (1990). Wave diffraction forces are of most interest and viscous forces are of less importance. This region is dominated by inertia forces and therefore similarity between inertia forces and gravitational forces are important.

Equal Froude number in full-scale and model-scale provides similarity between inertia and gravity forces given that geometric- and kinematic similarity is fulfilled. The dimensionless Froude number is given by:

$$F_N = \frac{U_M}{\sqrt{gL_M}} = \frac{U_F}{\sqrt{gL_F}} \tag{4.2}$$

Where U , is velocity, and L is the length of the structure which in our case corresponds to the diameter of the buoy. The dimensionless scaling ratios are given in table 4.1. These are derived from equation 4.2.

Parameter	**Unit**	**Scaling factor**
Length	[m]	$L_F = L_M \lambda$
Area	[m^2]	$A_F = A_M \lambda^2$
Volume	[m^3]	$V_F = V_M \lambda^3$
Time	[s]	$t_F = t_M \sqrt{\lambda}$
Frequency	[s^{-1}]	$f_F = f_M \lambda^{-0,5}$
Velocity	[m/s]	$U_F = U_M \sqrt{\lambda}$
Acceleration	[m/s^2]	$a_F = a_M$
Pressure	[Pa]	$p_F = p_M \frac{\rho_F}{\rho_M} \lambda$
Structural mass	[kg]	$m_F = m_M \frac{\rho_F}{\rho_M} \lambda^3$
Force	[N]	$F_F = F_M \frac{\rho_F}{\rho_M} \lambda^3$
Moment	[Nm]	$M_F = M_M \frac{\rho_F}{\rho_M} \lambda^4$

Table 4.1, Derived Froude scaling

The density of freshwater in the towing tank and seawater is different, and this has to be accounted for. Seawater has, $\rho_F = \rho_{Seawater} = 1025$ [kg/m^3] and $\rho_M = \rho_{tankwater} = 1000$ [kg/m^3]. Froude scaling is applied on the model test results.

5. Environmental Conditions

In this chapter a description of the governing wave climates of the operating area of the device is presented. Long time statistics is studied in order to calculate 1 year and 10 year survival conditions. These are considered as worst case for the Dynocean Buoy.

5.1 Long Time Statistics

Long time statistics are found from scatter diagrams from the designated operating area of the Dynocean Buoy. For this design the wave climate offshore of West-Africa has been studied at latitude between 10°N-30°N. This area has a moderate wave climate with gentle swells and small seasonal variations. The scatter diagram data presented below is gathered from Hogben et. al. (1986).

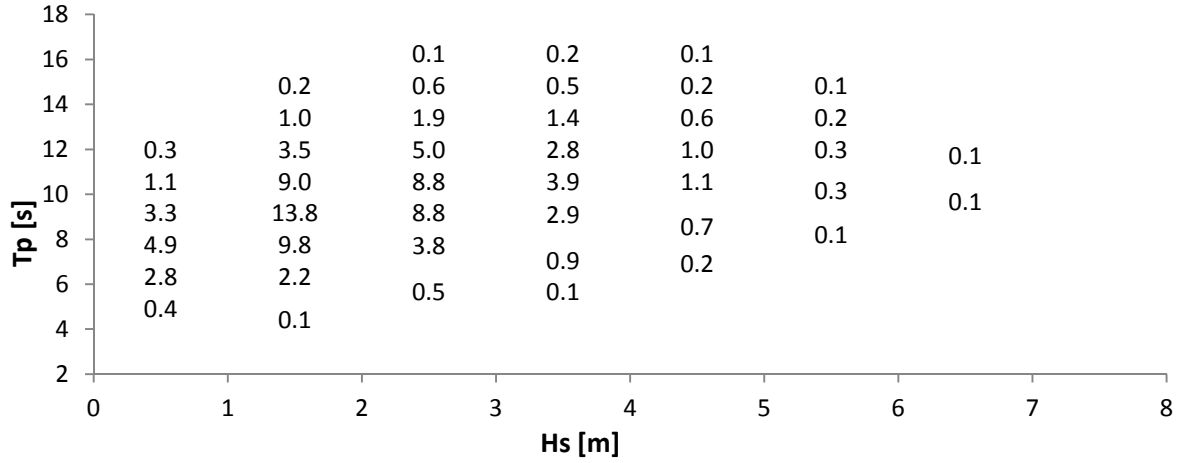

Figure 5.1, Annual distribution in per cent of significant wave height and spectral peak period.

The sea states are grouped into sea state classes for each significant wave height, Hs. The probability for each Hs is summed up by the following formula:

$$p_{H_s}(H_s) = \sum_{i=1}^{N_{T_p}} p_i \tag{5.1}$$

Where N_{T_p} is the total number of each T_p in the given H_s class and p_i is the corresponding probability. The corresponding spectral peak period for each sea state class is calculated by

$$T_{p,ave}(H_s) = \frac{\sum_{i=1}^{N_{T_p}} T_{p,i} p_{T_{p,i}}}{\sum_{i=1}^{N_{T_p}} p_{T_{p,i}}} \tag{5.2}$$

Where $T_{p,i}$ is the peak period for the ith peak period in each H_s class.

Hs class [m]	Probability [-]	Mean Tp [s]
0,5	0,13	8,09
1,5	0,397	9,38
2,5	0,296	10,26
3,5	0,128	10,86
4,5	0,039	11,22
5,5	0,010	11,65
6,5	0,002	10,72

Table 5.1, Probability of occurrence of sea-state given by Hs

The duration of each sea states is set to 3 hours. The total number of sea states for *m* years can be found by Myrhaug(2007):

$$N = \frac{365.25 days \cdot 24 hours \cdot m_{years}}{3 hours} \tag{5.3}$$

Based on the data provided in the tables above, predictions of 1 and 10 years sea states were calculated in the plot below.

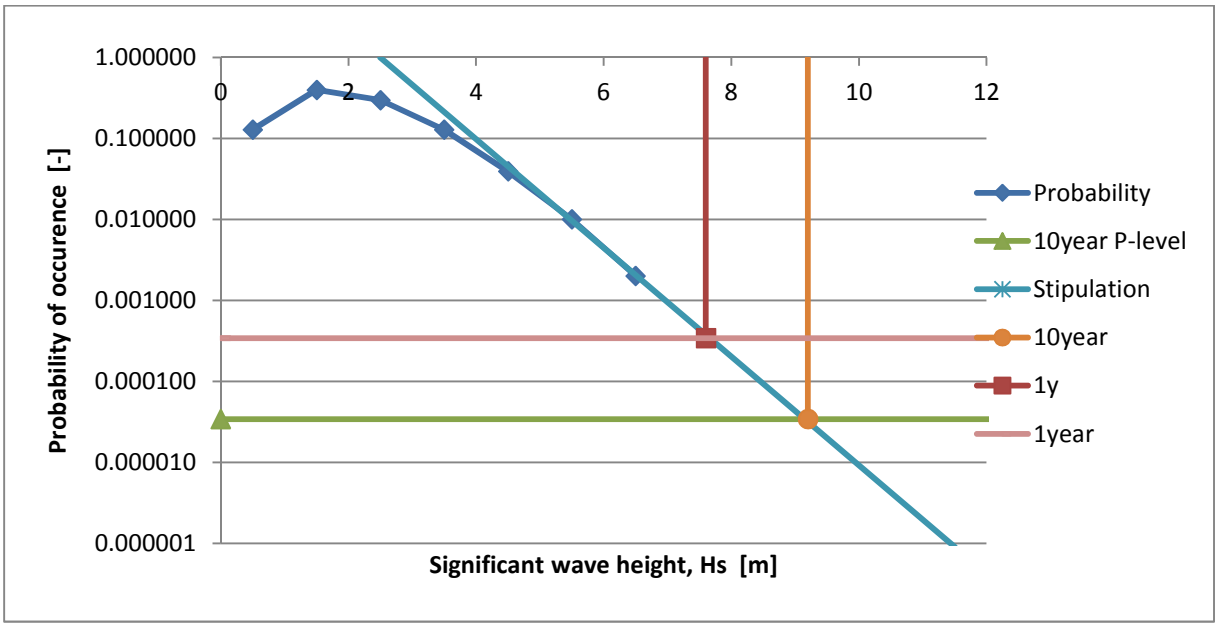

Figure 5.2, Estimation of survival conditions

The probability of occurrence of survival conditions is calculated by:

$$p_{survival} = \frac{1}{N} \tag{5.4}$$

The y-axis in the diagram above is in logarithmic scale. The stipulation line is constructed by making a trend line to match the probability curve for the highest significant wave heights. From the trend line predictions of 1 year and 10 year survival conditions is found.

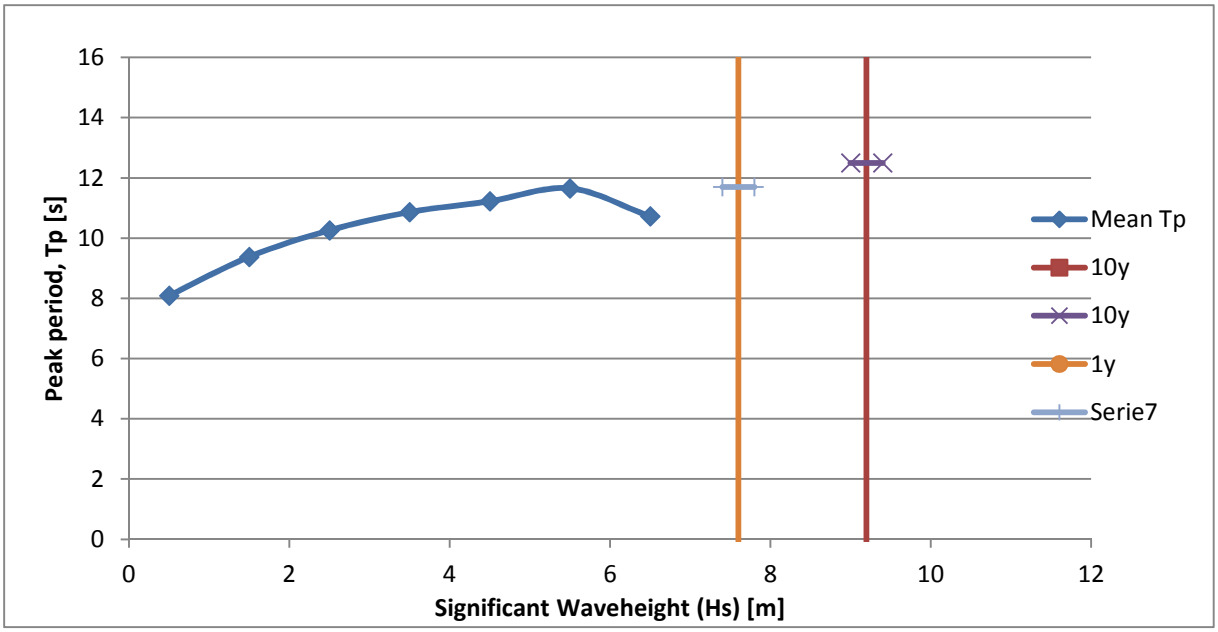

Figure 5.3, Estimation of spectral peak periods for survival conditions

Estimation of the peak period for 1 and 10 year is extrapolated from the graph above. A summary of the results is presented below.

Survival condition	1 year	10 year	Unit
Number of sea states	2922	29220	[-]
Probability of occurrence	3,42E-04	3,42E-05	[-]
Corresponding Hs	7,60	9,20	[m]
Corresponding Tp	11,70	12,50	[s]

Table 5.2, Summary of 1 year and 10 year survival condition parameters

6. Experimental Concept Phase

During the concept phase of designing the model many considerations and choices were taken. These are explained and discussed in this section. A presentation of the model instrumentation setup is also presented.

6.1 Problem Description

The main purpose of the model test is first and foremost to analyze the feasibility of the system. The second purpose is to compare the model test results with the results obtained from the SIMO analysis. Results from this model test can be used for calibration of the numerical model for further analysis of the system.

6.2 Tank Facility

A full description of the towing tank facility is presented in Palmstrøm (2010) and only a brief summary will be given in this section. Towing tank III at Marintek`s facilities was used for the model test. An illustration of the facility is presented in Figure 6.1 where the position of the wave maker is and wave absorbing beach is given. The tank is 85 meters long and has a width of 10.5 meters. The depth of the tank is 10 meters. The wave maker consists of a double flap and can produce both regular and irregular waves given by wave spectra. Max wave height is 0.9 meter and max steepness is 1:10. The wave period range is from 0.8 s to maximum 5 s.

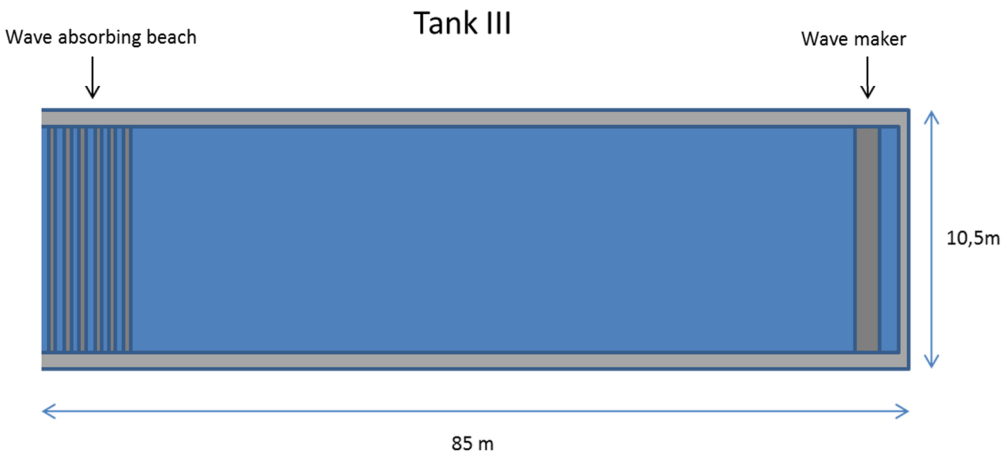

Figure 6.1, Illustration of the used model tank at Marintek

6.3 Concept Phase

Many factors had to be taken into account when designing the buoy. A concept study was therefore performed in the early stages of the design phase. A full description of the system is given in Palmstrøm (2010) and Johannessen (2009) and the reader is referred to these articles for a detailed description of the system.

6.3.1 Adjustable VCG

From previous numerical analysis performed in Johannessen et.al (2010) it was discovered that relative pitch motion contributed more than 30% of the total energy extraction from the system. This was highly dependent of the VCG (vertical center of gravity) of the main buoy.

Two factors became important from these observations; firstly, the VCG on the model should be adjustable to see if the results from model test agree with the numerical results. Secondly, it was an aim to get the VCG as low as possible, while still maintaining possibilities to vary the VCG.

6.3.2 Interchangeable Bottom Section

In early discussions the idea of interchangeable hull sections on the buoy were considered to examine the importance of hull shape for the power extraction of the system. The idea was good but it would require a complex model and increase the costs.

In order to get the correct displacement of the buoy as well as having a low VCG a steel keel was needed. It was decided to take use of interchangeable bottom sections below the keel, rather than large interchangeable hull sections. This was less expensive and it made the model simpler.

It was decided to study the effect of two different bottom sections. One bottom hull section was constructed with a flat bottom and a second one with a rounded bottom. The main purpose of this was to get an indication of the significance for the damping of the relative heave motion of the system. Relative heave motion will lead to large amounts of water flowing through the bottom opening. A rounded bottom should give less vortex shedding than a flat one, thereby giving less damping of the motions

6.3.3 Simulating the power extraction units

The largest challenge in the design process was how to simulate the power extraction units in the model test. In the full-scale version the coupling between the two floating bodies is pumps designed to deliver high-pressure fluid regardless of direction of the piston rod. A full description of these pumps is explained in Brandsvoll (2010).

The cylinders simulating the pumps show similar characteristics to the full-scale pumps. They have a minimum pressure that must be overcome before they start to contract/retreat because static friction between the cylinder and piston. The full scale water pump will have a threshold pressure to exceed before water can flow. The damping of the cylinder should be adjustable such that power output for different damping levels can be determined.

Figure 6.2, Picture of a similar type of air cylinder used to simulate the full-scale water pumps

7. The Model

The main dimensions stated in chapter 2 and the requirements in section 6.3 gives firm guidelines for the experimental design of the model. The design of the buoy is described in this section.

7.1 Main Buoy

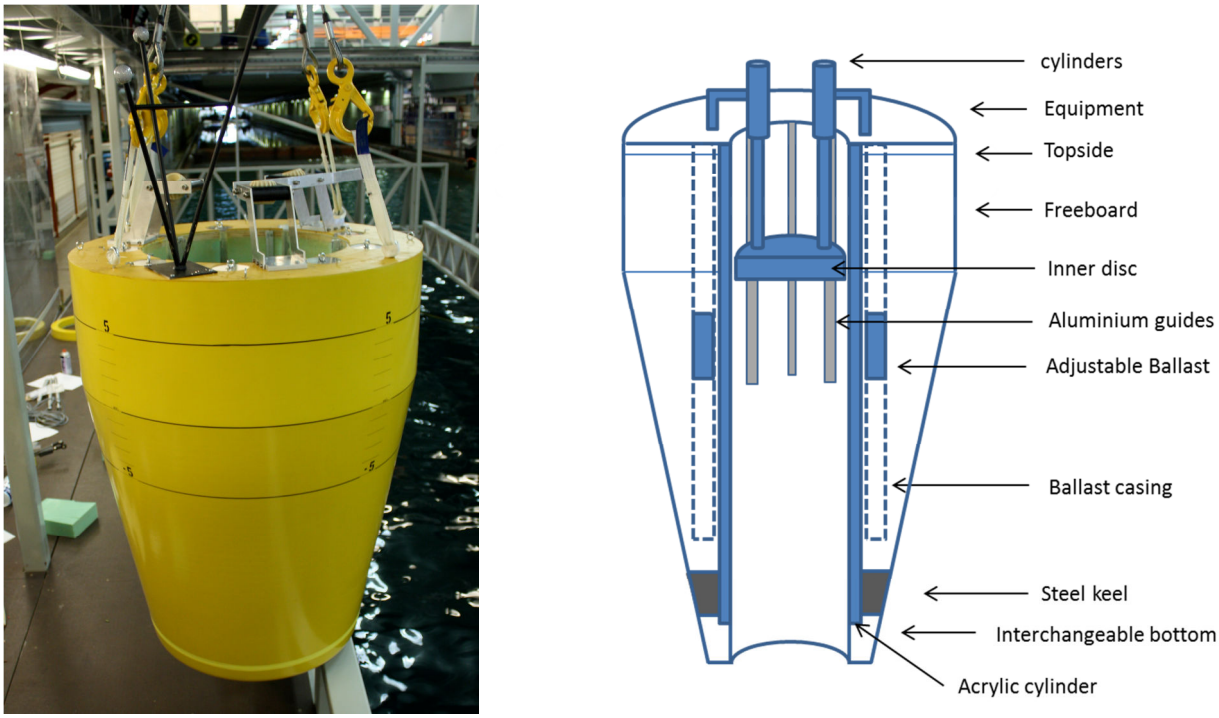

Figure 7.1, Picture and illustration of the main buoy

A picture of the buoy and an illustration of the cross-sectional components of the Dynocean Buoy are presented above.

The main buoy hull consists of a plywood top deck, a polyester coated divinycell hull, a steel keel and an interchangeable bottom section. To add strength to the structure, an acrylic cylinder is glued to the main hull inside the moonpool. The bottom part of the model consists of an interchangeable bottom sections. It is equipped with a total of six aluminum T-profiles attached to the acrylic cylinder. These T-profiles function as guides for the inner disc.

Nine small acrylic cylinders are inserted downwards from the topside in the divinycell hull (in a radial manner) with an angle of 40 degrees between each other. Weight is lowered into the cylinders, to give the correct displacement. By raising and lowering these weights the VCG can be adjusted.

To simulate the power extraction system, three pneumatic cylinders were mounted to brackets on the topside. These were installed in a radial manner with 120 degrees between. The disc inside the moonpool area is connected to the buoy only by the cylinders where the energy extraction occurs.

7.2 Power Extraction System

Different solutions were discussed on how to simulate the full scale water pumps in model-scale. Water pumps, frictional mechanisms (clamps), linear motors with a control unit, hydraulic cylinders and air cylinders were considered.

Because it was an aim to keep the system as simple as possible air cylinders were chosen to simulate the pumps. These have some of the qualities that can simulate characteristics in the real pumps. When exposed to a driving force, the air cylinders have a certain static frictional resistance that must be overcome before they start to contract/retreat, which simulates the pressure the pumps must overcome in full-scale.

Double acting pneumatic cylinders from Bosch Rexroth were used. A full technical description of the cylinders is attached in appendix 1. In order to control/vary the damping properties of the cylinders blind plugs drilled with different bores diameter were machined. These act as chokes on the cylinders.

Method for determining damping values

To get an insight of the damping properties of the cylinders a custom made test bench was constructed as shown in figure 7.2.

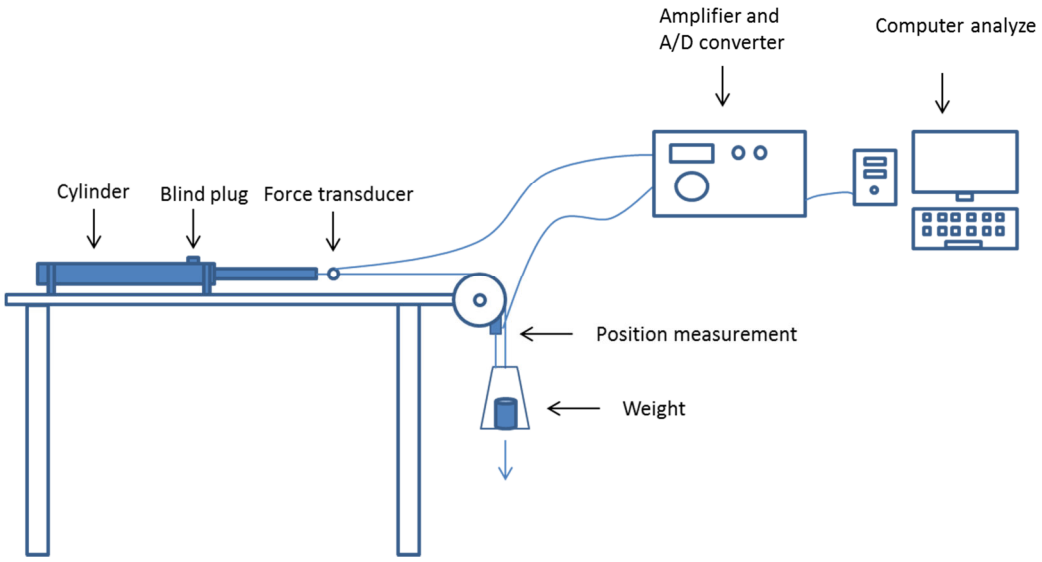

Figure 7.2, Test bench for calculating damping values for different bores

The cylinders are mounted to the bench in a fixed position. A weight is used to pull out the cylinder rod by gravity. The test bench is instrumented with a potentiometer to measure the displacement of the piston being extracted and a force transducer to measure the force used to extract the piston rod. Damping of the cylinders was calculated by:

$$B_{linear} = \frac{F_{average}}{V_{average}} \tag{7.1}$$

Where B_{linear}, $F_{average}$ and $V_{average}$ is the linear damping, average force and average velocity. The extraction of the piston rod was constant after the initial acceleration.

The effect of oil applied inside the cylinders where also analyzed. The following plot shows this effect as well as the linearity of the damping force for different velocities. Lubrication was applied prior to all tests.

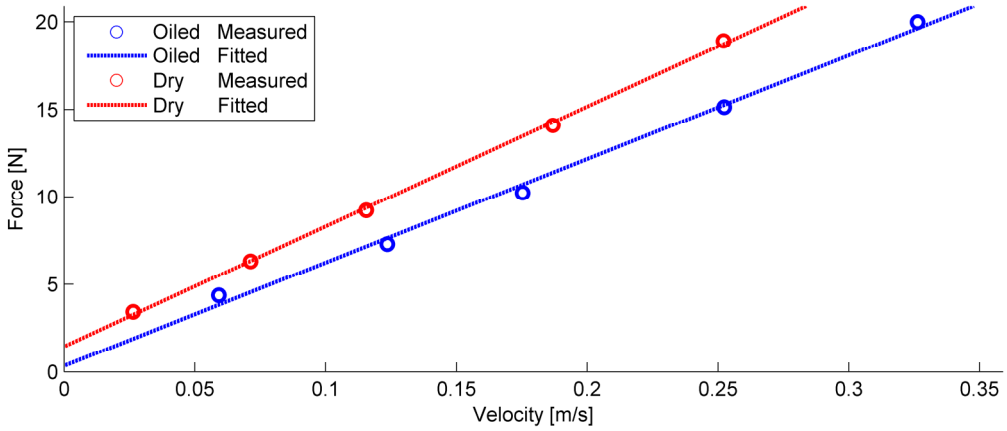

Figure 7.3, Force-velocity plot of damping force of cylinder tested in rig with and w/o lubrication

It should be emphasized that only extraction (not compression) of the cylinders were measured when determining the damping values. The measurements provide position and force measurements. By differentiating the position with respect to time the velocity could be found. An average of this velocity is used when determining the damping values.

Different types of bores were used in the calculation varying from 1.0 mm to 2.0 mm in the blind plug. In addition a test was taken when no blind plug was mounted (large opening → less damping). The test rig was built, instrumented and calibrated by the authors.

The results are presented in the table below:

Choke diameter	Average velocity	Force	Damping	Damping full-scale
[mm]	m/s	[N]	[N/(m/s)]	[kN/(m/s)]
no plug	0,396	6,8	17	76
2	0,289	6,8	24	104
1,5	0,246	6,8	28	122
1	0,143	6,8	48	210

Table 7.1, Estimates of damping values for different bores of blind plugs

In the model test bores of 1.0, 1.2 and 1.5 mm is used which correspond to a full-scale damping between 122 and 210 kN/(m/s) according to this test. It is emphasized that these results are not absolute, but used more as an indication.

A max stroke of the cylinder was 380 mm which represents 10.9 m in full-scale. This can handle relative motion amplitude above 5 meters which should be sufficient for the designated operating area.

7.3 Disc and Guide System

The Dynocean Buoy system extracts energy in relative heave, roll and pitch. By allowing relative yaw motion the disc inside the buoy would yaw without compressing the cylinders. Relative yaw motion between the buoy and the disc should be avoided.

The challenge was to minimize yaw motion and at the same time allow both pitch and roll. Also it is of importance that the disc is not allowed to "jump" out the guide system. Another reason for having guides is to minimize the friction of the system. The friction will be less by having a small portion of the disc in contact with the guides, rather than having a large area of the disc in direct contact with the buoy.

A consequence of allowing both pitch and roll motion is that some level off yaw motion must be allowed as well with current guide system. Since the model test is being performed in a towing tank with waves in only one direction, in theory no roll motion should occur. The guide system could therefore in theory be constructed very simple. The original idea was only to only have two guides into the disc illustrated in figure 7-4.

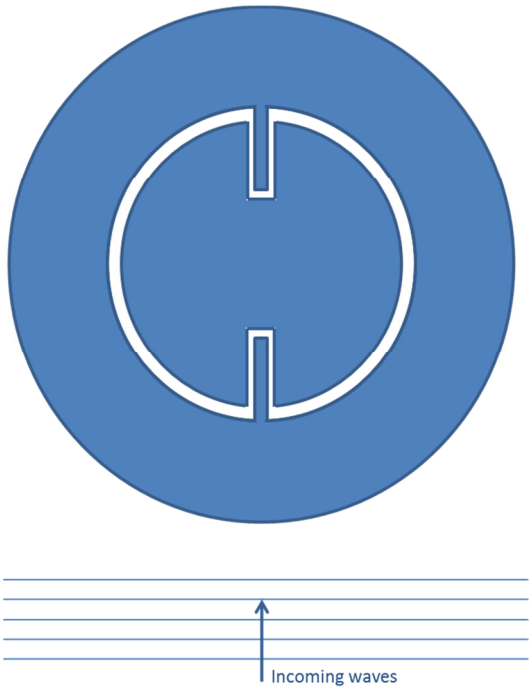

Figure 7.4, Early version of the guide system

It was later decided that this type of configuration was not the best idea. The damping properties of each cylinder could not be guaranteed to be 100% equal. This together with the fact that most of the model tests were performed in irregular seas and the introduction of tank wall reflections, it was likely that roll motion would occur. By utilizing the simple guiding system as in Figure 7.4 roll motion would be obstructed. This could give much friction in the system as well as introducing a "sticking" behavior between the disc and the buoy which would introduce errors in the measurements.

It was decided to make a guide system that did not obstruct roll motion. It was also of interest to construct a system that could be implemented in the full-scale version. A maximum rotation about a random horizontal axis has been set to 30 degrees. A MATLAB script “disc_geometry.m” was written to determine the disc dimensions on the following demands:

1. Obstruct the disc “jumping” out of guide system
2. Avoid jamming/sticking of disc in guide system
3. Minimizing yaw motion of the disc at the same time as allowing a rotation of 30 degrees around a random horizontal axis.
4. Reduce frictional forces

The number of guides was decided by a compromise between keeping the dimensions as small as possible still keeping the construction as simple as possible. From two guides too six guides there was a significant drop in the needed cross sectional length of the guides (in radial direction). It was also an aim to have the buoy as symmetric as possible, and it should therefore be either 6 or 9 guides to line up with the power extraction system. The increase from 6 to 9 guides did not give significant decrease size in radial direction, and therefore 6 guides with a spacing of 60 degrees were chosen. A top-view of the disc inside the buoy with the designed guide system is shown in figure figure 7.5 together with the dimensions of the aluminum t-profiles that were used.

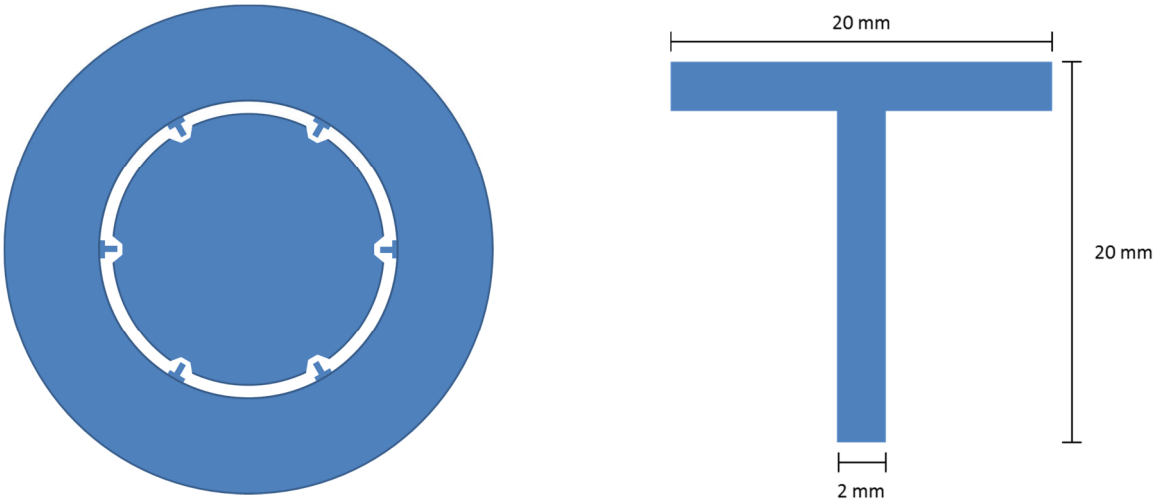

Figure 7.5, Illustration of the final version of the guide system

7.4 Summary of Body Geometry

Buoy	Model scale	Full-scale	Unit
λ (scaling factor)	1:28.7	-	[-]
Draught	0,784	22,50	[m]
Freeboard	0,300	8,60	[m]
MWL Diameter	0,836	24,00	[m]
Keel Diameter	0,592	17,00	[m]
Inner Diameter	0,488	14,00	[m]
Height of ballast cylinders	0,854	24,50	[m]
Numbers of ballast cylinders	9	9	[-]
Disc	**Model scale**	**Full-scale**	**Unit**
Draught	0,03	0,86	[m]
Freeboard	0,03	0,86	[m]
Diameter	0,478	13,72	[m]

Table 7.2, Body geometry of buoy and disc

7.5 Instrumentation

A total of 4 wave probes and 6 force gauges were used in addition to the global position measurement system. Global position measurements were logged with a frequency of 20 Hz. All force measurements are logged with a frequency of 200 Hz in model scale (37.3 Hz in full-scale) and a 20 Hz low-pass Butterworth filter was then applied. A review of the different types of measurements in the model test is given in this section.

7.5.1 Global Position Measurements

An optical measurement system was used to measure the global motion of the main buoy. A bracket with 3 ball shaped reflectors was mounted on the main buoy. By measuring the position to one of the reflectors in the local body coordinate system the system calculates the motion in all six DOF`s.

7.5.2 Relative Motion Measurements

An optical position measurement system could not be used in to measure relative motions since the buoy prevented a clear view to the disc from the cameras.

Use of potentiometers was first considered to measure the relative motion between the main buoy and the inner disc. These would only measure the relative vertical position next to each cylinder. The relative heave, roll and pitch motion could from this be calculated.

However the given potentiometers available at Marintek had relative large dimensions and weight. In addition the amount of force needed to extract/retract the potentiometers could affect the measurements.

The final solution consisted of three springs connected close to the fastening point of the cylinders on the disk and the main buoy. In between the cylinder brackets and the springs, force gauges were mounted. By Hooke`s law, the vertical position of the fastening point could be calculated by the following equation(Kreyszig 2006):

$$x = \frac{F}{k} \tag{7.2}$$

Where F is the force exerted on the spring, k is the known spring stiffness and x is the displacement. By differentiating the position with respect to time the relative velocity for each cylinder piston between could be calculated.

7.5.3 Force Measurements

Force gauges were mounted between the disk and each of the three piston rods. These measured the force on each cylinder from the disc.

By knowing the relative motion between the disk and the main buoy as well as the force on each cylinder, the power output can be calculated.

7.5.4 Fastening of Cylinders

Figure 7.6 below shows where the cylinders were fastened on the disc. The circles denote the fastening of the cylinders. The three crosses denotes where the spring was fastened to measure the relative motion of each cylinder. These were fastened 23 mm closer to the center in x-direction as shown in the figure. This was taken into account when calculating vertical motion of each cylinders fastening point. Relative heave, pitch and roll were calculated in real time by simple geometry.

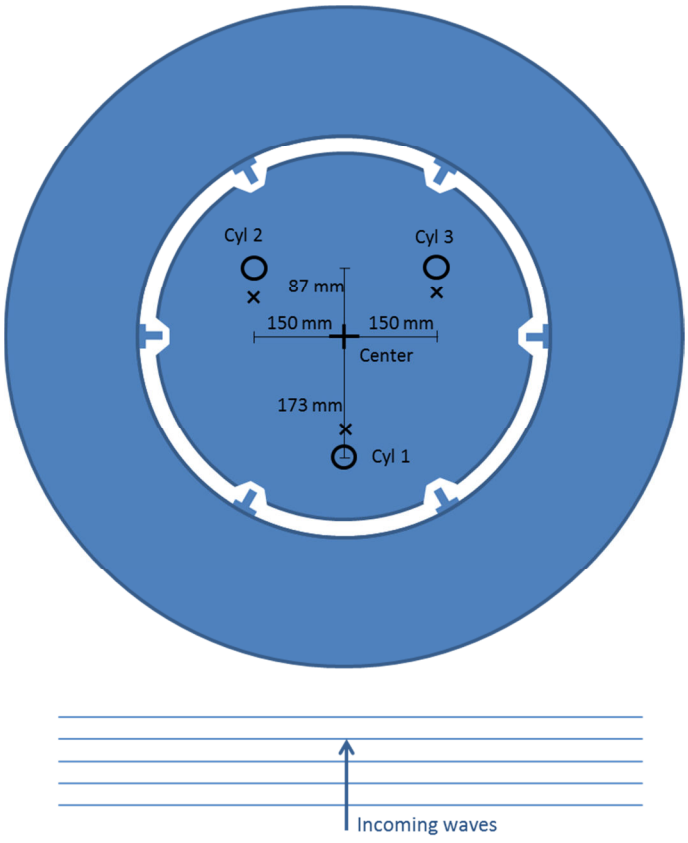

Figure 7.6, Positions of the cylinders and springs on the disc (model-scale)

8. Stability Analysis

A hydrostatic stability analysis of the system has been performed. This was done to determine important features of the Dynocean Buoy. The vertical center of gravity (VCG), center of buoyancy (COB) and metacenter were calculated. The moments of inertia with respect to the horizontal and vertical axis through the center of gravity were also calculated. Theory from this chapter is gathered from Amdahl. et. al. (2005) and Tipler (2004).

8.1 Theory

The GM value is a measure of stability of a floating structure. A positive GM value must be satisfied, if not the structure is unstable and will capsize if GM does not become positive due to the rotation. The GM value is calculated by the following formula:

$$\overline{GM} = \overline{KB} + \overline{BM} - \overline{KG} \tag{8.1}$$

Where;

$\overline{KG}$ is the distance from the keel to the VCG.

$\overline{KB}$ is the distance from the keel to the COB.

$\overline{BM}$ is the distance from COB to the metacenter calculated by

$$\overline{BM} = \frac{I}{\nabla} \tag{8.2}$$

Where I is the second moment of area and ∇ is the volume displacement.

$\overline{KG}$ is calculated by accounting for the all sub masses with the following formula:

$$\overline{KG} = \frac{\sum_{i=1}^{n} m_i y_i}{\sum_{i=1}^{n} m_i} \tag{8.3}$$

Where m_i and y_i represents each sub-mass and distance from keel to the point of gravity in each sub mass. If m_i is replaced with sub-volume, V_i, the same formula can be used to calculate Center of buoyancy of a floating structure.

In order to calculate the mass moment of inertia with respect to a given axis, the parallel-axis theorem can be used, this relates the moment of inertia about an axis through the center of mass of an object to the moment of inertia about a second, parallel axis:

$$I_{mass} = \sum_{i=1}^{N} I_{cm,i} + m_i h_i^2 \tag{8.4}$$

Here, $I_{cm,i}$ is the mass moment of inertia for a given sub mass, i. m_i is the mass of an object and I_{mass} is the moment of Inertia about a parallel axis a distance h away.

The radius of gyration is calculated by the following formula:

$$r_{gyration} = \sqrt{\frac{I_{mass}}{M}} \tag{8.5}$$

Where M denotes the total mass the body that is studied.

The mass moment of inertia about the diameter for a thin cylindrical shell is:

$$I_{xx} = \frac{1}{2}mr^2 + \frac{1}{12}ml^2 \tag{8.6}$$

Where r is the mean radius, m is the mass and l is the length of the shell.

For a hollow cylinder about the diameter the formula is:

$$I_{xx} = \frac{1}{4}m(r^2_{outer} - r^2_{inner}) + \frac{1}{12}ml^2 \tag{8.7}$$

8.2 Method

The stability analysis performed in MATLAB was used to vary different properties of the model. The bottom section height, steel keel height, displacement and position as well as number of ballast cylinders were varied in order to optimize the design. The total number of ballast cylinder was of importance when deciding the stability properties of the buoy. It was important to spread the weight equally in the horizontal plane to have the same radius of gyration in both roll and pitch to make the model realistic. By having a large quantity of ballast weights, the height of each weight was reduced, thus the VCG of the ballast could be raised and lowered a greater distance. This would give a larger specter to vary the GM.

For practical reasons it was of interest to spread the ballast weights in a symmetric fashion with respect to the cylinder and brackets mounted on the topside. Six, nine and twelve ballast cylinders were considered. By having too many ballast cylinders the model could become unnecessary complex. By having too few cylinders each ballast mass had a large weight and were unhandy to work with. By this a total of nine ballast cylinders were chosen and GM values were then calculated for different ballast conditions.

A first insight regarding stability considerations were performed during the concept phase. A MATLAB script, “Stability.m” was used to decide keel weight, number of ballast cylinders and the mass of each ballast weight. Mass moment of inertia was calculated about both the vertical and horizontal axis. These calculations were used at a later stage to get estimates for important natural periods of the system.

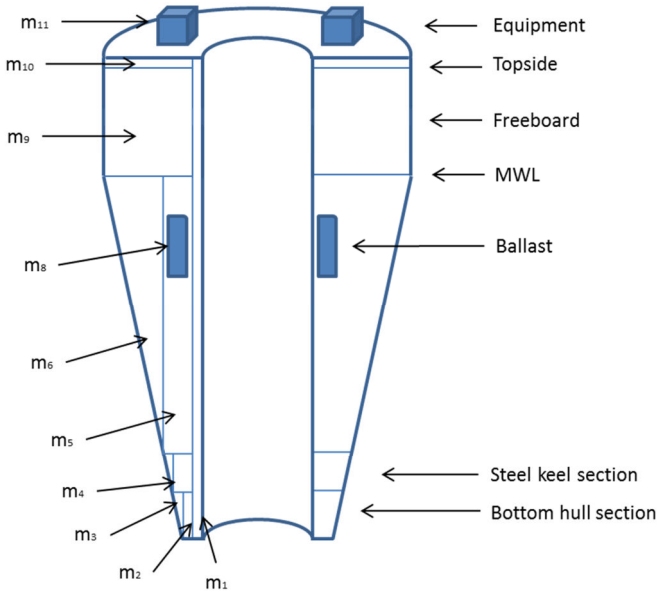

Figure 8.1, Mass distribution of the main buoy

In “stability.m” the buoy is divided into 11 sub- masses/volumes as illustrated in the figure above. All masses are kept in fixed positions except the ballast mass which can be raised and lowered. The GM value of the buoy is calculated with the formulas stated in chapter 7.1.

In order to calculate the mass moment of inertia about the horizontal axis some simplifications are used. The second term in equation 8.4 is used for all the sub-masses. The first term in the equation is used for the steel keel, the steel ballast cylinders and the topside which is illustrated in the figure below. The rest of the hull has relatively small mass and is therefore neglected. The steel keel is simplified as a hollow cylinder. The movable ballast weights where approximated as a thin walled cylinder with a representative mass and radius, see Figure 8.2.

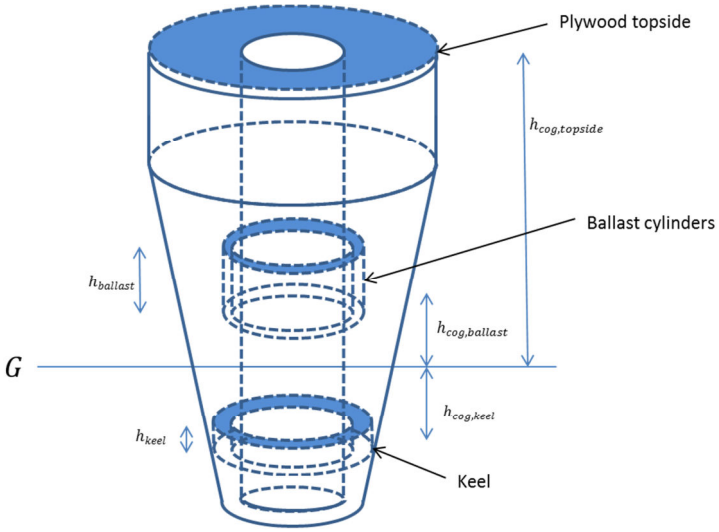

Figure 8.2, Simplifications of buoy properties when calculating mass moment of inertia

8.3 Results

An assessment of having a low VCG and having a fairly large capability to adjust the VCG was performed.

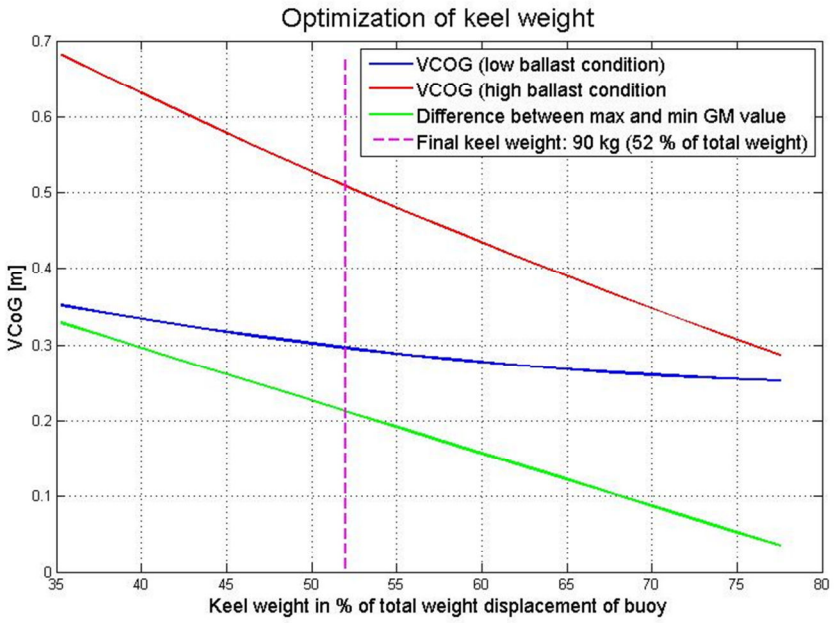

Figure 8.3, Max and min GM value for different keel masses

Figure 8.3 indicates GM values for different ballast condition. The green line in the figure above shows GM values for different keel mass in % of the total mass of the buoy. With a low keel weight (35% or less of total mass), the ballast weights becomes large and unwieldy. A high keel mass gives a potential small specter to vary the GM value of the buoy. From this analyze it was decided to have a 90 kg steel keel fastened to the hull right above the interchangeable bottom section. With this configuration the GM value could be varied from 3.35 m to 8.4 in full-scale.

Detailed analysis calculated in “stability.m” of buoy properties in low and high VCG condition can be found in Appendix 2.

It should be noted that the properties calculated in this analysis must be considered as preliminary design values. VCG, weight displacement and mass moment of inertia are updated at a later stage from inclination and pendulum tests.

Property	Model-scale	Full-scale	Unit
Displaced volume	0,171	4040	[m^3]
Displaced mass	171	$4140 \cdot 10^3$	[kg]
Steel keel mass	90	$2176 \cdot 10^3$	[kg]
Ballast weight	46	$1115 \cdot 10^3$	[kg]
Stability Analyze			
KB	0,47	13,50	[m]
BM	0,12	3,60	[m]
KG (low ballast position)	0,30	8,70	[m]
KG(high ballast position)	0,50	14,50	[m]
GM(low ballast position)	0,29	8,40	[m]
GM(high ballast position)	0,12	3,40	[m]
Radius of Gyration calculations			
r_{zz}	0,29	8,20	[m]
r_{xx} - Low ballast position	0,36	10,30	[m]
r_{xx} - High ballast position	0,46	13,30	[m]
I - Second moment of area	0,021	14417	[m^4]

Table 8.1, Buoy properties determined from the stability analysis

Here r_{zz} and r_{xx} denotes the radius of gyration of the vertical and horizontal axis through the VCG respectively.

9. Natural Periods

Calculations of natural periods of the system were assessed and calculated prior to the model test. Theory, method and results for uncoupled natural periods are presented in the following section. The calculations are performed in full-scale and compared to from results of the model test. Theory is collected from Faltinsen (1990) and if not otherwise stated.

9.1 Heave Natural Periods

The heave equation for an un-damped system can be described by the following formula:

$$(M + A_{33})\ddot{\eta}_3 + C_{33}\eta_3 = F_3(t) \tag{9.1}$$

The natural frequency for heave from equation is solved by putting the right hand side of equation 9.1 equal to zero. From this the following expression can be derived:

$$T_n = \frac{2\pi}{\omega_n} = 2\pi\sqrt{\frac{M + A_{33}}{C_{33}}} \tag{9.2}$$

Where M and A_{33} is the mass and added mass in heave of a floating body.

C_{33} is the water plane stiffness of a floating body and can be calculated as

$$C_{33} = \rho A_w g \tag{9.3}$$

Where ρ is the density of water, A_w is the waterline area and g is the acceleration of gravity.

When the disc inside the moonpool is oscillating in heave the water column inside the outer buoy is assumed to oscillate at the same frequency.

The natural period in heave of the disc inside the moonpool can be calculated by (Faltinsen 1990):

$$Tn = 2\pi\sqrt{\frac{h}{g}} \tag{9.4}$$

Where h is the draught of the moonpool. WADAM results collected from Brandsvoll (2010) for added mass have been used when calculating the natural frequency in heave for the buoy.

9.2 Pitch Natural Periods

Pitch and surge motion are highly coupled. In this pre-calculation the pitch motion is studied as an uncoupled one DOF system. The uncoupled natural period is calculated by the following formula

$$T_{55} = 2\pi\sqrt{\frac{I_{55} + A_{55}}{C_{55}}} = 2\pi\sqrt{\frac{Mr_{55}^{\ 2} + A_{55}}{C_{55}}} \tag{9.5}$$

Where r_{55} is the pitch radius of gyration with respect to an axis parallel with the y-axis through the CoG. Restoring force in pitch is given as:

$$C_{55} = \rho g V \overline{GM} \tag{9.6}$$

As an estimate for added mass in pitch the parallel-axis theorem (equation 8.4) is calculated for the water column inside the moonpool with respect to the buoy.

Natural periods for Buoy (full-scale)			
Heave	**Pre-calculated**	**Model test**	**Unit**
Mass	4 140	4 140	[10^3kg]
C33	3 000	3 000	[kN/m]
A33	414	834	[10^3kg]
Tn	7,70	8,10	[s]
Pitch, Low VCG	**Pre-calculated**	**Model test**	**Unit**
I5	439 402	456 175	[10^3kgm2]
C55	264 506	306 706	[kNm/angle]
A55	340 331	305 259	[10^3kgm2]
Tn	9,00	9,90	[s]
Pitch, High VCG	**Pre-calculated**	**Model test**	**Unit**
I5	735 645	744 059	[10^3kgm2]
C55	279 877	127 009	[kNm/angle]
A55	136 216	142 465	[10^3kgm2]
Tn	17,20	16,70	[s]
Natural periods for Disc (full-scale)			
Heave	**Pre-calculated**	**Model test**	**Unit**
Mass	3 686	3 686	[10^3kg]
C33	1 486	1 486	[kN/m]
A33	441	433	[10^3kg]
Tn	9,50	10,5	[s]
Pitch	**Pre-calculated**	**Model test**	**Unit**
Tn	N/A	4,20	[s]

Table 9.1, Natural period results

It should be noted that the calculations are performed prior to the model test and therefore the moment of inertia and GM values used in this calculation are the ones from chapter 7.

10. Model Test

10.1 Building of the Model

All design features, as the adjustable ballast system, interchangeable bottom section, the power extraction system, disc shape and guide system were all designed by the authors.

The construction of the model was mostly done by the staff at Marintek. However, the assembly of model was performed by the authors. The practical issues that emerged during the building phase were solved in cooperation with the staff.

Previous mass calculations from chapter 8 calculated the mass of the buoy without instrumentation and ballast cylinders to 117 kg. The ballast cylinders were calculated to have a total mass of 46 kg in and the total equipment dry weight was estimated to 8.2 kg.

When weighting the model after the construction was completed it the total weight of the buoy was 132 kg without the ballast weights and equipment. This was 15 kg more than calculated. The weight increase is most likely due to the following:

- During the milling process of the buoy an error was made and it had to be puttied at the freeboard section and then milled over again. This added weight to the top section of the buoy.
- Epoxy layer and paint was not taken into account when calculating the mass of the buoy.

All instrumentation that needed to be mounted on the buoy was measured to have a total weight of 3 kg, not 8.2 kg as estimated in previous calculations.

Because of this, the total mass ballast had to be adjusted. The total mass of the ballast was reduced from 46kg to 36 kg, giving each ballast cylinder a weight of 4 kg. The updated weight distribution is used in further calculations.

10.2 Pendulum Test

10.2.1 Theory

A pendulum test is a practical tool which can be used for determining the VCG and mass moment of inertia. Theory in this chapter is collected from Steen (2010).

The test is performed by initiating a rotation on the object of interest. Time measurements are noted for a given number of cycles. The average period of the oscillation is calculated from this. The period of a pendulum period is given by

$$T_0 = 2\pi\sqrt{\frac{I_O}{Mgh}} \tag{10.1}$$

Where I_O, g and M is mass moment of inertia about point O, acceleration of gravity and mass of the model respectively. h is the distance between the VCG and point O. A principle sketch is presented below. The model is assumed to rotate freely around point O. Equation (10.1) can be rewritten as;

$$4\pi I_O - MgT_0^2 h = 0 \tag{10.2}$$

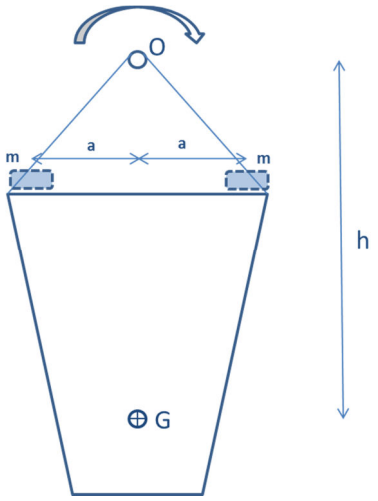

Figure 10.1, Principal sketch of a pendulum test

The period T_0 of the oscillating model is measured. Additional masses are mounted on each end, at a known distance from the rotation center. The new period, T_1 is now measured and the equation can be rewritten as

$$4\pi(I_O + 2Ma^2) - (M+2m)gT_1^2\left(h + \frac{2mh}{M+2m}\right) = 0 \tag{10.3}$$

Where m, a and T_1 represents the additional mass, horizontal distance from rotation axis and new pendulum period respectively. This equation can be solved for I_0 and h.

$$h = \frac{8\pi^2 ma^2}{Mg(T_1^2 - T_0^2)} \tag{10.4}$$

$$I_O = \frac{2ma^2T_0^2}{T_1^2 - T_0^2} \tag{10.5}$$

In order to obtain the mass moment of inertia about the VCG, the following equation can be used:

$$I_m = I_O - Mh^2 \tag{10.6}$$

10.2.2 Method

To get an accurate measure of the period of oscillation, the average of 20 oscillations were measured 7 times. The standard deviation was calculated for the 7 runs to get a sense of the reliability of the results. Full documentation of the analysis is provided in appendix 3. The result showed good consistency.

The cradle was first oscillated alone. Then two additional weights of 10 kg were placed an equal distance from the symmetric vertical axis. By use of equation 10.4 and 10.6 the VCG and I_m were calculated for the cradle.

Then the Dynocean Buoy was placed in the cradle and similar measurements as for the cradle was performed except the additional weights were increased to 40 kg.

To get the correct VCG and I_m for buoy, the VCG and I_m for the cradle was subtracted from the total VCG and I_m .

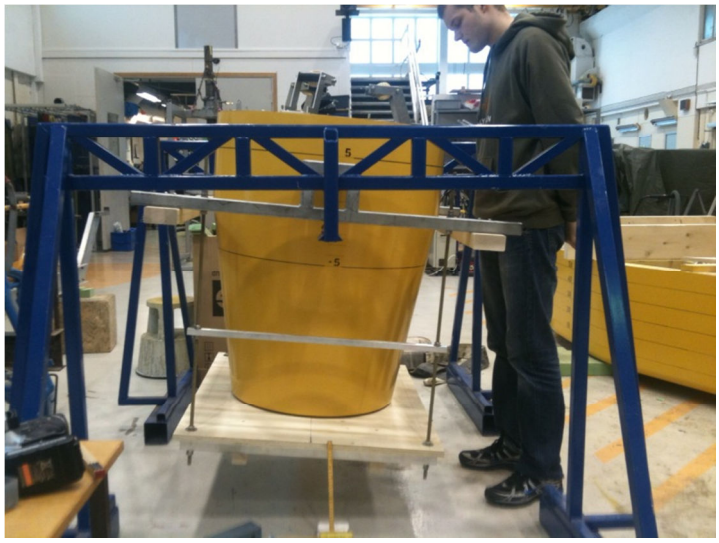

Figure 10.2, Mr. Brandsvoll oscillating of the Dynocean Buoy in the cradle

10.2.3 Results

Detailed calculations are found in appendix 3 and only a brief summary with key results is presented below.

Property	Model-scale	Full-scale	Unit
Ixx , Low ballast position	23,09	$449 \cdot 10^6$	[kgm^2]
Ixx , High ballast position	37,87	$737 \cdot 10^6$	[kgm^2]
rxx, Low ballast position	0,368	10,55	[m]
rxx, High ballast position	0,471	13,51	[m]
KG, low ballast condition	0,366	10,50	[m]
KG, high ballast condition	0,531	15,24	[m]

Table 10.1, Buoy rotation properties and KG from pendulum test

10.3 Inclination Test

An inclination test was performed when the Dynocean Buoy was launched into the water and equipped with instrumentation. The inclination test was performed to provide accurate information about the GM value in the two different VCG conditions.

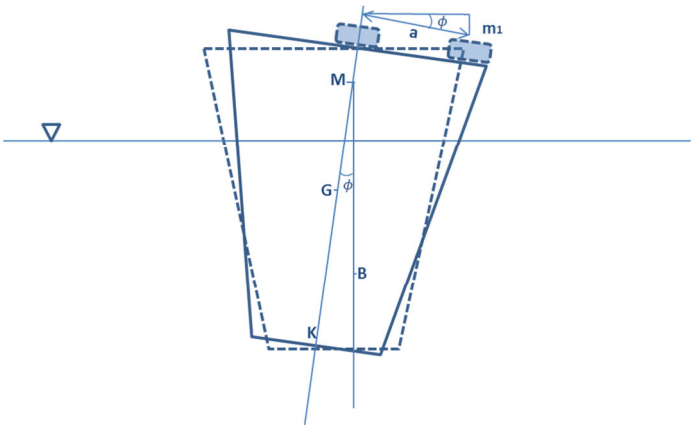

Figure 10.3, Principle sketch of the inclination test

A full description of the test method can be found in Amdahl et. al. (2005). The test is performed by letting the buoy float freely at MWL. A given mass, m_1, in the figure above is placed at a known distance, a, from the center line. The GM value can be calculated in the formula stated below. Results from the inclination test are found in the table below.

$$GM = \frac{m_1 a}{\nabla \rho \tan(\phi)} \tag{10.7}$$

Property			Model-scale	Full-scale	Unit
K - keel			0,000	0,00	[m]
B - center of Buoyancy			0,469	13,47	[m]
M - Metacenter			0,594	17,05	[m]
a: distance between center line and CoG of m1			0,355	10,19	[m]
Inclination test 1 - Ballast weights are lowered at a minimum					
mass [kg]	**bank angle [deg]**	**GM-model [m]**	**KG-model [m]**	**GM-full-scale [m]**	**KG-full-scale [m]**
4	1,80	0,264	0,329	7,59	9,46
6	2,70	0,264	0,329	7,59	9,46
8	3,65	0,260	0,333	7,48	9,57
Average		***0,263***	***0,331***	***7,55***	***9,50***
Inclination test 2 - Ballast weights are lowered at a maximum (0,77m higher)					
mass [kg]	**bank angle [deg]**	**GM-model [m]**	**KG-model [m]**	**GM-full-scale [m]**	**KG-full-scale [m]**
2	2,170	0,110	0,484	3,15	13,90
4	4,390	0,108	0,485	3,11	13,94
Average		***0,109***	***0,485***	***3,13***	***13,92***

Table 10.2, Buoy properties from inclination test

10.4 Mooring lines Setup

The Dynocean Buoy was kept at a mean horizontal position by 4 mooring lines. These were fastened on the topside of the buoy and to the tank walls as illustrated below.

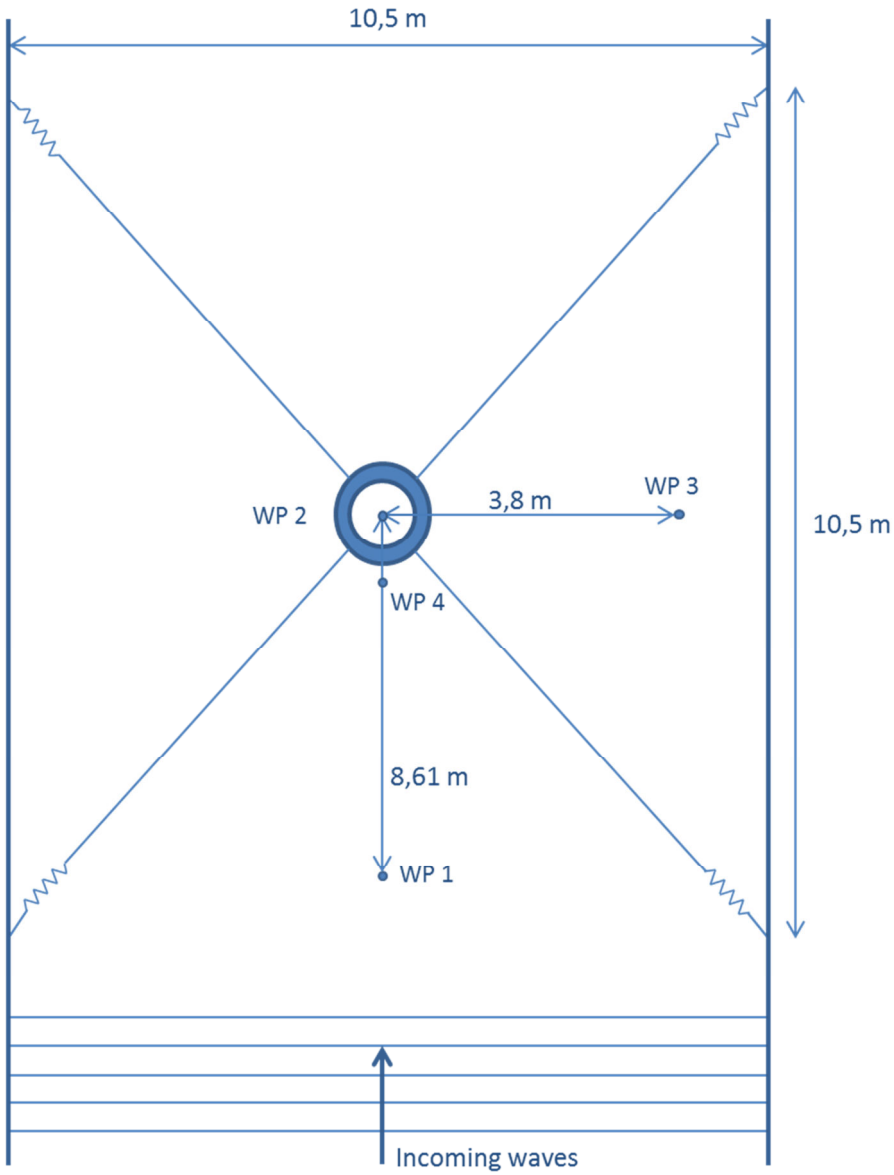

Figure 10.4, Sketch of the mooring setup used in model testing

Ideally the fastening of the buoy should be as soft as possible, but still prevent slack. It is important to prevent interference from natural periods of the mooring with natural periods expected to occur. Therefore a pre-calculation of the natural periods for the mooring setup was performed. A study of surge and yaw natural periods of the mooring setup was performed. Equations for surge and yaw motion is given below respectively from Faltinsen(1990).

$$T_{11} = 2\pi\sqrt{\frac{m + A_{11}}{k_{surge}}} \tag{10.8}$$

$$T_{55} = 2\pi\sqrt{\frac{I_{55}}{k_{yaw}}} = 2\pi\sqrt{\frac{mr_{zz}^{\ 2}}{k_{yaw}}} \tag{10.9}$$

Where m, A_{11} and k_{surge} represents the mass, added mass and the system stiffness of the system in surge respectively. I_{55} and r_{zz} represents moment of inertia and radius of gyration about the vertical axis. k_{yaw} is the system stiffness in yaw.

$$k_{surge} = 2\left(\frac{\sqrt{2}}{2}(k_{sl} + \frac{P_0}{L})\right) \tag{10.10}$$

$$k_{yaw} = 4(r_{fairlead}P_0) \tag{10.11}$$

Between the fastening points on the buoy and the mooring lines, force transducers were attached during the setup. This gave real-time measurements of the pre-tensioning, P_0. The stiffness of each single spring was 30 N/m, denoted as k_{sl} in the formulas. The fairlead radius, $r_{fairlead}$ and line length, L, is used to calculate the system stiffness for yaw and surge motion. Natural periods below 20 s in full-scale should be avoided to prevent conflict with natural periods of the buoy motions.

By setting the pretension to 20 N in model-scale, the natural periods from the mooring system should not interfere with expected natural periods of the buoy. A table with the current calculations is given below.

Property	Model-scale	Full-scale	Measured	Unit
Line length	7,78	223	N/A	[m]
Pretension single line	20,000	472·10[3]	N/A	[N]
Spring stiffness, single line	30,000	24711	N/A	[N/m]
System stiffness (kx=ky)	46,063	37941	N/A	[N/m]
Fairlead radius	0,418	12	N/A	[m]
Yaw Stiffness	0,000	22·10[6]	N/A	[Nm]
Added mass, surge[1]	287,649	6800·10[3]	N/A	[kg]
mass	170,890	4040·10[3]	N/A	[kg]
r_{zz} about CoG (spec)[2]	0,285	8,18	N/A	[m]
Surge natural period[3]	19,82	106,2	101,0	[s]
Yaw natural period[4]	4,05	21,7	22,7	[s]

Table 10.3, Mooring calculations

[1] The added mass in surge is collected from WADAM results found in Brandsvoll (2010)
[2] The r_{zz} is collected from the stability analyze
[3] The analysis of the measured value can be found in appendix 7.31
[4] The analysis of the measured value can be found in appendix 7.30

10.5 Summary of Model and Model Properties

During the inclination test the Dynocen Buoy was floating at MWL, it was correct ballasted and the weight is distributed in the same manner as all of the following tests were performed. Therefore the KG values from the inclination test are chosen to be used for further calculations since these are considered more accurate than KG values from the pendulum test.

The highest expected natural period is pitch in high VCG condition (16.6 s). Both surge and yaw natural period are higher than pitch natural period and will not interfere.

For further calculations the radius of gyration about the horizontal axis from the pendulum test is used. The radius of gyration about the vertical axis calculated from the stability analysis is still used for further calculations.

A summary of all the important properties of the Dynocean Buoy used for further calculations is presented in the table below:

Property	Model-scale	Full-scale	Unit
Displaced volume	0,171	4040	[m^3]
Displaced mass	170,890	$4140 \cdot 10^3$	[kg]
Hull including steel keel	131,00	$3096 \cdot 10^3$	[kg]
Ballast mass per cylinder	4,00	$95 \cdot 10^3$	[kg]
Total cylinder ballast mass	36,00	$851 \cdot 10^3$	[kg]
Div. equipment and ballast	3,90	$91 \cdot 10^3$	[kg]
Ixx - Low ballast position	23,40	$456 \cdot 10^6$	[kgm^2]
rxx - Low ballast position	0,3703	10,63	[m]
Ixx - High ballast position	38,21	$744 \cdot 10^6$	[kgm^2]
rxx - High ballast position	0,473	13,57	[m]
Izz	13,887	$277 \cdot 10^6$	[kgm^2]
rzz	0,285	8,18	[m]
B - center of buoyancy	0,469	13,47	[m]
M - metacentric height	0,594	17,05	[m]
KG - low ballast condition	0,331	9,50	[m]
KG - high ballast condition	0,485	13,92	[m]
GM - low ballast condition	0,26	7,55	[m]
GM - high ballast condition	0,11	3,13	[m]

Table 10.4, Summary of properties of the Dynocean Buoy estimated prior to the model test

11. Parameter Input

It was of interest to see the effect of varying different input parameters. This chapter describes the different parameters that were investigated in the model test. The different sea states the buoy was exposed to are also presented. A comparison study of the different input parameters is performed with a “base case standard” used as a reference.

11.1 Bottom Section Shape

Two different bottom sections have been selected as shown in figure 11.1. The edged bottom (a) should give larger damping for relative heave. A semicircular bottom section presented in (b) should give better vortex shedding and reduce unwanted drag damping. By comparing results between the two cross sections the importance of the shape of the moonpool inlet can be decided.

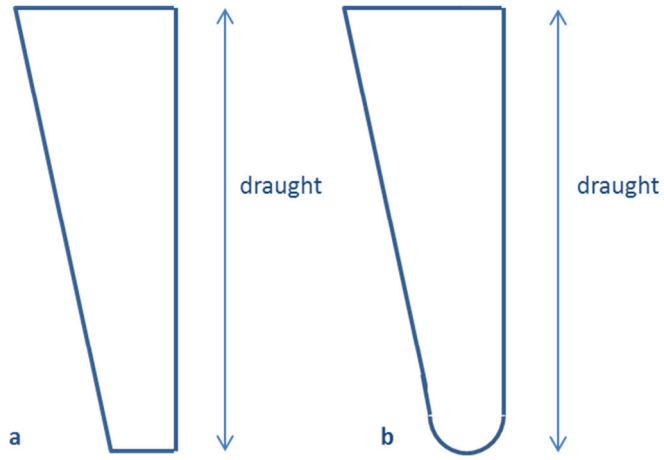

Figure 11.1, Different bottom sections

11.2 Vertical Center of Gravity

Two different positions of the ballast weights were used during the tests to vary the VCG. It was of interest to investigate system performance with different VCGs. The resulting VCG for both ballast positions were measured from inclination tests which is considered to be more accurate than results from the pendulum test.

#	Property	Full-scale	Unit
1	KG: Low ballast position	9,50	[m]
2	KG: High ballast position	13,92	[m]

Table 11.1, KG by different ballast positions

11.3 Damping of Cylinders

Damping properties for the pneumatic cylinders calculated in section 7.2 were used on the device in the model test. A total of three different bores of the blind plugs were used. The damping values found from preliminary analyses are presented in the table below.

#	Property	Full-scale	Unit
	Stroke	10,9	[m]
1	Damping; plug with 1 mm bore	210	[kN/(m/s)]
2	Damping; plug with 1,5 mm bore	122	[kN/(m/s)]

Table 11.2, Damping properties of power extraction units (cylinders)

11.4 Sea States

It was of interest to study how much energy the system produced in different sea states of the designated operating area of the Dynocean Buoy. The irregular sea states (irregular wave 1-4 in the table below) are typical sea states that represent short wind driven waves and swell components.

An interesting test parameter to check the feasibility of the system is the response of the survival conditions. Both visual inspections and position measurements can give a good indication of the feasibility of the system.

The regular and irregular waves used in the model test are presented in Table 13.3 below.

Irregular waves	**Specified**		**Measured**	
	Hs [m]	**Tp [s]**	**Hs [m]**	**Tp [s]**
Irregular wave 1	1,50	6,50	1,38	6,17
Irregular wave 2 (base case condition)	2,50	9,00	2,14	8,98
Irregular wave 3	3,50	11,50	3,60	12,28
Irregular wave 4	4,50	14,00	6,69	14,10
1 year survival condition	8,00	11,00	7,71	10,90
10 year survival condition	10,50	13,00	10,59	12,45
Regular waves	**Specified**		**Measured**	
	H [m]	**T [s]**	**H [m]**	**T [s]**
Regular wave 1	1,50	4,83	N/A	N/A
Regular wave 2	2,50	8,98	N/A	N/A
Regular wave 3	3,50	10,47	N/A	N/A

Table 11.3, Planned sea states for the model test

11.5 Base Case Standard

In order to have a efficient way to compare the different results, a base case standard was defined for the buoy with both high and low VCG. The base case standard will be used as a basis when discussing the results. The base case standard for high and low VCG is illustrated in figure 11.2.

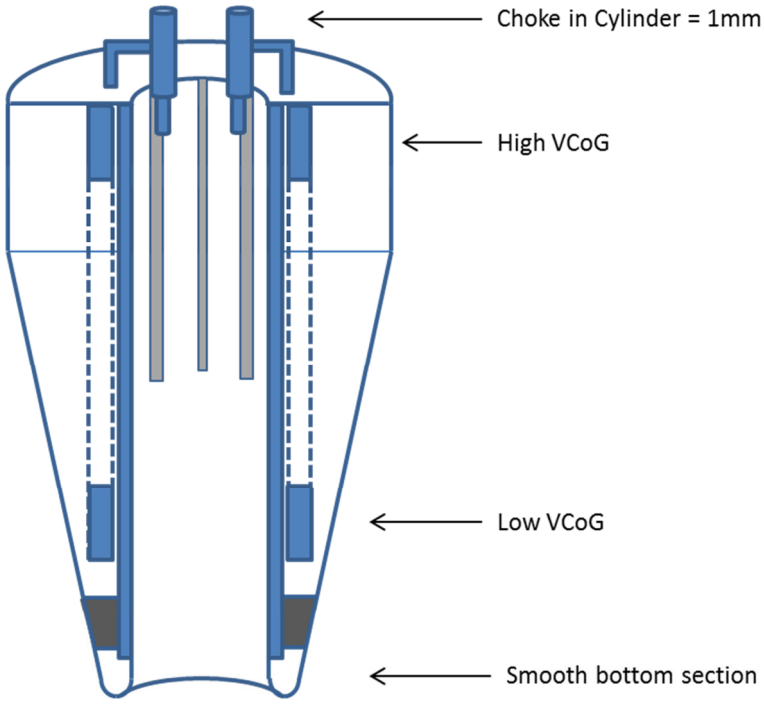

Figure 11.2, Sketch of the base case standard for the Dynocean Buoy

A table summarizing the base case standard is presented below:

Property	Full-scale	Unit
Bottom section	rounded	[-]
Damping of cylinders[5]	210	[kN/(m/s)]
Significant wave height	2.5	[m]
Spectral peak period	9.0	[s]

Table 11.4, Properties for the base case standard model

[5] The damping of 210 kN(m/s) is estimated. This represents the a 1 mm bore in the end plug of each cylinder.

12. Uncertainty Analysis

There is uncertainty in all measurements from a model test. This model test is primarily used to calculate the power output from different sea-states and to validate numerical results. It is essential that the uncertainty is considered when analyzing the results from the model test.

This chapter is based on the information and methods described in Steen (2010). For this model test a formal uncertainty analysis has not been performed. This chapter focuses mainly on indicating the uncertainty factors involved in the model test.

The definition of error is the difference between the measured value and the true value:

|Error| = |measured value – true value|

Accurate error is very hard to calculate since the true value is not known. Therefore an estimation of the error calculated based on statistics, called uncertainty, are performed for model tests. Error estimations are usually divided into two main categories: Bias and precision errors.

The steps in an uncertainty analyze is given as follows:

- Identify all error sources
- Determine the individual precision and bias errors for each error source
- Determine the sensitivity of the end result to error sources
- Create the total precision interval
- Create the total bias uncertainty
- Combine the total bias and precision

12.1 Precision Errors

Precision errors are “scatter” or variations in the result and can be found by comparing the results of repeated measurements. Precision error is calculated based on an assumption of Gaussian distribution.

When calculating the precision error one should ideally repeat the measurement up to ten times. An important factor when calculating the precision error is the *replication level*. The replication level is defined as how large part of the experimental set-up that is re-made as part of the repetition.

The setup of the model test took more time than expected and there were little time to run repeated measurements. For this reason, estimation for precision error is not obtained for any cases.

12.2 Bias Uncertainty

Bias errors are systematic errors that cannot be revealed by repetition of the experiment. Bias errors cannot be measured, only estimated. Bias uncertainties that are of interest for this case are:

- Calibration factors of the sensors and measurement equipment
- Geometric accuracy of the model
- Tank wall effects

- Scale effects
- Instrumentation and measuring errors

Bias errors will not affect the comparison results when varying input parameters because these are equal for all the input parameters. For values that require accuracy, i.e. max and min values and power output, bias errors will affect the results.

12.2.1 Calibration

Before mounting force transducers to the model they must be calibrated. This also applies for the wave probes. Table 12.1 below shows the deviation between pre- and post-calibration of the force transducers and wave probes used in the model test. The position of each wave probe is given in section 7.5.

Syl_kraft1_8686, Syl_kraft2_8687 and Syl_kraft3_8688 are the force transducer placed directly beneath each cylinder. These measured the force exerted on each cylinder from the disc.

The force transducers Snorkraft_1_8141, Snorkraft_2_8135 and Snorkraft_3_8142 were each connected to a spring with known spring stiffness. These transducers were used to calculate relative positions of each cylinder as well as relative heave and pitch between the outer buoy and inner disc explained in section 7.5.

Transducer	Sensitivity	Pre calibration	Post calibration	Unit	Deviation
Wave probe 1	1 [mV/V]	0,08840	0,09206	[m/V]	4,14 %
Wave probe 2	1 [mV/V]	0,08730	0,09581	[m/V]	9,75 %
Wave probe 3	1 [mV/V]	0,08820	0,09785	[m/V]	10,94 %
Wave probe 4	1 [mV/V]	0,12900	0,13267	[m/V]	2,84 %
Syl_kraft1_8686	1 [mV/V]	345,40	345,11	[N/V]	0,08 %
Syl_kraft2_8687	1 [mV/V]	341,00	342,13	[N/V]	0,33 %
Syl_kraft3_8688	1 [mV/V]	338,30	338,76	[N/V]	0,14 %
Snorkraft_1_8141	2 [mV/V]	-81,52	N/A	[N/V]	N/A
Snorkraft_2_8135	2 [mV/V]	-75,56	N/A	[N/V]	N/A
Snorkraft_3_8142	2 [mV/V]	-57,90	N/A	[N/V]	N/A

Table 12.1, Result from calibration of the force gauges and wave probes

From table 12.1 negligible difference between pre- and post-calibrations for the force measurements of the cylinders is documented.

Large deviations for the pre- and post-calibration of the wave probes were observed. During the week in the towing tank, there were some minor oil spills from the hydraulic walkway bridges in the test facility. The oil film in the water can interfere when measuring the wave height. A typical sign is when they measure fewer peaks above MWL. The wave probes were properly cleaned after the oil-spills to avoid this. This could be the reason for why the post calibration for the wave probes are 4-11 % higher than for the pre-calibration and result in higher measured wave heights than it actually was.

This does not affect the results from the model test because the wave probes were primarily used under the calibration of the waves in the beginning of the model test.

The relative vertical displacement of each cylinder was calculated with the use of a spring and force transducer as explained in section 7.5.2. The stiffness of all the three springs used in the model test was performed and can be found in appendix 5. The calculated stiffness for the different springs is used when post-processing the results.

The spring stiffness was calculated by displacing the spring a known distance. A force transducer measured the force for in the spring for each displacement. Each point was then plotted and a trend line was applied to check for linearity.

As a reliability test one of the springs the stiffness was calculated three times. The largest deviation found for the estimated spring stiffness was found to be 4 %.

12.2.2 Geometrical Accuracy

The Dynocean Buoy was milled from divinycell at Marintek`s facilities. The staff at Marintek estimated the accuracy of the mill to be of an order of 1mm. Examination of the moonpool showed that there were more deviations than 1mm. The acrylic cylinder placed inside of the moonpool was skewed in a way that the cross section had an elliptic form. This was a small deviation is not taken into consideration when analyzing the results.

12.2.3 Tank Wall Effects

The model will generate waves in all directions when oscillating. The waves generated from the model will eventually reach the wall and wave maker and be reflected back to the model. A system of transverse waves will be generated and affect the response of the structure. The effect of this is especially pronounced when testing stationary structures like the Dynocean Buoy. The diameter of the Dynocean Buoy compared to tank width is around 1:12 which is the ratio Marintek recommends to avoid tank wall effects. In addition, the Dynocean Buoy has a circular cross-section, therefore; not much of the radiated waves are reflected straight back to the buoy.

When calculating the total power output of the system different input parameters were used as explained in chapter 11. Tank wall effects will not influence the results when comparing the different input parameters to each other since they are equal for all the test runs.

12.2.4 Scale Effects

The ratio between full scale and model scale is 28.7 which is considered as a decent scale ratio for this type of model test (Cruz 2010).

Scale effects are important in cases where viscous forces give significance force contribution. Viscous force contributions consist of skin friction forces and pressure drag forces. The roughness of the hull is important for the frictional drag forces. For pressure drag the shape of the hull is of importance. By applying a rounded bottom section instead of an edged bottom section, the pressure drag term is expected to drop significantly.

The Dynocean Buoy is a large volume structure in the environment of the operating area. Drag forces will be present and have influence the results. For wave frequency motions the buoy will experience forces that are mainly dominated by mass and not by drag forces.

12.2.5 Instrumentation and Measuring Errors

Bias error in the measured value from force transducers is estimated to be around 1-1.5 %.

The accuracy of the motions measured by the optical system is estimated to be in the order of 1 mm for positions in model scale and 0.05 degrees for all rotations.

The bias error of the wave probes is estimated to approximately 1 mm.

All error estimates of the instrumentation are provided by Sandmark (2011).

12.3 Uncertainty Discussion

Different uncertainty aspects have been pointed out. The precision error has not been obtained, and a quantitative uncertainty analysis has for this reason not been performed.

It is important to keep in mind that the model test results as well as all the post-processing of the results involve uncertainty. For calculations of relative motions two main uncertainty factors are involved:

- Springs stiffness measurement
- Non-linear spring stiffness for large deflections
- Calibration of the force transducers

High frequency force fluctuations in the springs were filtered out by a low-pass filter when post-processing the results.

13. Wave Calibration

The input needed to make an irregular sea is the specter type together with the parameters specifying this specter. The equation defining an irregular sea is given below:

$$\eta = \sum^{\infty} a_n \cos(\omega_n t + \varepsilon_n) \tag{13.1}$$

The correct spectrum and a realization are drawn. The set of random phases, ε_n, is called the wave seed. Different seeds can be used to obtain different realizations of a wave spectrum. Time series from realizations with the same spectrum and seed should be identical.

The wave maker machinery is a complex system. The digital information has to become analog, and the wave flap has to start making waves. The wave maker is hydraulic driven and the movements will depend on oil pressure and other factors.

By measuring the irregular waves Hs, Tp and γ -value and the spectrum shape is calculated. The γ -value is a measure of the peakedness. These parameters define the sea state. When the object is to use the actual wave time series in a numerical analysis afterwards the recording of the waves are especially important.

In practice the process goes like this:

1. The model test operator gives the wave spectrum and a seed to the wave maker via software
2. The wave elevation time series is recorded and analyzed.
3. If the measured spectrum is close enough to the specified spectrum the wave calibration is accepted. This is checked with a plot of the spectrum shape including the key parameters; Hs and Tp.
4. If the measured spectrum is too far off the specified spectrum adjustments have to be made.
5. The operator adjusts the wave maker input (by experience or software) and runs the sea state once again. If the new spectrum is close enough the sea state it is ready for use. The threshold for being satisfied with the run is dependent on the customer and the application of the subsequent model test.

Theory for this chapter is collected from Pettersen (2007). In order to calculate the Hs for each irregular wave the spectral 0^{th} moments must be calculated.

$$m_n = \int_0^{\infty} \omega^n S(\omega) d\omega \tag{13.2}$$

Where ω is the circular frequency and $S(\omega)$ is the wave spectrum. m_n is the spectral n^{th} moments, the 0^{th} moment can be found by setting $n = 0$.

The Hs can now be found by the following formula:

$$H_s = H_{m_0} = 4\sqrt{m_0} \tag{13.3}$$

The spectral peak period, Tp, is defined as the period where the power spectrum has its maximum.

This procedure has been used when calculating the Tp and Hs for the different irregular waves in the MATLAB script “Calibration_irr.m”.

The specified and measured Hs and Tp for each irregular wave run are given in appendix 5. This is found by Fourier transforming the full time series to the frequency domain by the PWELCH function in MATLAB. This function calculates a PSD (Power Spectral Density) estimate via Welch's method. This is a method based on FFT (Fast Fourier Transform), but the Welch method is an improvement in that way that it reduces noise in the estimated power spectra (Welch 1967).

Appendix	Run	Specified			Measured		Result
		Hs[m]	Tp[s]	Gamma	Hs[m]	Tp[s]	
5.1	8100	1.5	6.5	1	1.38	6.17	Accepted
5.2	8110	2.5	9.0	1	2.20	8.98	Accepted
5.3[6]	8115	2.5	9.0	1	2.14	8.98	Accepted
5.4	8120	3.5	11.5	1	3.02	12.32	Not Accepted
5.5	8121	3.5	11.5	1	3.60	12.28	Accepted
5.6	8130	4.5	14.0	1	4.00	14.10	Not Accepted
5.7	8131	4.5	14.0	1	4.69	14.10	Accepted
5.8	8140	8.0	11.0	3.3	6.59	10.64	Not Accepted
5.9	8142	8.0	11.0	3.3	7.71	10.90	Accepted
5.10	8150	10.5	13.0	3.3	9.02	13.15	Not Accepted
5.11	8151	10.5	13.0	3.3	10.59	12.45	Accepted

Table 13.1, Results from the wave calibration of irregular waves

The specified irregular waves are estimated from the basis of scatter diagrams from the operating area. It is not important that the irregular waves are exactly the same as the specification. The only important point is that the wave measurements are logged.

[6] The buoy was moved to a new position after the mooring setup. Therefore a re-run of wave 8110 with the wave probe at the new buoy location was performed.

14. Decay Tests

The body is excited in one isolated degree of freedom to a reasonable amplitude. The amplitude should not be too large to keep the problem linear. All decay tests are excited by hand.

In some DOFs it is best to give the body a deflection from the equilibrium position (surge, sway) and then let it go. In other DOFs i.e. heave, pitch the structure should be oscillated at resonance for a few periods before the motion is left to decay. It was difficult to isolate the desired degree of freedom. For some decay tests this affected the results.

The purpose of the decay tests is to find the natural period and damping. With a known stiffness the added mass can be calculated.

A total of 31 decay tests were performed. Time series and results is provided in appendix 7.

14.1 Theory

The theory in this chapter is collected from Steen (2010). The theory is implemented in MATLAB scripts to make the analyzing effective.

Natural periods and Added mass

The natural period has been found by the same method as described in chapter 13. From the power spectrum the top peak defines the Eigen frequencies ω_n.

For calculations of added mass the formulas in chapter 9 have been used. The result is given in the same chapter.

Damping

A one-degree of freedom system is assumed when determining the dampening of the oscillating buoy and disc when they are not connected. The differential equation describing the motion is:

$$M\ddot{x} + B_1\dot{x} + B_2\dot{x}|\dot{x}| + Cx = 0 \tag{14.1}$$

Where M is the total mass (body mass and added mass), B_1 is the linear damping, B_2 is the quadratic damping term and C is the restoring stiffness.

This equation can be divided by M to get the following equation:

$$\ddot{x} + p_1\dot{x} + p_2\dot{x}|\dot{x}| + p_3x = 0 \tag{14.2}$$

To determine the linear- and non-linear damping the method of equivalent linearization is used. By this method the non-linear damping term is replaced with a linear term. This method is based on the requirement of equal damping energy per cycle for the equivalent linear term (Steen 2010). This is satisfied using:

$$p_{EQ} = p_1 + \frac{8}{3\pi}\omega x_0 p_2 \tag{14.3}$$

Where x_0 and ω is the motion amplitude and oscillation frequency respectively. The linearized equation of motion can be given by:

$$\ddot{x} + p_{EQ}\dot{x} + p_3 x = 0 \tag{14.4}$$

p_{EQ} is called the equivalent damping and can be obtained for each cycle by the following formula:

$$p_{EQ} = -2\omega \frac{\delta}{\sqrt{\pi^2 + \delta^2}} \tag{14.5}$$

Where the logarithmic decrement, δ , is given by:

$$\delta = \ln\left(\frac{x_i}{x_{i-1}}\right) \tag{14.6}$$

Where x_i and x_{i-1} are two succeeding amplitudes.

The results for p_{EQ} for each period can be plotted versus the equivalent velocity, $\frac{8\omega x_i}{3\pi}$. A trend-line can be fitted to the p_{EQ} points on the plot by linear regression. The linear damping coefficient is found where the trend line intersect with the y-axis, p_1 . The linearized quadratic coefficient is now identified as the slope of the fitted trend line, p_2 .

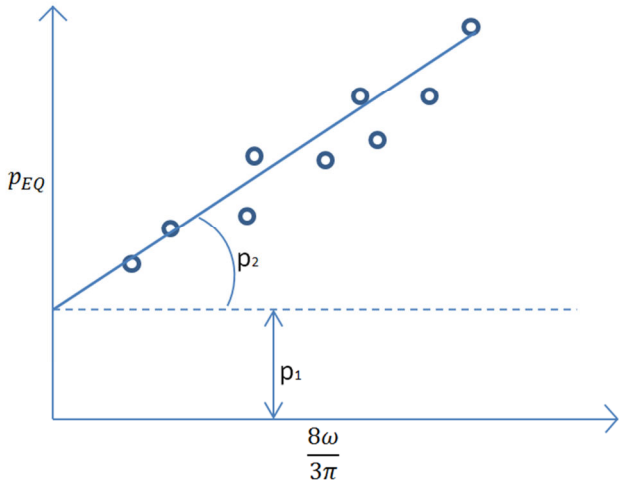

Figure 14.1, Illustration of damping from a decay test

Correlation

When studying the damping properties with linear regression it is important to consider the correlation between the variables. The correlation tells if there is a pattern in the data points being investigated. Figure 14.2 a shows an example of uncorrelated x and y values while Figure 14.2 b shows an example of a correlated x and y values. By expressing the relationship between x and y in the form of a straight line, the square of the deviation of the actual values of y and their predicted straight line approximation is minimized. The formula for calculating the straight line is given as (Newland 1993):

$$\frac{y-m_y}{\sigma_y}=\left\{\frac{E[(x-m_x)(y-m_y)]}{\sigma_x\sigma_y}\right\}\frac{x-m_x}{\sigma_x} \tag{14.7}$$

Where σ_y and σ_x is the standard deviation of the random variable x and y. m_y and m_x is the mean values of x and y respectively.

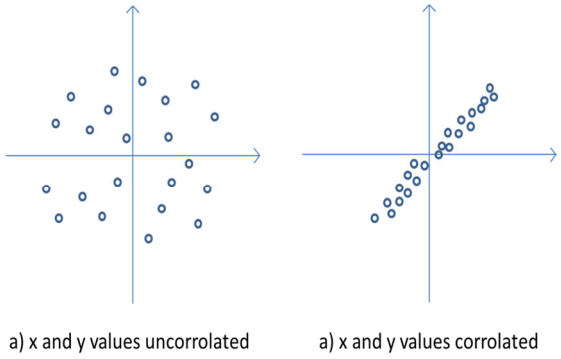

Figure 14.2, Illustration of correlation between two variables, based on Newland (1993)

Once the straight line is fitted to the data sample of interest, the correlation coefficient or normalized covariance should be examined. This is calculated by following formula (Newland 1993)

$$\rho_{xy}=\frac{E[(x-m_x)(y-m_y)]}{\sigma_x\sigma_y} \tag{14.8}$$

Here ρ_{xy} is the correlation coefficient. Figure 14.3 provides examples of different correlation coefficients. With a ρ_{xy} = +/- 1 it is perfect correlation. With ρ_{xy} = 0 there is no correlation what so ever. This implies that a line of regression is not representative for the sample. For each decay test the correlation coefficient is calculated to see how well the linear line fits to the data.

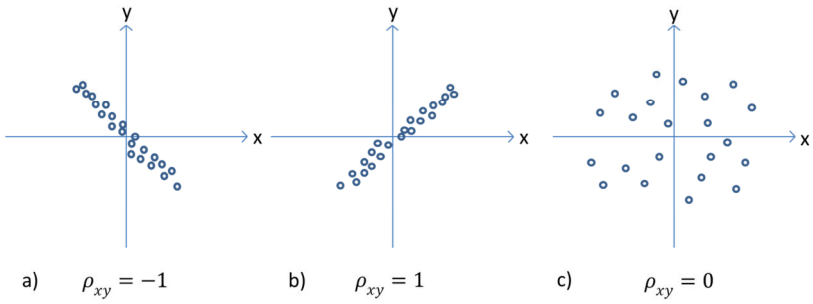

Figure 14.3, Regression lines for different correlation coefficients, based on Newland (1993)

14.2 Results and Discussion

Full analyses of the decay tests can be found in appendix 7. Only important discoveries from the decay tests are presented in this section.

14.2.1 Correlation

The correlation coefficients of the damping coefficients varied significantly for the different decay tests. For some of the decay tests these were very good, but for other some it was not as good. For many of the tests the correlation very good, but in some cases it was bad. Examples of this is illustrated in figure 14.4 and 14.5.

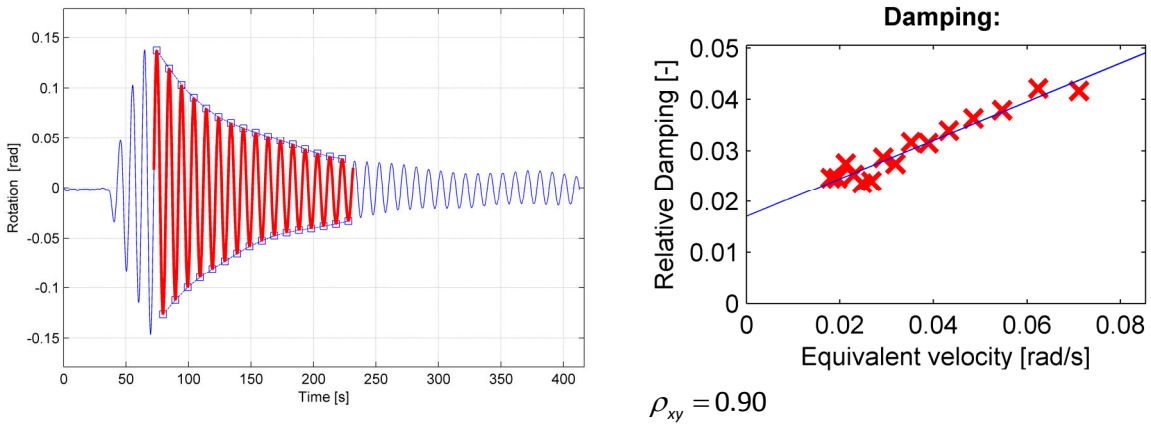

Figure 14.4, Pitch buoy decay test with good correlation – Appendix 7.24

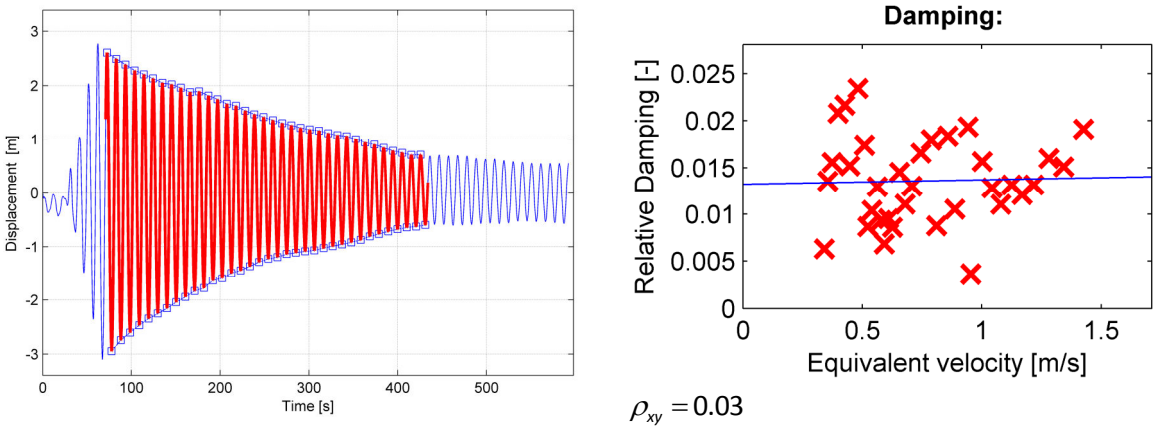

Figure 14.5, Heave disc decay test with bad correlation – Appendix 7.19

For decay test 1020 the correlation coefficient for relative damping in heave motion is low. This implies that the regression line is not representative for the data. The large deviations in the relative damping are probably due to inaccurate measurements.

14.2.2 Disc Motion inside Stationary Buoy

The ballast weights were removed from the buoy. Beams were used between the walkways in order to push the outer buoy down to MWL. This gave a completely stationary buoy.

The three cylinders were removed, but the equipment for measuring the relative distance between disk and buoy were still intact. The disc was oscillated in pitch and heave motion to determine the natural period and damping of the disc.

This test was performed primarily to investigate the effect of the rounded section compared to the edged bottom section.

Detailed information from the decay test for rounded and edged bottom section can be found in appendix 7.19 and 7.21 respectively.

Bottom section	Linear damping term	Quadratic damping term	Correlation coefficient
Rounded	0.013	0.000	0.031
Edged	0.018	0.025	0.033

The damping of an edged bottom section is clearly larger than for the rounded bottom section. With a rounded bottom section the damping of the disc motion is almost entirely governed by the linear term. With the edged bottom section the damping consists of both a linear term and a quadratic term which is significant.

14.2.3 Pitch with Different VCG

In this test configuration only the buoy motions are measured. The disc and all its coupling components are removed and the buoy floats freely. The variation of damping in pitch in the two different ballast conditions is compared.

For this analysis the edged bottom section has been used because these tests proved to have a better correlation coefficient. Full description of these test are found in appendix 7.23 for the high VCG case and in 7.24 for the low VCG case.

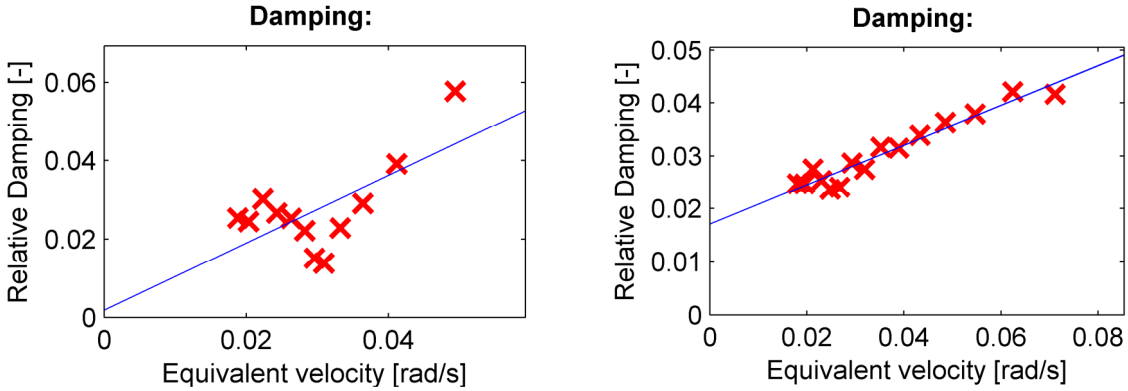

Figure 14.6, Left: Damping with high VCG, Right: Damping with low VCG

Firstly, the correlation coefficient for low VCG is 0.966 which is very good. The linear line is a good fit for this sample. However for high VCG condition, the correlation coefficient is only 0.666 and for this reason it is difficult to have a clear conclusion. The quadratic damping term with high VCG is over two times larger than with low VCG. Even with a low correlation coefficient, this still implies that a larger portion of the damping is proportional to the velocity squared for the case with high VCG.

The linear damping term is over eight times larger with low VCG than with high VCG. The natural period is measured to 16.7 s with high VCG and 9.9 s with low VCG. Because of this the pitch motion is slower with high VCG than with low VCG as illustrated in Figure 14.7.

From the figure below it can be seen that the pitch damping for low VCG is significantly larger than for high VCG

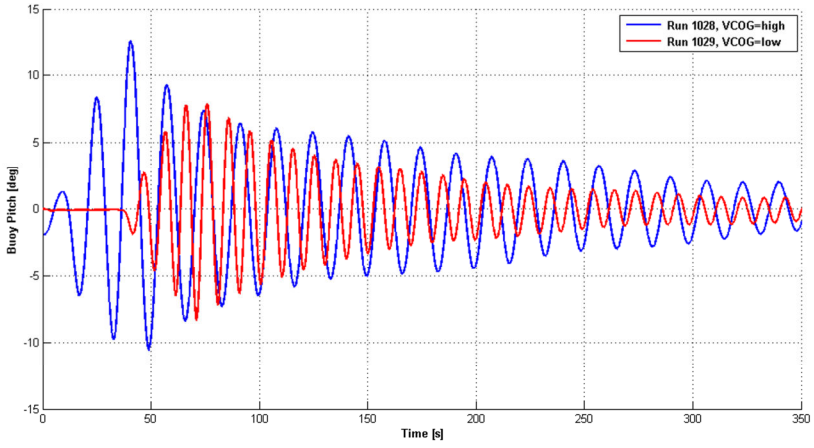

Figure 14.7, pitch decay test for high and low VCG

14.2.4 Hydrodynamic Coupling

Hydrodynamic coupling are clearly present in some DOF. This is illustrated in the time series for pitch decay test 9925 (appendix 7.27) which is given in. Here the pitch motion oscillates in the natural period of the pitch motion around 16 seconds. From a spectral analysis it can be shown that there is a small peak in the response spectrum at around 0.0101 Hz (the surge natural period is 99 s) which explains the slowly varying oscillation in the figure.

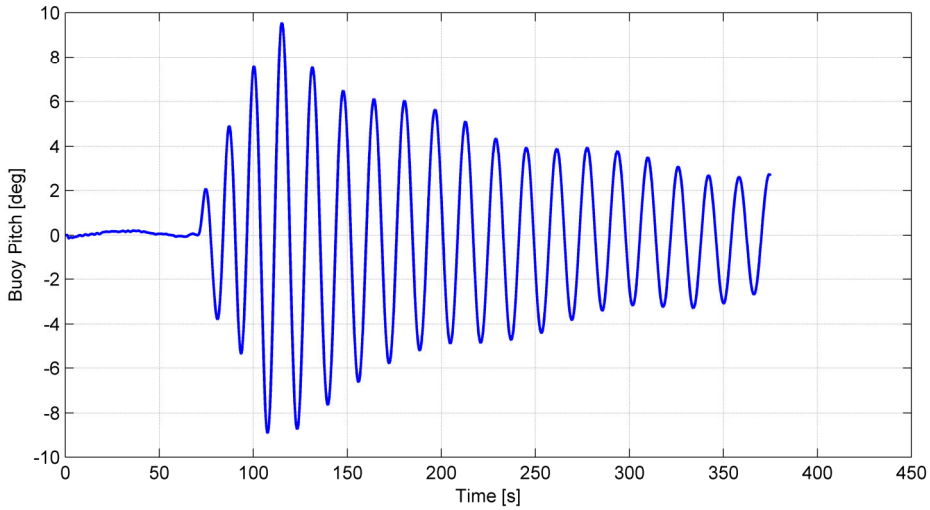

Figure 14.8, Decay test 9925: Pitch motion

Figure 14-9 shows the same decay test in addition to surge motion of the buoy. A spectral analysis revels that the high frequency motion of both surge and pitch lies around a period of 16 s and the low frequency motion lies in a frequency of 0.0101 Hz. The low frequency oscillations of both motions are in phase. The frequency of 0.0101 Hz corresponds to the natural frequency of surge from the mooring system.

It is clear that pitch and surge is a coupled motion and an isolated damping for pitch cannot be obtained.

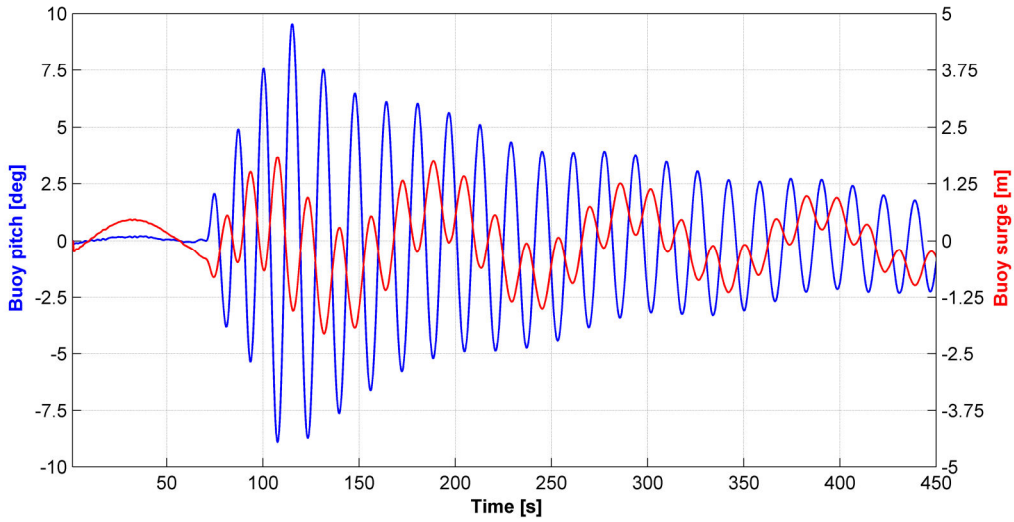

Figure 14.9, Decay test 9925: Pitch and surge motion

14.2.5 Damping of cylinders

Decay tests were also performed when buoy and disc were in connected by the cylinders. The chokes were varied from 1.0 mm till 1.5 mm. These tests were performed for both pitch and heave. These tests are performed with edged bottom section and with low VCG.

Heave decay tests for the two different chokes are given in Figure 14.10. The buoy is oscillated in heave motion by hand and released after approximate 60 seconds (green line). There are too few points to get quantitative data for the damping. From the figure it can be shown that there are two oscillations with a choke of 1.0 mm while four for 1.5 mm before the motion is damped out. The effect of applying a choke of 1.5 mm compared to 1.0 mm is very pronounced for this case. (Note, the plot below shows the global heave motion of the buoy).

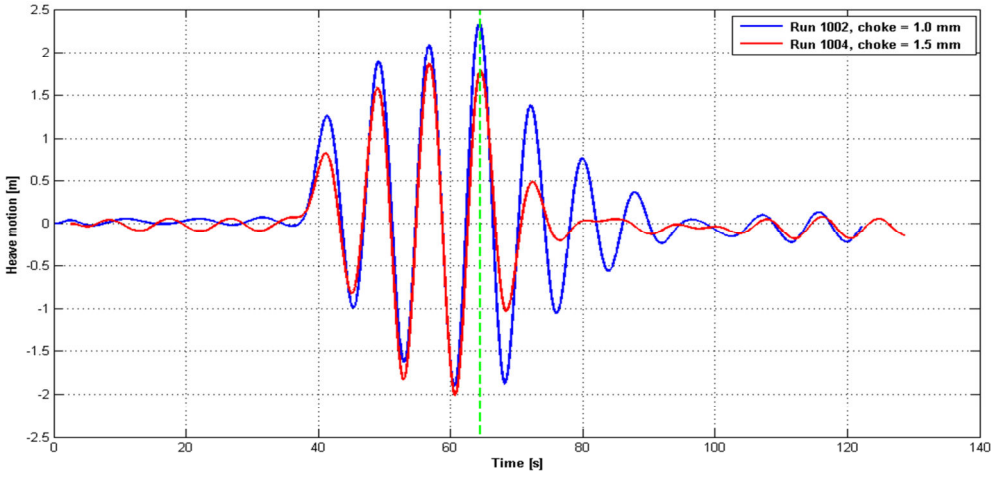

Figure 14.10, Heave decay tests with disc in coupling. Different chokes are used.

One should expect more damping in pitch motion with 1.5 mm choke than with 1.0 mm. Pitch motion is rather unaffected by change in damping levels. This is a interesting observation.

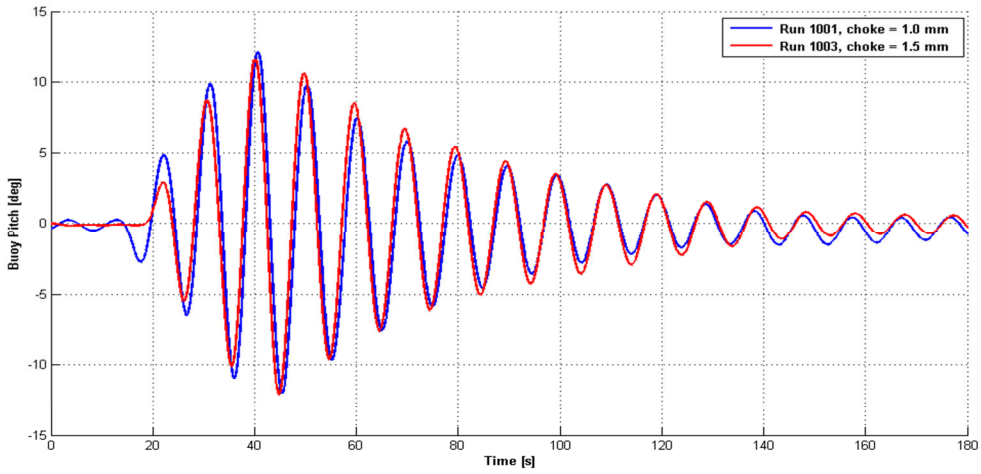

Figure 14.11, Buoy pitch decay test: Disc in couplings. Different chokes are used.

15. Irregular Wave Tests

A total of 17 irregular tests were performed. There are two main reasons for these tests. The main purpose of these test are to examine how much energy that can be extracted by the system in realistic sea states. Secondly, it is of importance to study the effect of the different input parameters mentioned in chapter 11.

15.1 Filtering

Before results can be examined the time series must be filtered to avoid high frequency noise from the force transducers applied to calculate force and relative motions. The time-series of all the measurements of interest were transformed to the frequency domain from the time-domain by FFT (Fast Fourier Transform).

In the frequency domain unwanted high frequency noise can be removed by a low-pass filter. This removes all the frequency components above a given cut-off frequency. After the high frequency noise is removed the signal can be transformed back to time-domain by inverse FFT.

It is an aim to filter as little as possible in order to avoid loss of information. At the same time, noise in the measurements needs to be removed.

The two plots below shows the effect of filtering with different cut-off frequencies. By applying a too low cut-off frequency (blue line, 0.2 Hz) the time-series gets to smoothed and do not represent the actual time-series. By applying a too high low-pass filter (red line, 1.2 Hz) the time-series gets too little rounded.

Peak period used for the irregular tests varies from 6.5 s to 14.0 s (0.071 Hz to 0.154 Hz). The motions of interest are linear wave-induced motions; a cut-off frequency of 0.5 Hz (3.14 rad/s, green line) has therefore been used when filtering all measurements used to estimate power (force in cylinder 1-3, position of cylinder 1-3, relative heave and relative pitch).

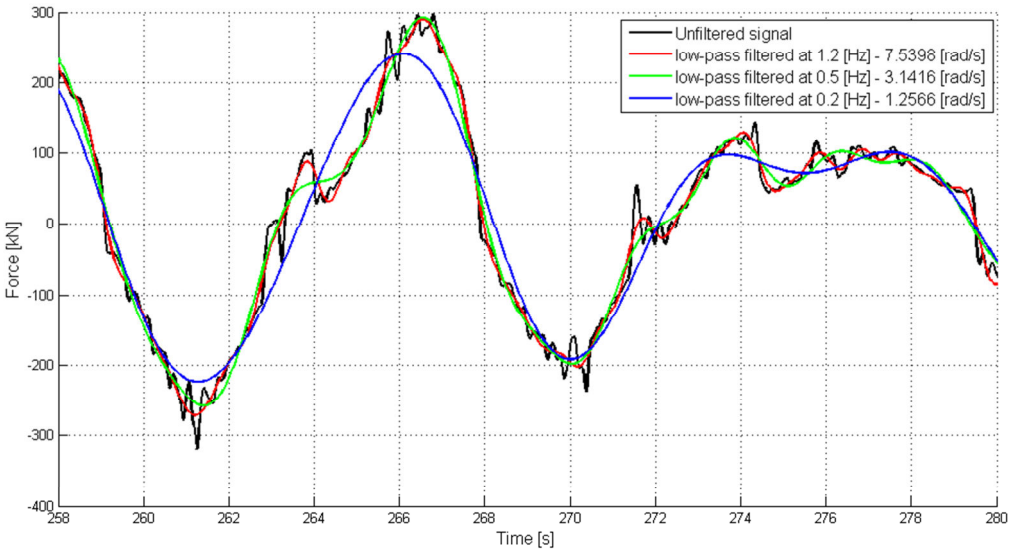

Figure 15.1, Effects of different cut-off frequencies for force from 'freq_analyze.m' (Run 6001)

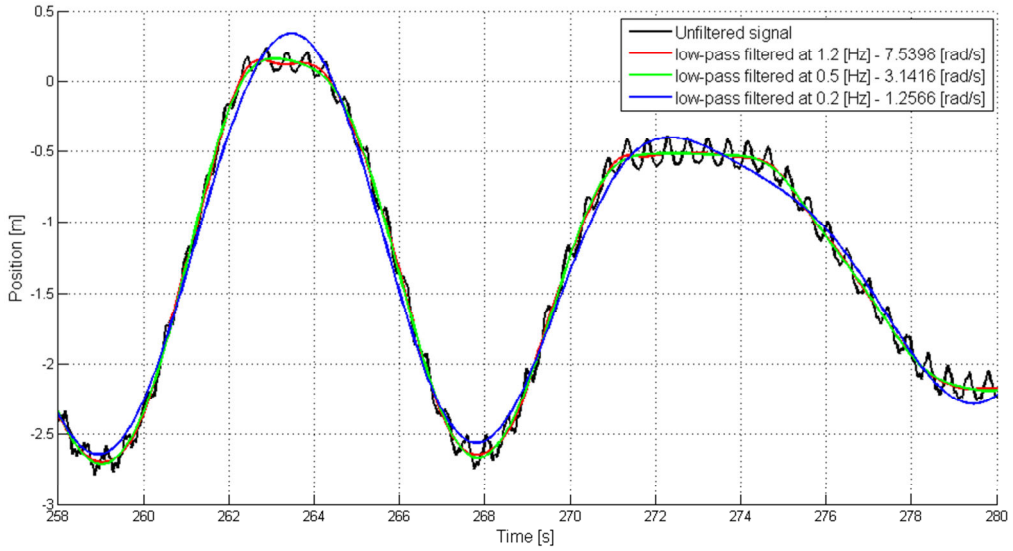

Figure 15.2, Effects of varying the cut-off frequency for position from 'freq_analyze.m' (Run 6001)

15.2 Power Calculations

The power of the system can be calculated by the simple formula (Tipler 2004):

$$P(t) = \vec{F}(t) \cdot \vec{v}(t)$$

Where $\vec{F}(t)$ and $\vec{v}(t)$ is the time dependent force and relative velocity respectively. In this case $\vec{v}(t)$ is the velocity of the piston rod in the power extraction unit.

In order to calculate the total energy output of a system the power must be integrated over the time the measurements are performed. The method for calculating the power of the system is described below.

A MATLAB script named "Irreg_Analyze.m" has been written in order to calculate the power and statistical values for each irregular run. The relative position and force measured for each run is calculated and the mean is subtracted for all position and force measurements.

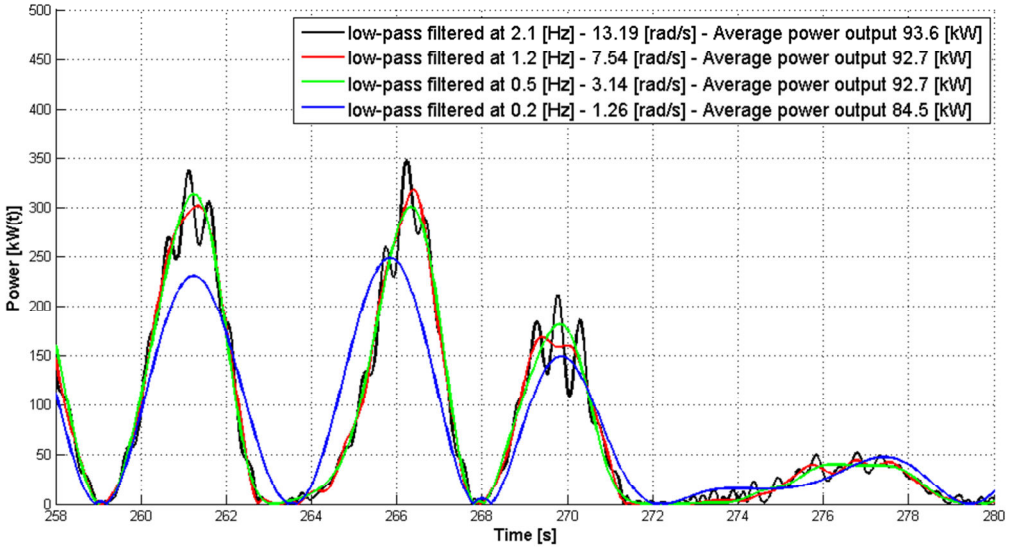

Figure 15.3, Effect of filtering the power output from cylinder 1 (Run 6001)

"filter.m" is used to filter out high frequency noise from the measurements. By applying a cut off frequency of 0.2 Hz the power is reduced too much, as illustrated in figure 15-3. By using a low-pass filter of 0.5 Hz the unwanted high frequency noise is removed and all the relevant information is still retained.

The velocity of all the cylinders is calculated by differentiating the position. The power for each cylinder is then calculated as a function of time. The total energy output for each cylinder is calculated by integrating the power of each cylinder with respect to time by the trapezoidal method (Edwards and Penney 2002). The power produced in each cylinder is added together to get the total energy output of the system during the time interval. Average power is then computed by dividing the total energy output on the total time of the each run.

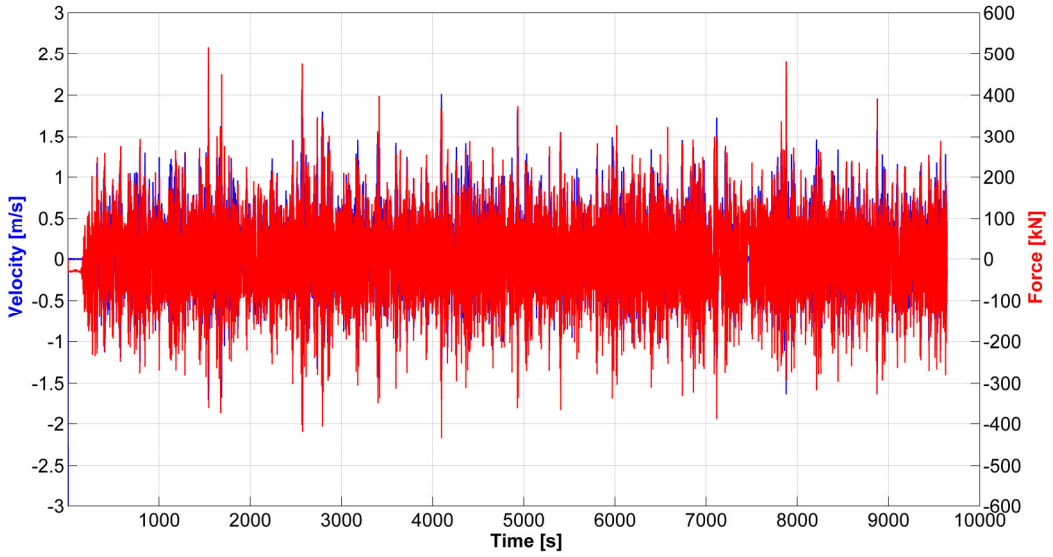

Figure 15.4, Full time-series of the relative velocity and force in cylinder 1 (Run 6110)

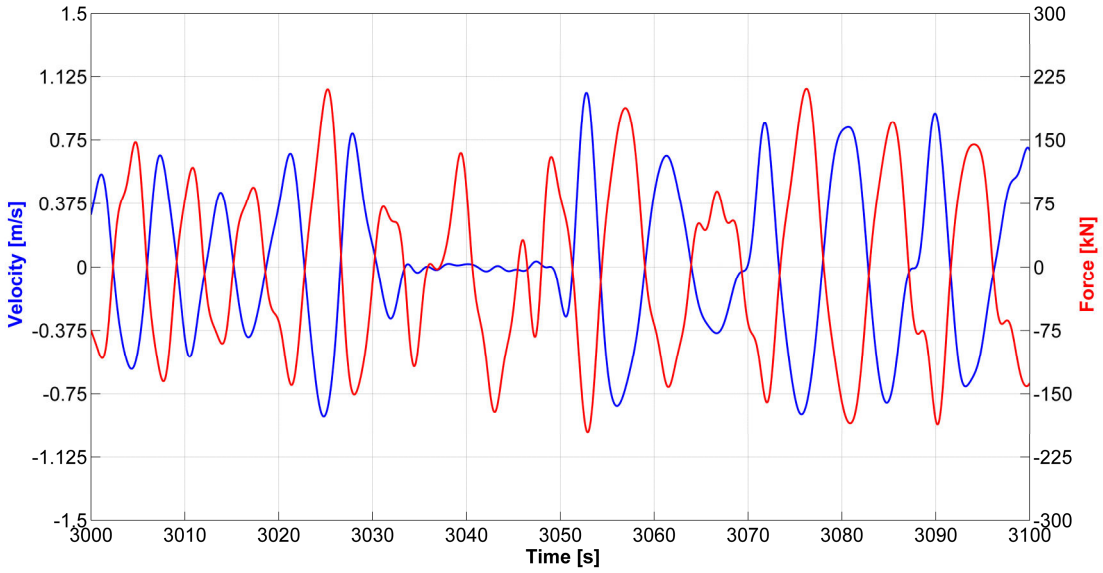

Figure 15.5, Illustration of the friction in cylinder 1 (Run 6110)

In Figure 15.4 the full time-series of run 6110 is plotted. In Figure 15.4 the velocity is approximately zero from time = 3035 s to 3050 seconds, this is a clear evidence of the static friction in the cylinders.

Before power calculations were performed the transient part of each regular run was removed. Approximately the first 500 s was removed when performing the power analysis. The transient part in run 6110 is shown in Figure 15.6 below. The cylinder is exposed to force induced by the waves at around 150 s, however there is small/negligible relative velocity for approximately the 300 first seconds. This is due static friction in the cylinders. The two bodies (buoy and disc) move together as one body. This is clearly illustrated by the global heave motion in the figure below by the pink plot. At 300 s the static friction is exceeded by the force from the waves and relative motion initiates.

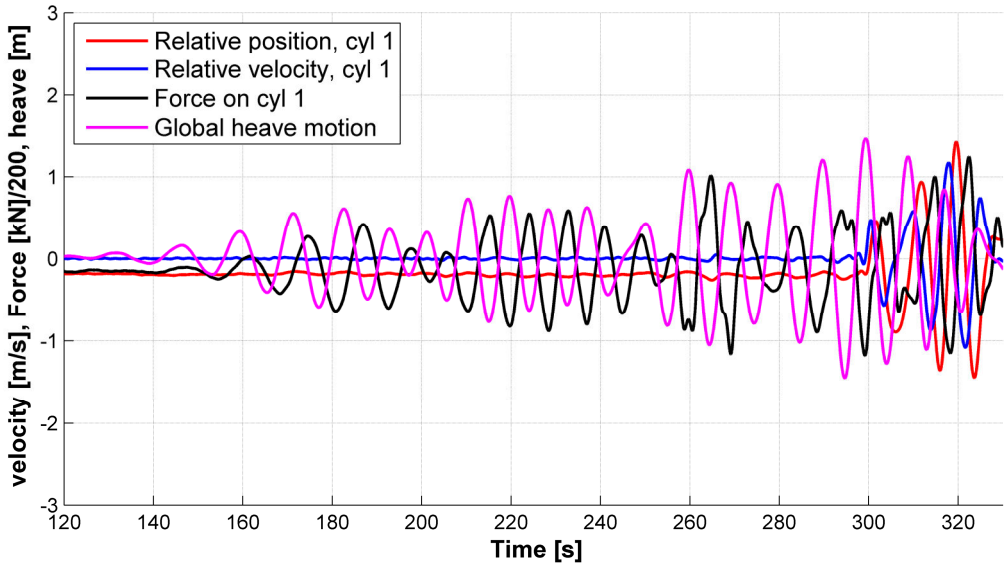

Figure 15.6, Transient part of time series (Run 6110)

15.3 Results

The power output was calculated for all irregular runs. A comparison study with the different input parameters will be compared to the base case standard. The base case sea state (Tp=9s, Hs = 2.5m) was used for this study.

15.3.1 Power output

Run Number	Hs	Tp	Choke	VCG	Bottom section	Model test results
[-]	[m]	[s]	[mm]	[-]	[-]	[kW]
3000	2,5	9	1	High	Edged	126
5520	2,5	9	1	Low	Edged	162
6001	***2,5***	***9***	***1***	***Low***	***rounded***	***180***
6010	4,5	14	1	Low	rounded	350
6020	1,5	6,5	1	Low	rounded	16
6030	3,5	11,5	1	Low	rounded	358
6040	1,5	6,5	1,5	Low	rounded	16
6052	2,5	9	1,5	Low	rounded	159
6100	2,5	9	1,5	High	rounded	127
6110	***2,5***	***9***	***1***	***High***	***rounded***	***133***
6120	4,5	14	1	High	rounded	291
6130	4,5	14	1,5	High	rounded	278
6140	3,5	11,5	1	High	rounded	286
6161	3,5	11,5	1,5	High	rounded	271
6170	4,5	14	1,5	High	rounded	275
6181	2,5	9	1,2	High	rounded	131
6190	1,5	6,5	1	High	rounded	7

Table 15.1, Power calculations from the model test

Table 15.1 presents the calculated power output from the different irregular runs. Run 6001 and 6110 are used as the base case standards for low and high ballast position respectively.

The power estimates for the device in a sea-states characterized by small Hs and Tp like run 6020, 6040 and 6190 is very small. By visual observations both global- and relative motions were very small. Figure 15.7 below shows the whole time-series for run 6190. The force measured on cylinder 1 is significant throughout the run. However the Tp and Hs are too small to excite any motions except for a couple of times indicated by the blue line. Even with large force on a cylinder, the power of the system is small when there is no relative velocity between the buoy and disc. This explains the low power calculated for these sea-states. However, for the larger sea states with Hs=2.5 m and up, the power output calculated show very promising results.

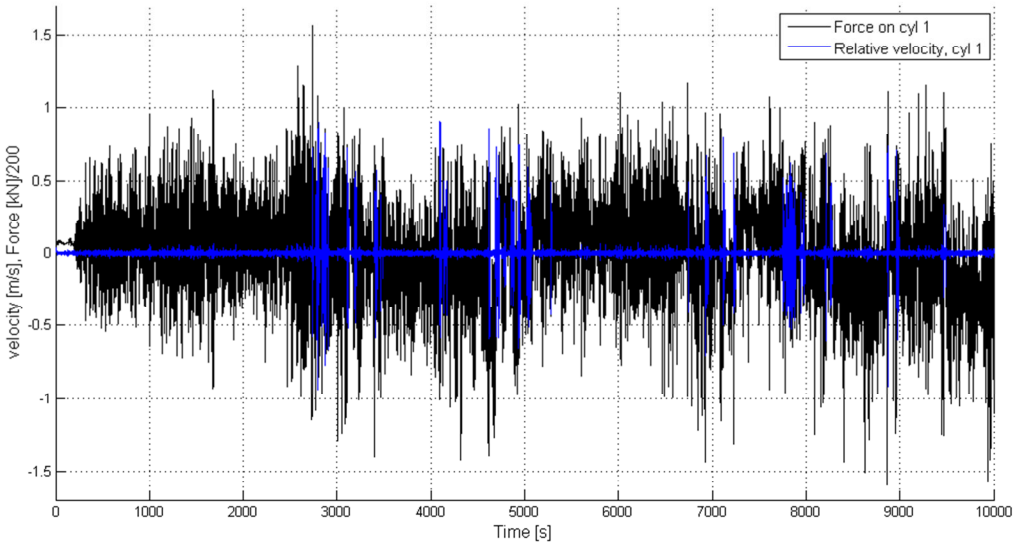

Figure 15.7, Relative position, velocity and force for Hs=1.5, Tp=6.5

15.3.2 Damping of the cylinders

The characteristics of the dampers were determined from the irregular wave tests. The relation between force and velocity were plotted and a line was fitted. Only points with a velocity between 0.1 and 1.0 m/s were used in the line fit to avoid introduction of error from static friction or nonlinear effect at high velocities. Upward velocity is positive. Separate lines for the positive and negative values were drawn. The discontinuity at zero velocity can be explained by dynamic friction – Force acting opposite of the direction of motion for all velocities. The dynamic friction was in the order of 10kN for all cases analyzed.

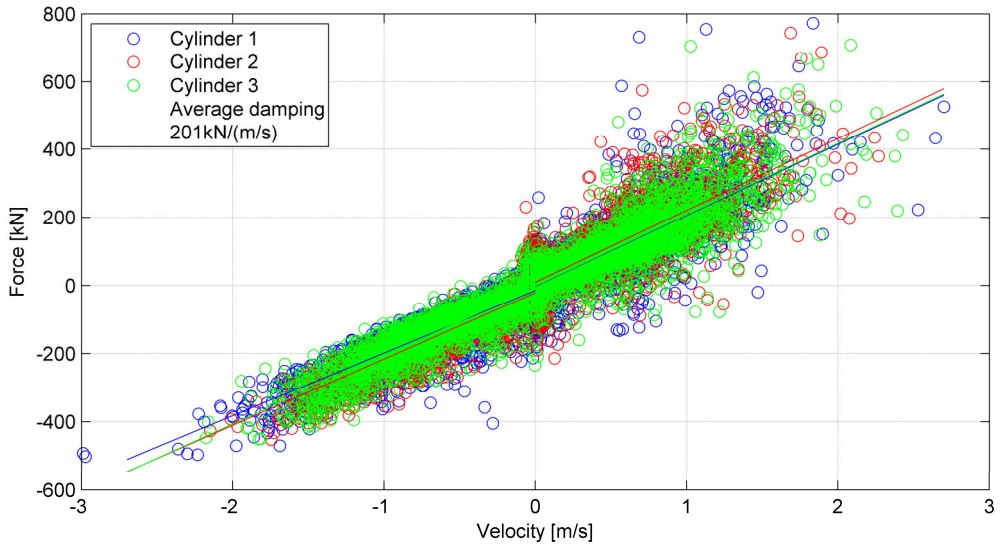

Figure 15.8, Force-velocity plot for 1.0 mm choke diameter (Hs=3.5, Tp=11.5)

Nonlinear behavior was discovered for high positive velocities. The same nonlinearities were not seen for negative velocities.

The two plots below show the force-velocity plot of the two larger choke diameters. Because the forces present in this time series are generally smaller, the static friction is more pronounced. The force reading at zero velocity represents the force that must be overcome to initiate movement. The static friction can be estimated to approximately 150 kN.

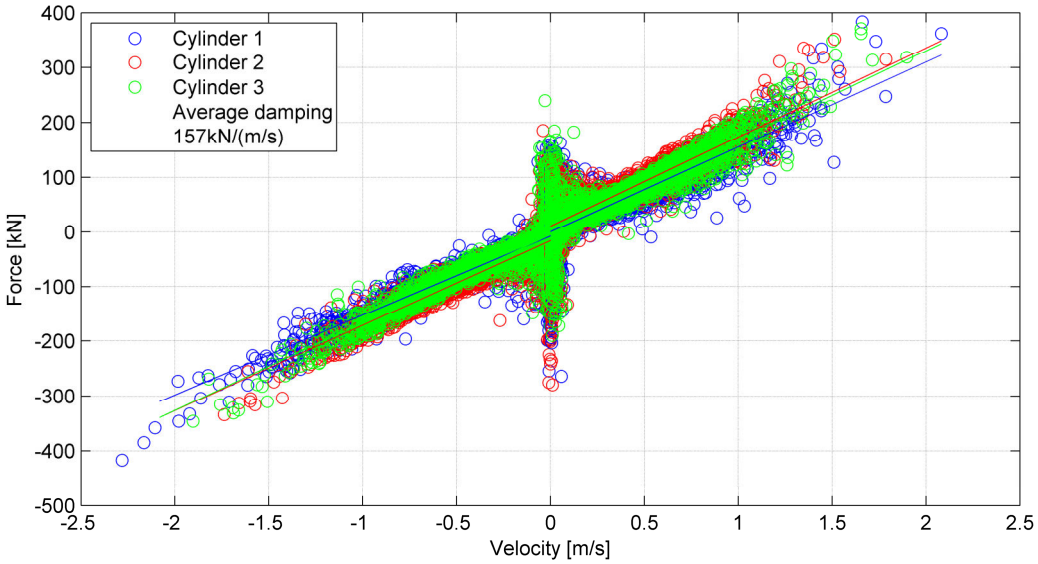

Figure 15.9, Force-velocity plot for 1.2 mm choke diameter (Hs=3.5, Tp=11.5)

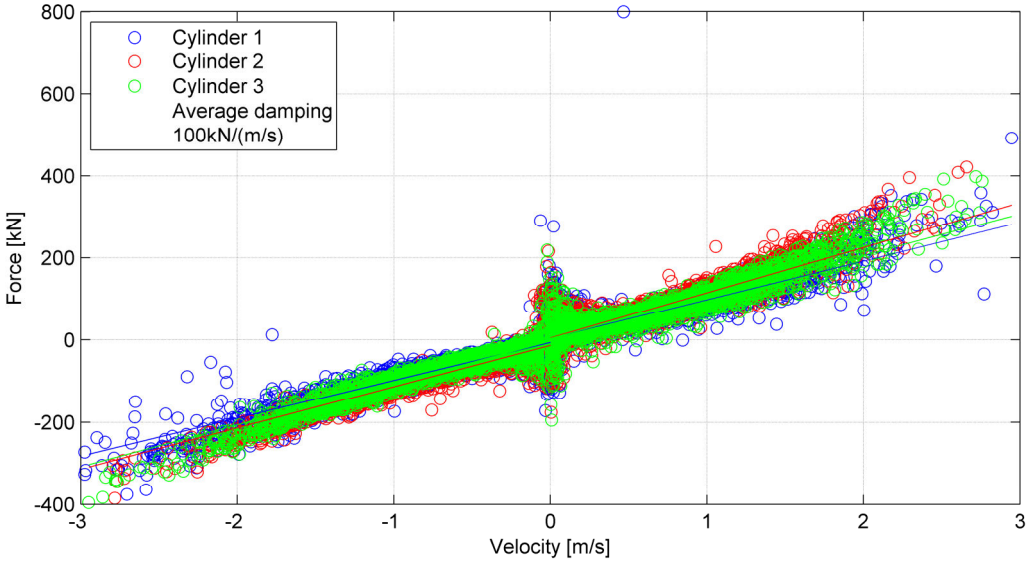

Figure 15.10, Force-velocity plot for 1.0 mm choke diameter (Hs=3.5, Tp=11.5)

15.3.3 Input parameters

1. *Different chokes on Cylinders*

Choke diameters of 1.0 mm, 1.2 mm and 1.5 mm in model-scale have been used to investigate the effect of the damping properties of the cylinders. This corresponds to an approximate damping of 201, 157 and 100 kN/(m/s) for the respective chokes estimated in the previous section.

Run	Choke diameter	Power cylinder 1	Power cylinder 2	Power cylinder 3	Total Power	Deviation
[-]	[mm]	[kW]	[kW]	[kW]	[kW]	[%]
High VCG						
Run 6110	1	45	42	46	133	0,0
Run 6181	1,2	47	40	44	131	-1,7
Run 6100	1,5	45	40	43	127	-4,6
Low VCG						
Run 6001	1	93	44	44	180	0,0
Run 6052	1,5	94	33	32	159	-11,9

Table 15.2, Power output by applying different chokes on the cylinders

The results indicate that by reducing the choke (increasing the choke diameter) the system extracts less energy from the waves.

The power output when applying the largest choke diameter (1.5 mm), is 4.6 % less than when applying the smallest choke diameter of 1 mm when the VCG is high. With low VCG the power output is 11.9 % less when applying the largest choke diameter.

With high VCG the damping properties are of little importance compared to other input parameters and the efficiency of the system is rather unaffected by altering the damping characteristics of the cylinders.

With less choke on the cylinders, more relative motion is allowed. At the same time less force is measured on each cylinder. The increase in velocity does not weigh out for the loss in force, thus the total power of the system is less with a small damping of the cylinders. This is illustrated in figure 15.12 and 15.13 below.

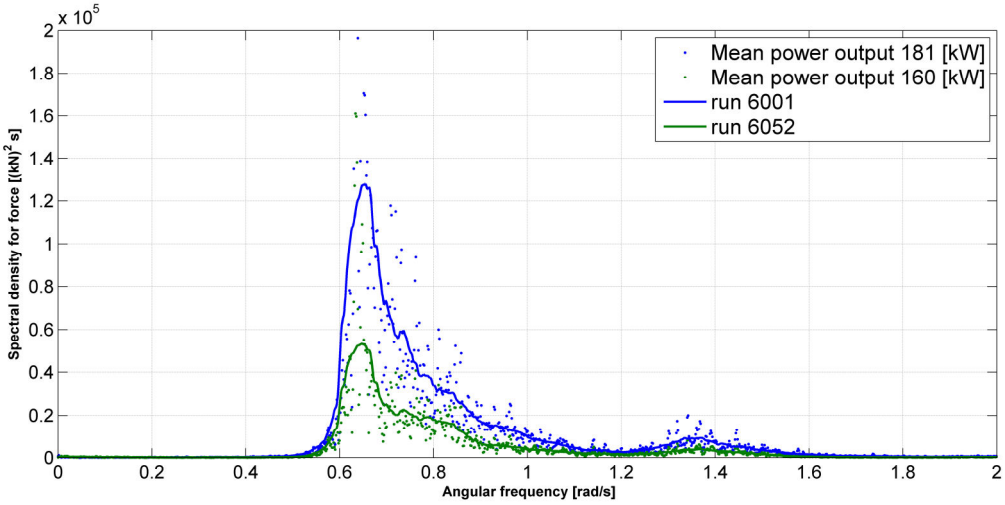

Figure 15.11- Response spectrum for relative force in cylinder 1. (1.0- and 1.5 mm choke)

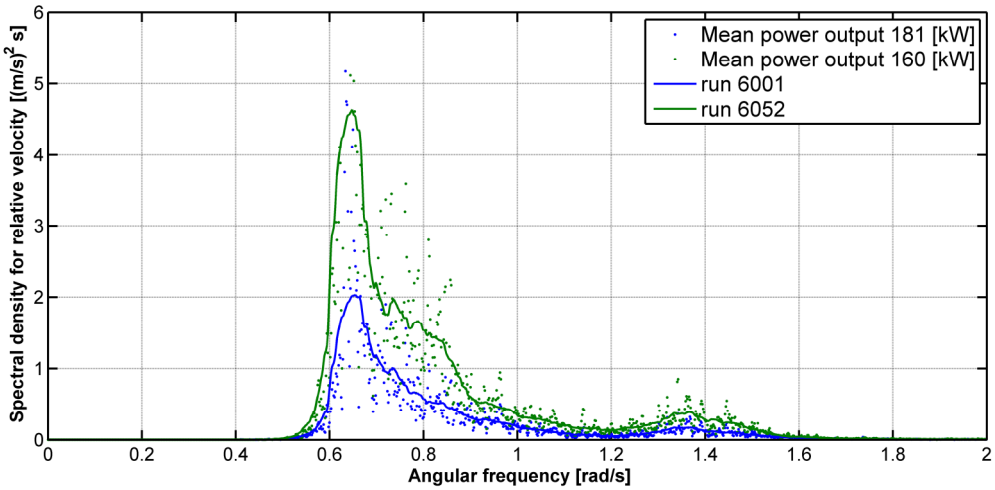

Figure 15.12 - Response spectrum for relative velocity in cylinder 1. (1.0- and 1.5 mm choke)

The SD as well as the maximum relative heave motion is clearly less with 1.0 mm choke than with 1.5 mm choke in both low and high VCG condition. The SD for relative pitch between the buoy and disc show similar trends. The max values in pitch are somewhat equal for high VCG, but in low VCG the max measured pitch motion is approximate 2 times larger with 1.5 mm than with 1.0 mm choke.

2. *Interchangeable Bottom Section*

The rounded bottom section gave as expected more power output from the system than the edged bottom section. Statistical values from the time domain analysis provide a deeper insight into why this is the case.

Run	Bottom section	Power cylinder 1	Power cylinder 2	Power cylinder 3	Total Power	Deviation
[-]	[-]	[kW]	[kW]	[kW]	[kW]	[%]
High VCG						
Run 6110	rounded	45	42	46	133	N/A
Run 3000	Edged	43	39	44	126	-6
Low VCG						
Run 6001	rounded	93	44	44	181	N/A
Run 5520	Edged	90	36	35	162	-11 %

Table 15.3, Power output by applying different bottom sections

It was observed that the force on each cylinder is generally much larger with the rounded bottom section than the edged. The force in cylinder 1 is more affected by different bottom sections than cylinder 2 and 3 in both VCG conditions. The SD of measured force on the three cylinders is 8-19 % higher with low VCG and 4-12 % higher with high VCG. The spectral plot in figure 15-14 of the force in cylinder 1 also supports this.

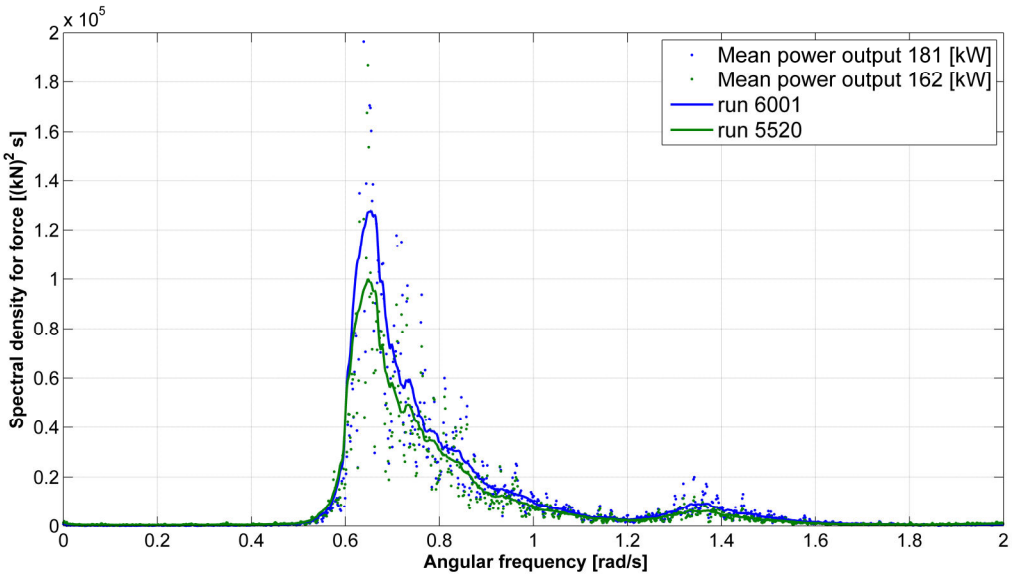

Figure 15.13, Response spectrum of force with low VCG, cylinder 1 (Bottom section analysis)

The SD of the relative velocity of the cylinders is fairly equal for the two bottom sections for both VCG conditions. From the frequency domain analysis, the spectral density for the relative velocities of the cylinders coincides fairly well in both cases shown in figure 15.15.

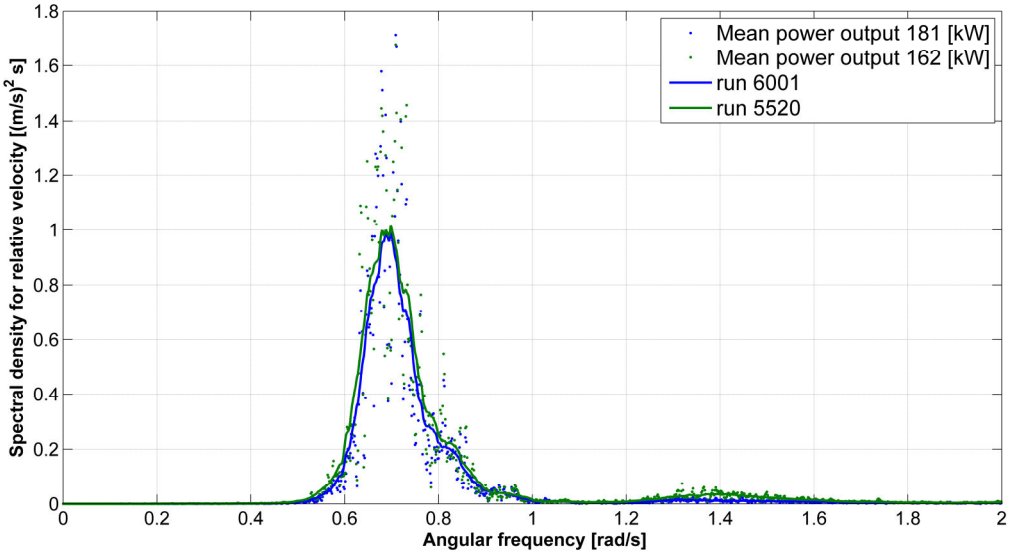

Figure 15.14, Response spectrum of velocity with low VCG, cylinder 2 (Bottom section analysis)

A general observation from the tests is that there are small changes in the relative velocity for all the cylinders when changing bottom section. An increase (between 4-17%) in the measured force on each cylinder is however measured for the rounded bottom section compared to the edged one.

3. *Different VCG Conditions*

As previous stated the VCG is of great importance for the efficiency of the system. With low VCG the power output is 36% higher than with high VCG in the base case sea state. This is due to an increased contribution in pitch motion. Most of the added power output is generated in the fore cylinder (cylinder 1).

Run	VCG	Power cylinder 1	Power cylinder 2	Power cylinder 3	Total Power	Deviation
[-]	[-]	[kW]	[kW]	[kW]	[kW]	[%]
Run 6001	Low - [KG=9.50 m]	93	44	44	181	N/A
Run 6110	High - [KG=13.92 m]	45	42	35	133	-26

Table 15.4, Power output in different VCG conditions

Tp in the sea-state is measured to 9.0 s for the irregular wave used in this test. The natural period in heave of the buoy was found to be 8.2 s which is very close to the Tp in the wave spectrum. Therefore large heave motions occur around this region with both high and low VCG as illustrated in figure 15.16 below.

The heave natural period is not affected by VCG in theory. It is however obvious that large pitch motion alters the heave response, see figure 15.16.

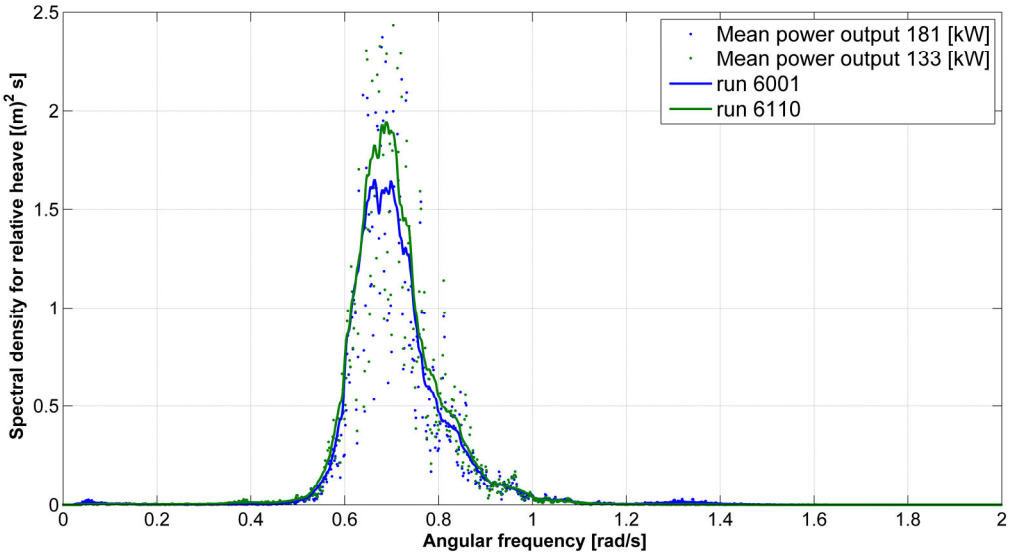

Figure 15.15, Response spectrum for relative heave motion (VCG analysis)

Pitch natural frequency is measured to 16.7 s in high ballast condition and 9.9 s in low ballast condition. The natural period in low ballast condition is very close to the Tp in the sea-state. Figure 15.17 illustrates the significant difference in pitch response for both VCG`s.

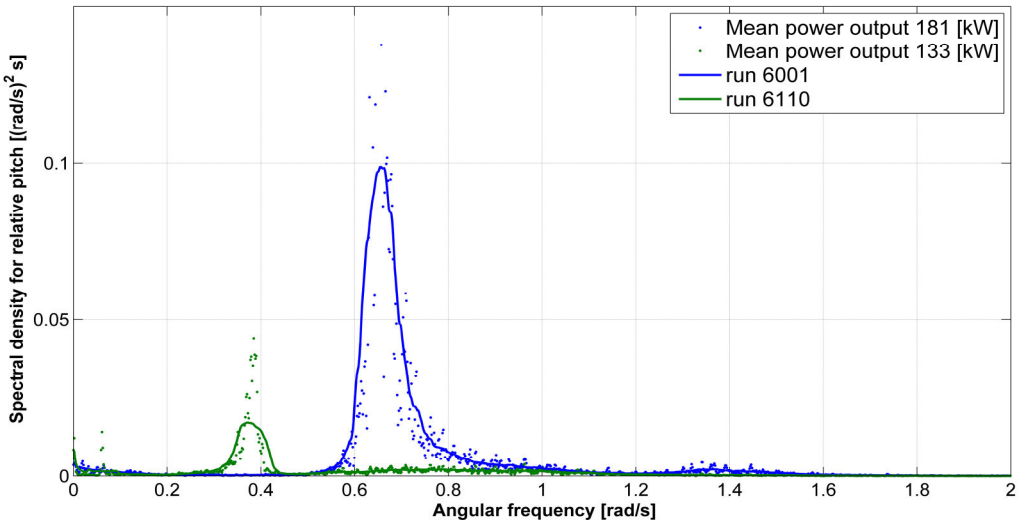

Figure 15.16, Response spectrum for relative pitch motion (VCG analysis)

The small peak in figure 15.17 at 0.4 rad/s for run 6110 corresponds to the uncoupled natural period in pitch for low VCG. A small peak in the spectral density for relative pitch can be found at 1.4 rad/s for high VCG. This corresponds to the pitch natural period for the disc inside the moon-pool seen in decay test appendix 7.20 (approximate 4 s).

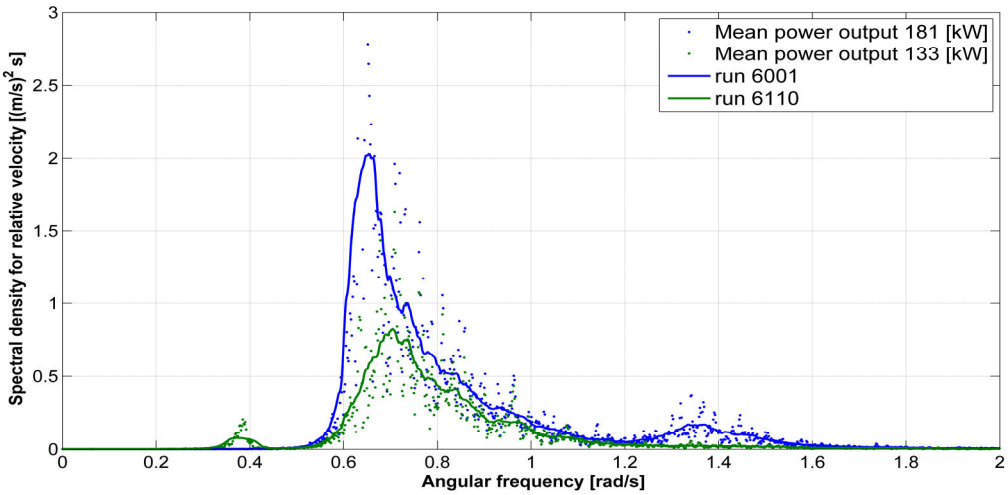

Figure 15.17, Response spectrum of velocity for cylinder 1 (VCG analysis)

As seen in figure 15.19 the spectral density for relative velocity of cylinder 3 are more or less equal in both high and low VCG condition. The same applies for cylinder 2.This implies that the relative vertical motion of the pistons is of same magnitude in both high and low VCG condition. Cylinder 1 shows however a large increase in spectral density for relative velocity in low VCG.

This may be explained by the fact that during low VCG condition the disc pitches about the axis through the fastening points of cylinder 2 and 3 on the disc. Visual observations strengthen this statement.

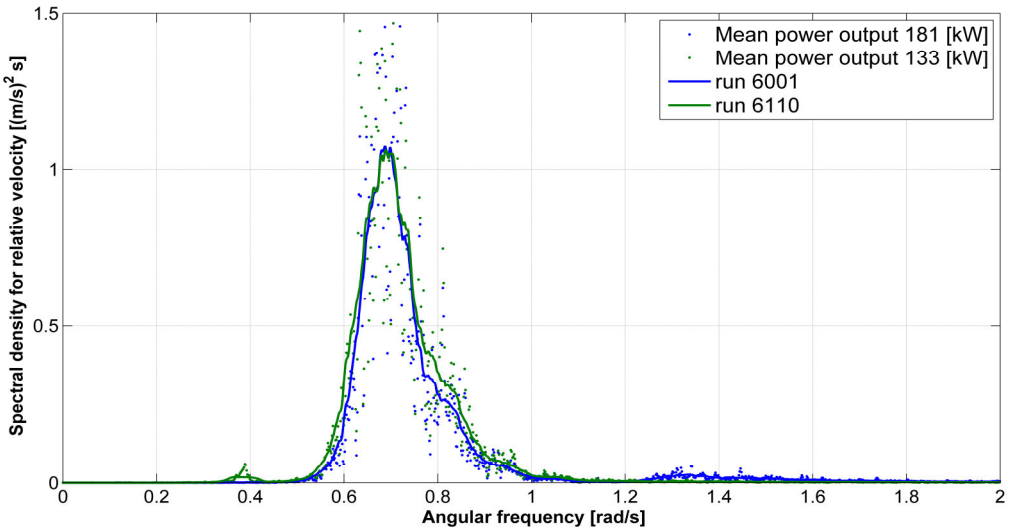

Figure 15.18, Response spectrum of velocity for cylinder 3 (VCG analysis)

As seen in figure 15.20 below the force on cylinder 1 is much larger with low VCG than with high VCG. This applies for cylinder 2 and 3 as well. Because the magnitude of the force is higher with a low VCG, the relative velocity in of each cylinder also increases.

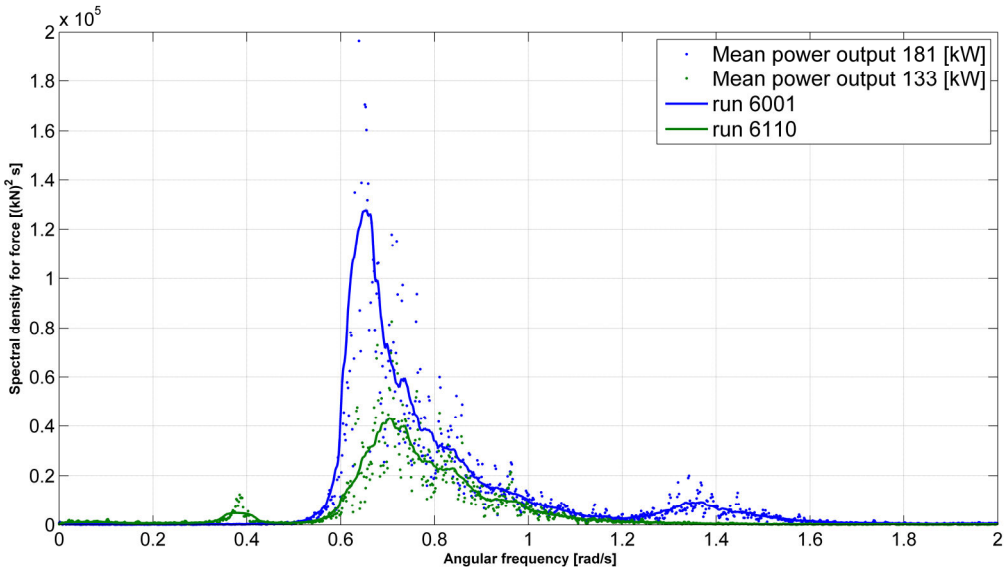

Figure 15.19, Response spectrum for force in cylinder 1 (VCG analysis)

By altering the natural period in pitch motion to be around the same Tp as the sea state significantly increases the total power output of the system, and for this it is clearly the most important design parameter of the buoy.

In order to take advantage of the pitch and roll motions the system has to be designed in such a fashion that the pitch/roll natural period is close to the same as the most typical Tp in the given operating region.

16. Survivability

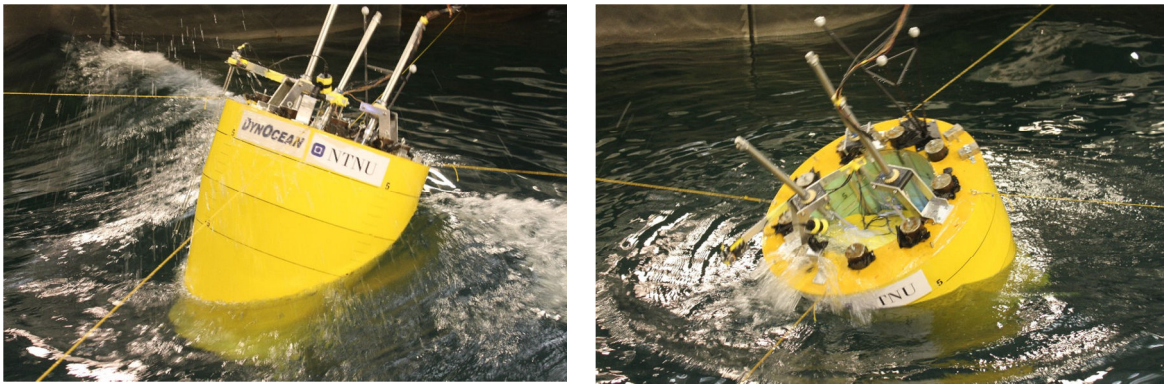

Figure 16.1, Pictures from 1 year survival condition run 4011

A survival condition was run as the last test in the tank. The buoy was set up with high VCG and 1.0mm choke.

The buoy showed an extreme behavior in the one year survival condition. Measurements showed that the pitch motion of the buoy reached an angle of 44 degrees. The less critical heave offset peaked at 13 meters.

The relative heave and pitch also reached the maximum possible amplitudes

A camera mounted on the topside of the buoy shooting downwards in the moonpool captured large amounts of water on top of the disc quite often. This water flushed out over the topside occasionally. Parts of the deck became submerged due to large pitch and a large negative heave occurring at the same time, ref figure 16-2.

Figure 16.2, Green water on deck

The piston inside the cylinders reached the end stops multiple times during the run. This represents a total stroke length of 10.9 meters in full-scale.

When the Tp in the sea condition lays around 12.5 s the structure goes from being a large volume structure to a small volume structure(MacCamy and Fuchs 1954). The inertia forces from the waves are more dominating and large motions are difficult avoid, but some action can be done to damp the motions.

$$\lambda = \frac{T^2 g}{2\pi} = \frac{12.5^2 \cdot 9.81}{2\pi} = 243[m] \tag{16.1}$$

$$\frac{\lambda}{D} = \frac{243}{24} \approx 10[-] \tag{16.2}$$

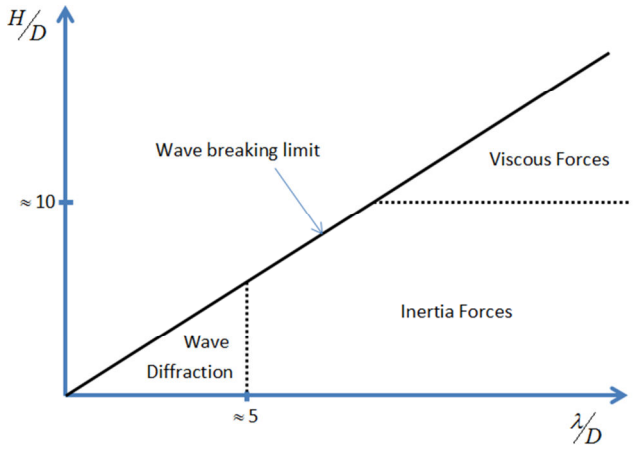

Figure 16.3, Wave loading regimes based on MacCamy & Fuchs (1954)

Large impact forces from the pistons reaching the endstops of the cylinder was observed. This will definitely reduce the longevity of the full-scale water pumps. An increasing of the cylinder damping, even a complete lock of the disc could eliminate this problem. End cushioning mechanisms would also be an improvement.

As stated earlier a max pitch angle of 44 degrees were recorded in the model test. From visual observations large pitch motion was present during the entire run and green water flushed the topside frequently. The Tp in the irregular survival sea was measured to 10.9 s. The pitch natural period of the buoy was measured to 16.7 s. The wave spectrum contained significant energy also at this frequency. It is crucial from to move the natural period of pitch motion away from the Tp of the sea states in survival conditions. This can be done by adjusting VCG and thereby the radius of gyration.

17. Numerical Simulation

Numerical simulation in time domain is the solution of a physical problem modeled mathematical. If the theory was perfect and the numerical capabilities of computers were unlimited one would not have to perform model tests. This is not true and the numerical results have to be verified by model tests.

The goal was to reproduce the results from the model test and to show that SIMO describes the desired effects sufficiently for further use in the design process.

To achieve this, a number of parameters had to be tuned to match the model. The approach was to start replicating decay tests – tuning the results when the SIMO output differed from the model test. When the decay results were satisfying the irregular seas where analyzed.

Steps performed

1. Construction of a panel model (GeniE)
2. Linear radiation-diffraction analysis (HydroD)
3. Implementation of couplings and body properties (MATLAB)
4. Time domain simulation (SIMO)
5. Post-processing of results (MATLAB)

Since numerical simulation is both faster and cheaper than a model test this method is commonly used in new designs. But for new concepts and modes of operations a model test should be performed at an early stage. The DYNOCEAN concept is unconventional. It is a coupled hydrodynamic system in the resonance area. The relative movement and the interaction between the two bodies are complex and very important for the viability of the design. The goal is to determine if the software and the numerical model is too far off the real solution. If the software is unable to describe the motion sufficiently it may be rejected as a tool for design purposes.

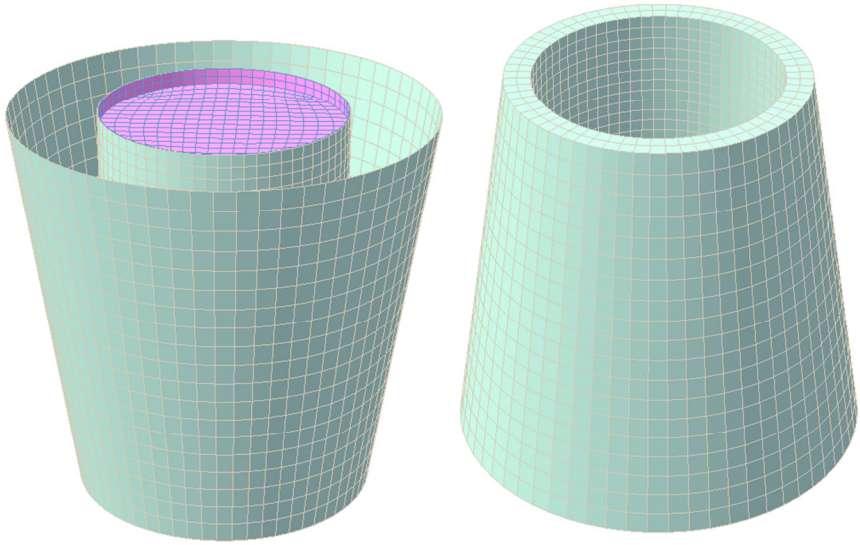

Figure 17.1, Panel model used in the linear radiation-diffraction analysis

17.1 Software and Theory

GeniE

The panel model and mesh were constructed in GeniE, which is a DNV software available in the SESAM software package.

HydroD (WADAM/WAMIT)

HydroD is an interface by DNV to various numerical codes. WADAM is the only part used in this analysis. WADAM is a general hydrodynamic analysis program built on top of WAMIT. WAMIT is in turn the hard code which does the calculations. It tool was made by a group at MIT. WAMIT builds on potential theory which is described in Faltinsen (1990). A linear radiation-diffraction analysis is performed to determine the hydrodynamic coefficients of one or more bodies. The output from the frequency domain analysis is input in the time domain analysis performed in SIMO.

SIMO

SIMO is a software distributed by DNV but developed and owned by Marintek. It is a time domain simulation tool built for complex marine operations (**Si**mulation of **M**arine **O**perations). It uses input information from different sources to calculate the motions of one or more bodies in the time domain. The input can be given by user or other software. Information about body/water interaction is for example given by WADAM. All input is gathered in one text file. Incoming waves can be given by a wave spectrum or recorded time series.

The routine solves all applicable dynamic equilibrium equations for each time step for coupled systems. The length of each step has to be determined based on the nature of the movement to be analyzed.

17.2 Construction of a panel model (GeniE)

The mesh has to be applied with caution. Any discontinuities internal on a body must be avoided. Any discontinuity between the inner vertical wall of the buoy and the outer wall of the disc must also be eliminated. The mesh size of all surfaces was determined by the relation between the diameters to keep the number of panels identical. This gave vertical lines dividing the panels in a radial pattern from the outer water line of buoy until it reached the disc. On the disc they got transformed to a square pattern.

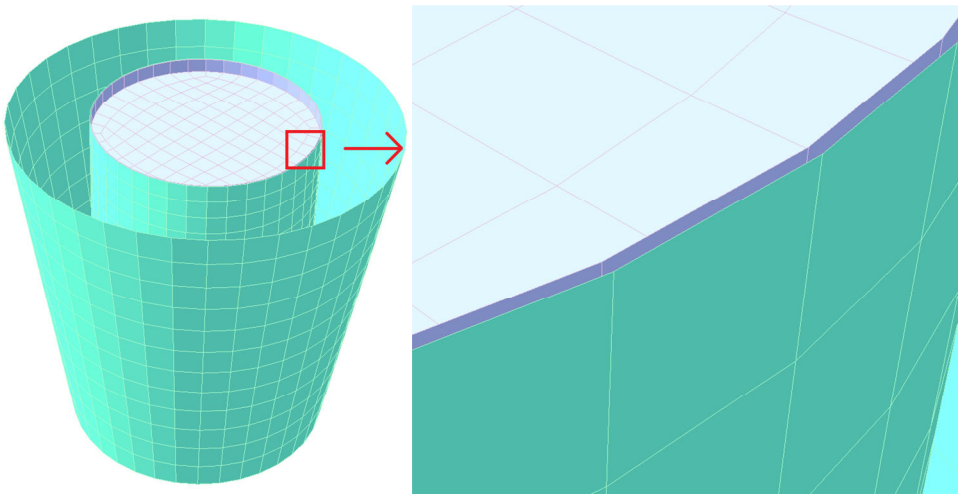

Figure 17.2, Illustration of mesh alignment between the two bodies

The accuracy of an analysis like this is related to the number of panels. Many panels give good accuracy but high computation time. A simple mesh convergence test was performed by running identical body geometry with different mesh sizes. It became evident that the results did not change significantly with a finer mesh when a certain level was reached. The mesh seen on the previous page is the actual mesh used. It consists of approximately 6000 panels which gave a computation time of nine hours for sixty frequencies.

The geometries of the two bodies are as similar as possible to the physical model. Since WADAM is only solving the potential flow problem (Faltinsen 1990) the bottom part does not have to be rounded perfectly to achieve good results. The contribution from viscous drag damping has to be accounted for (with linearization) in the time domain analysis.

17.3 Linear radiation-diffraction analysis (HydroD)

Output used from the frequency domain analysis are the wave force transfer functions, added mass and damping coefficients as a function of frequency. Since this is a coupled system the output is divided into three groups

- Buoy with the disc stationary.
- Disc with the buoy stationary.
- Coupling forces; the resulting forces on one body with the other body moving and vice versa.

17.4 Implementation of couplings and body properties

When hydrodynamic data from the WADAM analysis are available a time domain analysis can be performed. For coupled systems additional information need to be given.

The base case choke diameter of 1.0 mm was modeled in SIMO. The damping of the power extraction units were set to 200 $kN/(m/s)$ as estimated in section 7.2.

17.4.1 Drag model – Slender elements

SIMO lets the user define a second model of slender elements. Each cylinder depicted below gets assigned drag coefficients that will give a drag force from Morrison's equation. This is a completely different model from the panel model used in WADAM/WAMIT linear radiation-diffraction problem.

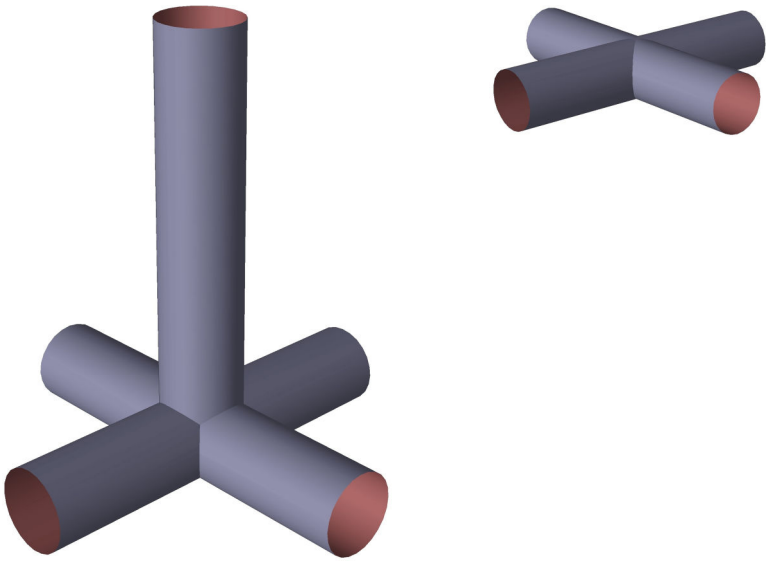

Figure 17.3, Illustration of slender element models of buoy and disc.

The damping coefficients needed for the different slender elements are hard to calculate. Numeric decay tests are performed in SIMO and compared with the model test.

Replications of the model decay tests will give the correct damping levels by comparing the results.

17.4.2 Coupling elements

The two bodies are coupled through interaction in the water and the physical/mechanical parts that connects the two floating bodies to one coupled system. The mechanical link and physical effects of the complete system has to be modeled by mathematics. The SIMO software has a variety of different coupling elements available (Marintek 2004). The following elements were used building up the model as realistic as possible.

Cylinders

The power take off cylinders can be modeled in SIMO with the help of force/elongation couplings. The input needed is the coordinates of the end points and the force characteristic of the piston. The coupling can exert forces proportional to displacement (spring) and/or velocity (damper).

The cylinders, which in reality are piston pumps, are modeled like dampers. The force transferred through a cylinder is linear proportional to the relative velocity between the two bodies at the fastening points of the coupling.

The damping of the cylinders was set to 200 $kN/(m/s)$ to match the 1.0mm choke analyzed in section 15.3.2.

Pilots

This is the same SIMO coupling object as the piston explained above. The characteristic is given differently to measure relative distance between two points.

The pilots were set up with a stiffness of 1 kN/m and no damping. The force reading of this element will then be proportional to the relative movement between main buoy and disc (at the horizontal fastening location). Pilots were placed next to (on top of) each piston in addition to one in the disc center, see Figure 17.4.The water plane stiffness is approximately 1500 kN/m ,calculated in chapter 9.1. The contribution from the 4 kN/m total stiffness provided by the pilots can be neglected.

Fenders (Guides)

SIMO has no physical feel of the geometry of the two bodies. They interact only through mathematical elements implemented by user. A lot of the properties of the two bodies are obviously determined by the body shape but SIMO reads only the matrixes given by WADAM. It is necessary with mathematical objects to prevent the two bodies from floating into each other. This was achieved by fenders.

Fenders are defined by a fender plane connected with local coordinates of one body, and a fender point connected to the second body. A characteristic of the forces acting between the point and fender (normal to the plane) as a function of the distance between them is given by user.

Implementation of coupling elements

All coupling elements were implemented in the SIMO input file together with the WADAM output by a MATLAB script [sysgen.m]. In addition to writing the input file the script plots a graphic display of the buoy and all the coupling elements assigned.

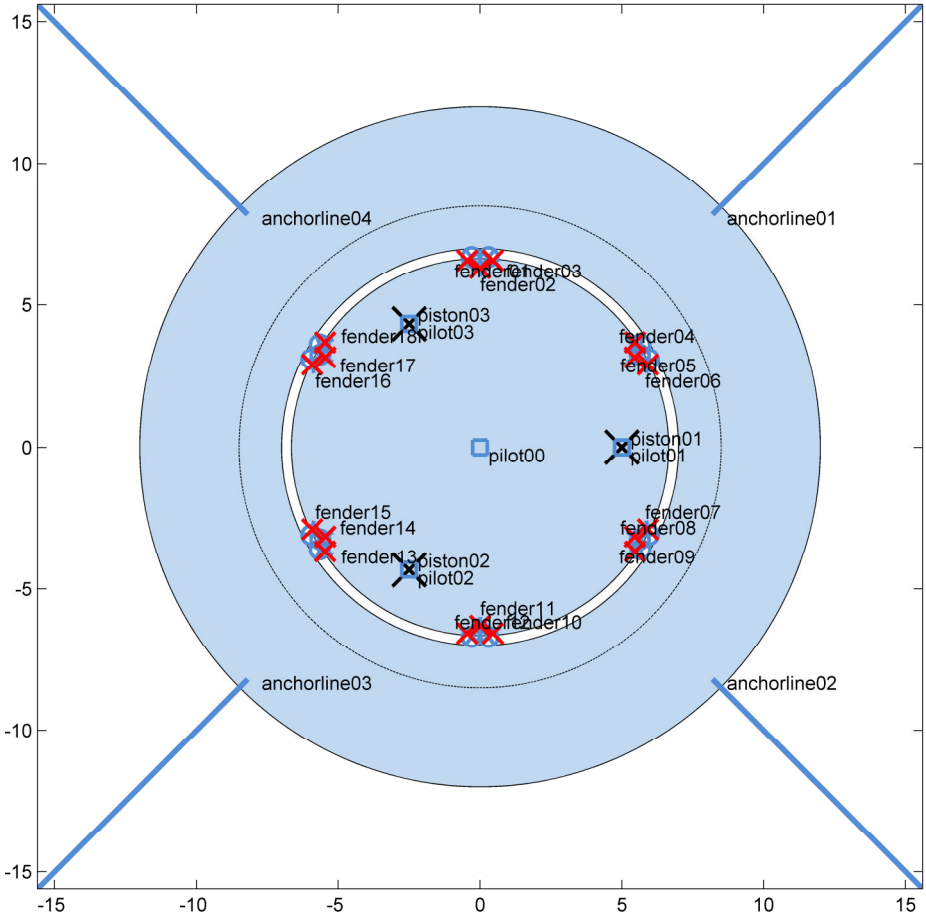

Figure 17.4, Top view of elements implemented in the SIMO input file

17.4.3 Mooring setup

The moorings in SIMO were modeled according to the actual model setup, explained in chapter 10.4.

The full scale width of the model tank equals 300 m. This is also the distance in the wave propagation direction between fore and aft mooring fastening point. This gives mooring lines of approximately 200 meters. The springs used at the end of the mooring lines in the model test was measured to a spring stiffness of 30N/m. This scales to approximately 25kN/m in full scale.

During the mooring installation in the tow tank force gauges were mounted between buoy and mooring lines to read the pretension. The lines were stretched to a pretension of 20 N. This scale to approximately 450kN in full scale.

A spring stiffness of 25kN/m and a pretension of 450kN were given the mooring lines in SIMO. The effect from a mooring setup like this should be minimal on the response, see chapter 10.4. The system and its sources of errors will not be analyzed further.

17.4.4 Properties of the Buoy

Mass properties

The mass properties summarized in chapter 10.5 are implemented SIMO.

Hydrostatic stiffness

The total stiffness matrix should account for the mooring stiffness. The stiffness matrix presented here is for the freely-floating body only, since SIMO will implement the effect from the moorings automatically.

The flotation point, the center of gravity and the submerged volume center are all on the same vertical axis. The stiffness matrix reduces therefore to three elements on the diagonal.

$$K_{hydro} = \begin{bmatrix} 0 & 0 & 0 & 0 & 0 & 0 \\ 0 & 0 & 0 & 0 & 0 & 0 \\ 0 & 0 & k_{33} & 0 & 0 & 0 \\ 0 & 0 & 0 & k_{44} & 0 & 0 \\ 0 & 0 & 0 & 0 & k_{55} & 0 \\ 0 & 0 & 0 & 0 & 0 & 0 \end{bmatrix} \tag{17.1}$$

k_{33} is the vertical water plane stiffness. The value is not measured from the model test. The theory is simple and should not introduce errors.

$$k_{33} = \rho g A_w \tag{17.2}$$

$$k_{33} = 1000 \cdot 9.81 \cdot (12^2 - 7^2) \cdot \pi = 2.93 \cdot 10^3 \left[kN/m \right] \tag{17.3}$$

$$k_{44} = k_{55} = \rho g V \overline{GM} \tag{17.4}$$

Since the Dynocean Buoy is axisymmetric the term k_{44} and k_{55} are equal. These parameters represent the ability to resist applied moments about an axis in the water plane. This is only true for small angles. Since large angles are expected, this will introduce an error.

CoG	**Mass** $[kg]$	**Bank Angle** [deg]	$k_{44} = k_{55}$ $[kNm/rad]$
High			
	4	1.8	300 840
	6	2.7	300 840
	8	3.65	296 719
Low			
	2	2.17	124 772
	4	4.39	123 351

Table 17.1, Determination of rotation stiffness determined from the inclination test

The results from the inclination test show consistent results. The values below will be used without further discussion.

$$\begin{aligned} \left[k_{44} = k_{55}\right]_{High\ CoG} &= 300\ 000\ [kNm/rad] \\ \left[k_{44} = k_{55}\right]_{Low\ CoG} &= 124\ 000\ [kNm/rad] \end{aligned} \tag{17.5}$$

17.4.5 Properties of the disc

No experimental measurements of the disc were taken except for the dry weight; this will have to be estimated. The mass coefficients of the fairly light disc are not that important, since the real (hydrodynamic) second body consists of both the disc and the water column inside the buoy. The mass of the oscillating water column which the disc caps is several time the mass of the disc.

	Model		Full Scale	
Radius	0.24	m	6.89	m
Mass	6.5	kg	153 659	kg
Draught	0.03	m	0.86	m

Table 17.2, Scaling of disc properties

CoG (estimated)

The disc was constructed with a plastic center plate and divinycell plates glued to both sides. The top foam plate was carved out to fit a plywood plate to fasten the cylinder piston rod and the force gages. Total mass was measured to 6.5 kg. It is assumed that the center of gravity is in the water plane in the center of the disc for the numerical analysis.

Moments of inertia (estimated)

We assume a homogeneous mass distribution and apply basic moment of inertia formulas[REF, physics book].

Solid cylinder about diameter through center:

$$I = \frac{1}{4}MR^2 + \frac{1}{12}ML^2 \tag{17.6}$$

Solid cylinder about the cylinder axis:

$$I = \frac{1}{2}MR^2 \tag{17.7}$$

These formulas give together with the geometry of the disc the following mass properties

$$\begin{aligned} M &= 154 \cdot 10^3 \, kg \\ I_{YY} &= I_{XX} = 1.86 \cdot 10^6 \, kgm^2 \\ I_{ZZ} &= 3.65 \cdot 10^6 \, kgm^2 \end{aligned} \tag{17.8}$$

17.5 Time domain simulation

17.5.1 Decay tests

An efficient way of tuning a numerical model is to replicate decay tests from the model test. By this fairly simple method errors in the wave force part of the equation is removed. Only one degree of freedom is analyzed in one test, so only one component of each of the governing six by six matrixes have to be changed.

The damping level of a hydrodynamic system is important, for wave power extractors it becomes essential. The determination of damping is the main objective of a decay test. A comparison of the natural frequency in the numerical analysis and the model test will give a clear indication of the quality of the model.

The iterative procedure tuning the model can be broken in to the steps below.

- Adjust SIMO input file
- Run SIMO
- Export results from SIMO
- Import SIMO results to MATLAB
- Process, plot and evaluate results
- Start from top

Two decay tests where replicated in SIMO; disc heave with the buoy stationary(a) and heave of the buoy without the disc installed(b). These were decided to be the most critical degrees of freedom for the power output of the system.

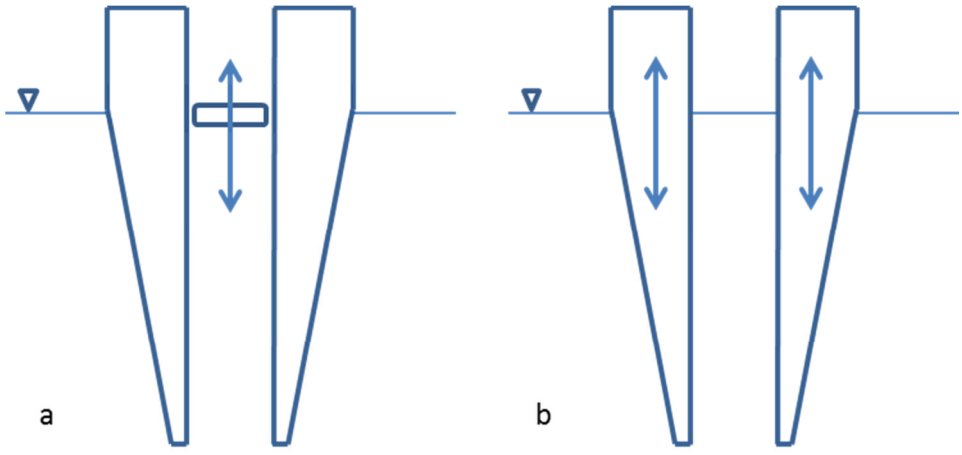

Figure 17.5, Illustration of decay tests performed in SIMO

By using the same MATLAB script analyzing the model decay test the damping of the SIMO model could be tuned. The drag coefficient of the slender element model, explained in 17.4.1, governs the quadratic damping, while the six by six linear damping matrix determines the linear component. The damping level was tuned with good results to resemble results from the model test.

Disc Heave

The heave motion of the disc is in practice the movement of the oscillating water column of the moonpool of the outer buoy. For this test no coupling elements were attached to the disc. It is freely floating on top of the moonpool inside the buoy.

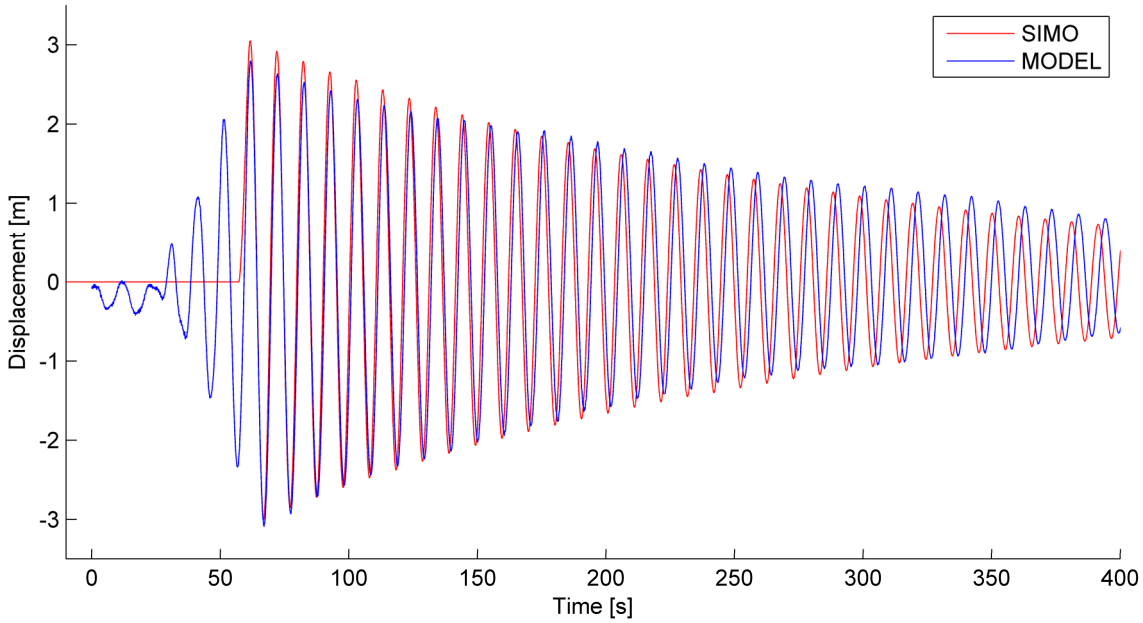

Figure 17.6, Decay test: Disc heave - Model/SIMO comparison

Negligible waves were generated from this decay test. The damping mechanisms that govern the motion are the skin friction and the flow of water through the bottom opening of the buoy. The motion is generally very low damped.

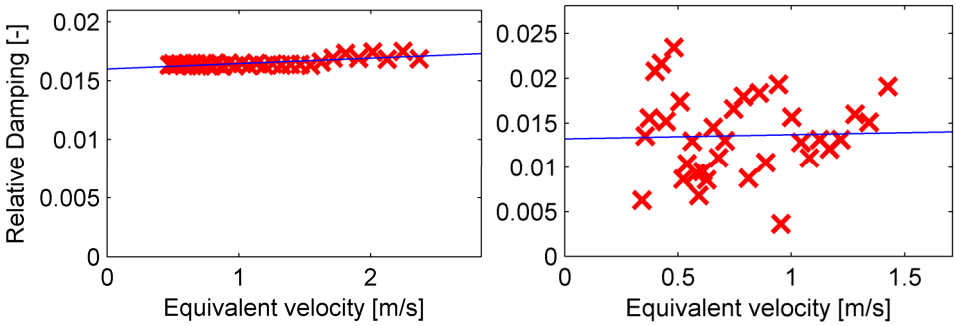

Figure 17.7, Relative damping for heave decay of buoy. SIMO (left) and the model test (right)

Due to very low damping the damping and limited precision of the measurements in the model test results came out significantly scattered. The numerical software shows a perfect line. See appendix 7.19 and 8.1 for all data from the tests.

Buoy Heave

The buoy heave has a significant damping due to the inclined outer wall. Large damping is associated with the devices ability to extract energy from waves. A good wave power extractor must also be a god wave maker(Falnes and Budal 1978).

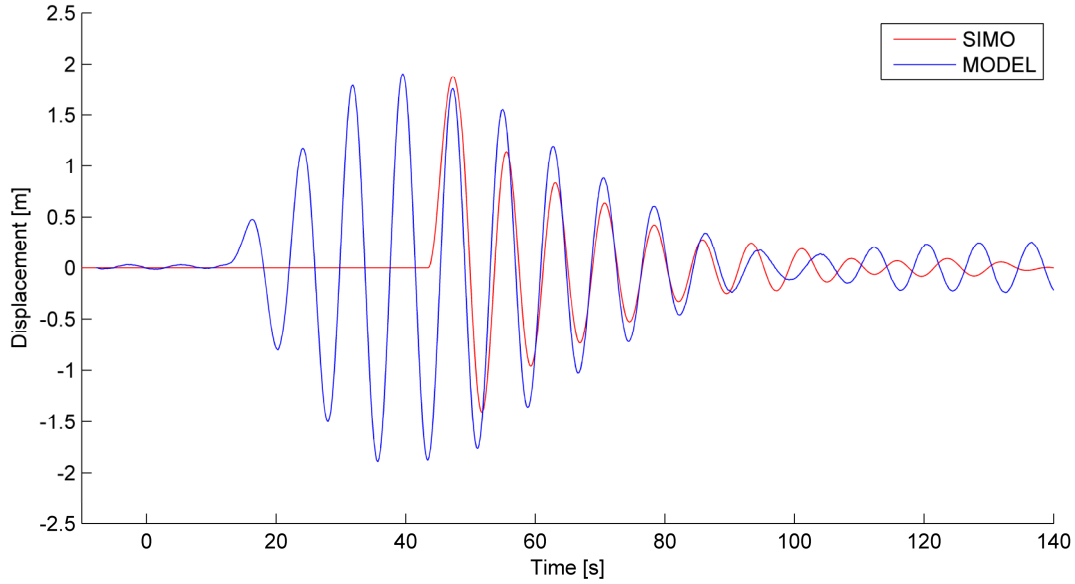

Table 17.3, Decay test: Disc heave - Model/SIMO comparison

The plot shows that the damping level is approximately equal, although the characteristics seem different.

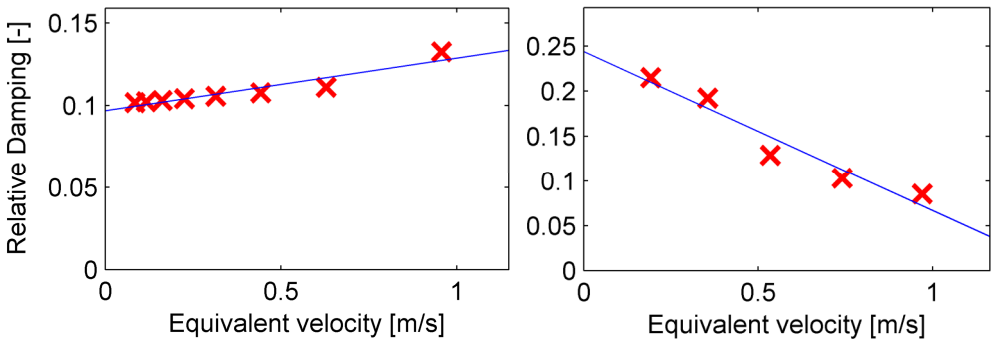

Figure 17.8, Relative damping for heave decay of disc. SIMO (left) and the model test (right)

17.5.2 Irregular sea

The waves where calibrated with two wave probes in place, one regular wave probe at the prospective buoy location and an ultra sound wave elevation measuring device mounted on the towing carriage. Due to an oil film on the water surface from previous oil leaks the measurements from the generic wave probes could measure an error - especially in the wave troughs. For the runs used for comparison in the frequency domain and power output wave time series from the acoustic device was used. For visual comparison in time domain the wave from the wave probe at the buoy location were used.

Time plots

To get an impression of the goodness of the numerical model time plots can be useful to compare. The below plot shows the numerical results plotted together with the time series from model test 6001.

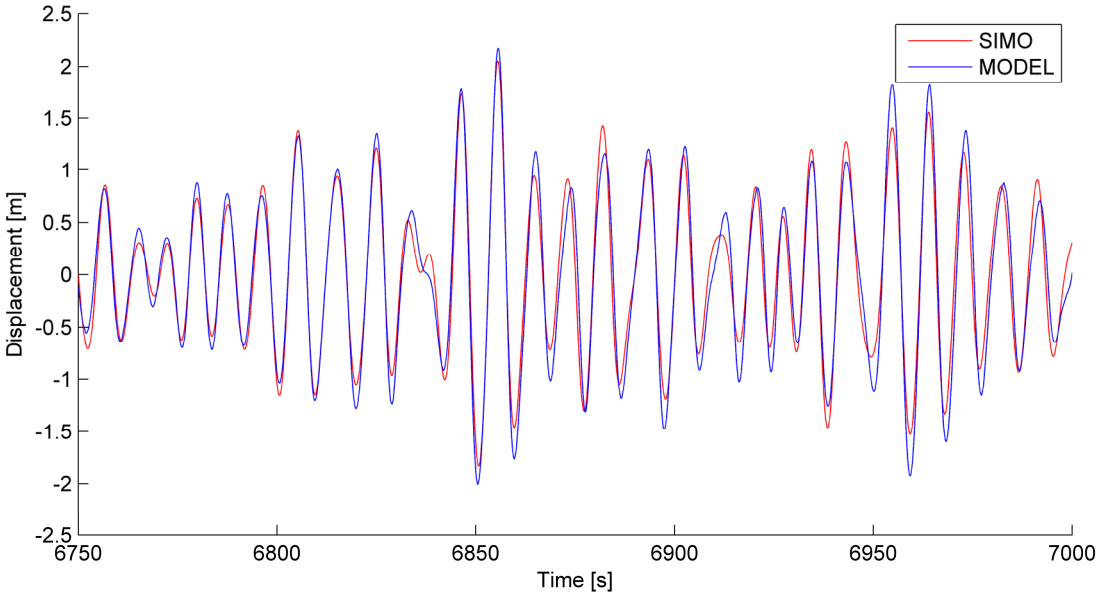

Figure 17.9, SIMO/Model test comparison: Heave of the outer buoy. (Hs = 2.5m, Tp=9.0s)

Static Friction

As already shown in section 15.3.2 the cylinders used showed significant static friction. This can be clearly seen in the figure below. The figure show unfiltered signals. The strokes of the pistons were measured by a spring and a force gauge. The static friction kicks in when the velocity is zero. The pistons will not move until the static friction is overcome. This gives a short lag in the motion at local maxima and minima. This can be seen at every point where the velocity changes direction.

The high frequency fluctuations at the maxima and minima are the out of axis vibration of the spring used for measuring the relative distance between the two bodies.

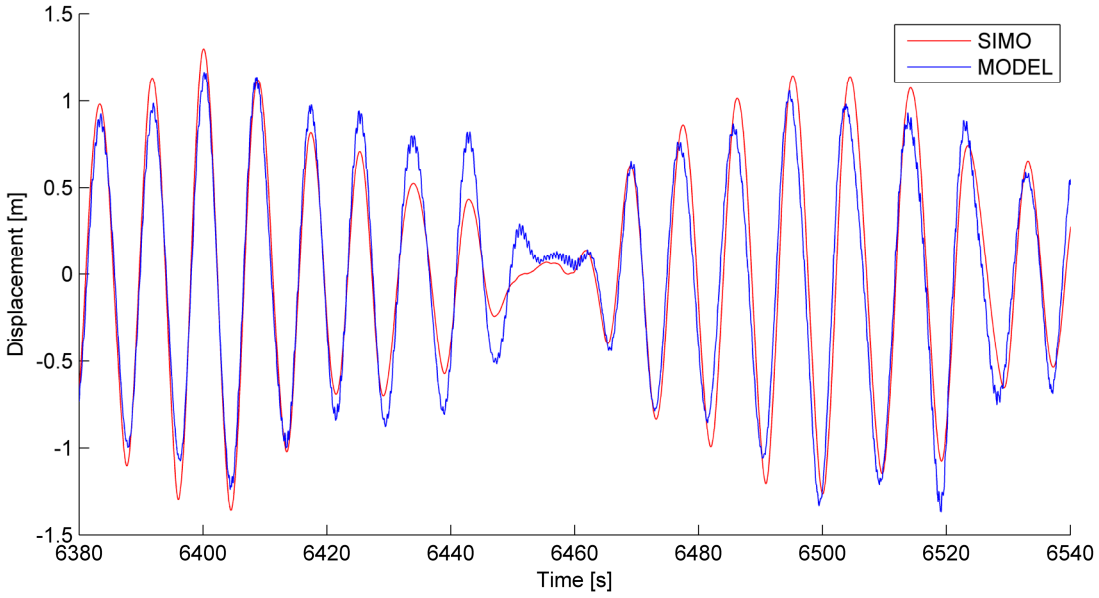

Figure 17.10, Unfiltered signals of buoy heave (Hs=2.5, Tp=9.0)

Static friction was attempted modeled in SIMO without a satisfying result. As explained earlier in this chapter the software used is primarily made for analyzing marine operations, not wave power extractors. Different methods and built in elements were tried without getting the desired effect. The effect from static friction is assumed to have a significant impact on the system performance.

Cylinder characteristics

The cylinder model in SIMO shows a strict linear relation between force and velocity. This can be clearly seen in force velocity plot of each separate cylinder.

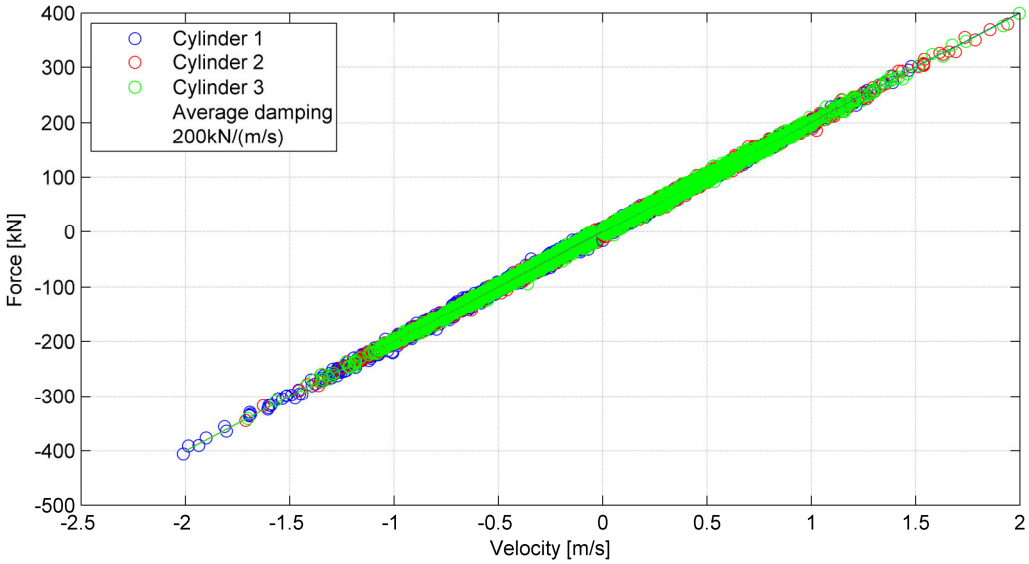

Figure 17.11, Force-velocity plot of the SIMO cylinders (Hs=2.5, Tp=9.0)

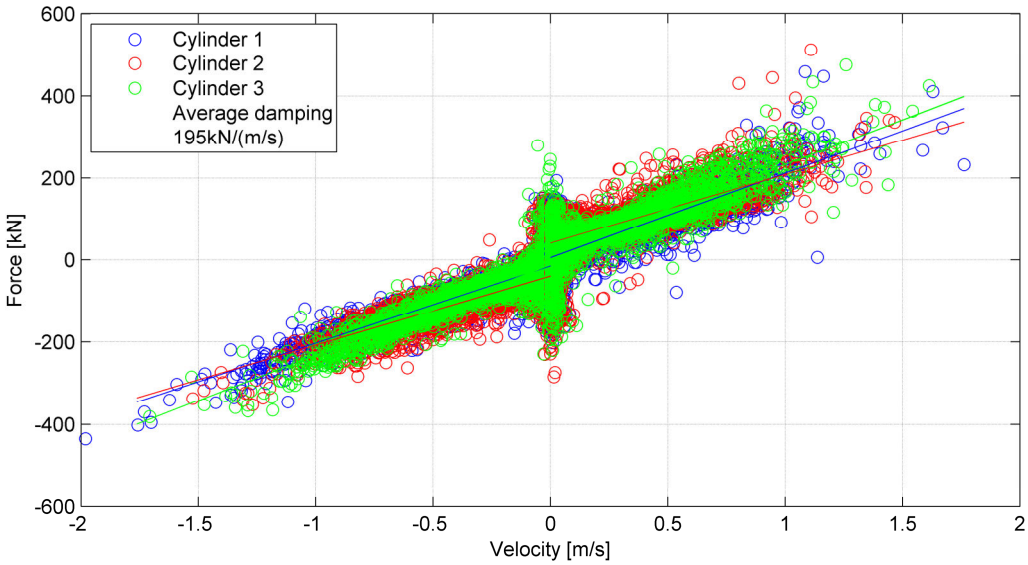

Figure 17.12, Force-velocity plot of the cylinders for 1.0 mm choke (Hs=2.5, Tp=9.0)

Power output

The most interesting parameter comparing the physical and numerical model is the estimated power output. This is together with the costs/kWh are the two main factors giving the viability of the concept. The data from the model test and the SIMO time series were analyzed with the same MATLAB procedure, explained in section 15.2 with the following result:

Run	VCG	Hs [m]	Tp [s]	Power output [kW]		Appendix
				MODEL	SIMO	
6110	**High**	2.5	9.0	133	131	9.1
6140		3.5	11.5	286	351	9.2
6120		4.5	14.0	291	414	9.3
6001	**Low**	2.5	9.0	180	194	9.4
6030		3.5	11.5	350	477	9.5
6010		4.5	14.0	358	525	9.6

Table 17.4, Comparison of power output from model test versus SIMO.

The SIMO model overestimated the power output in the higher seas quite significantly. This could be from a number of reasons.

Static friction in the cylinders prevents some small motions in the model test. This property was not properly implemented in SIMO. The product of the force multiplied with velocity, in the areas where SIMO allows motion in contrast to the model test, will be small but could make a difference.

Friction in the guides keeping the disc from yawing is not analyzed in dept. In the model test it was seen that the disc jammed for a split second during large deflections in heave and pitch. This cannot happen in the SIMO model.

Pitch motion of disc contributes to larger power output in SIMO than in the model test. The figure below shows the velocity response spectrum of all cylinders accumulated up for each frequency. This parameter is directly proportional to the piston force in the SIMO model. For the model test this is a truth with modifications. In the model test the compressibility of air result to a not completely linear relation between force and velocity in the cylinders. This is not taken into account in the discussion.

SIMO accounts for linearized quadratic and linear damping of the bodies. The physical damping could very well be proportional to other exponents of the velocity. This is beyond the scope of this study and will not be further discussed.

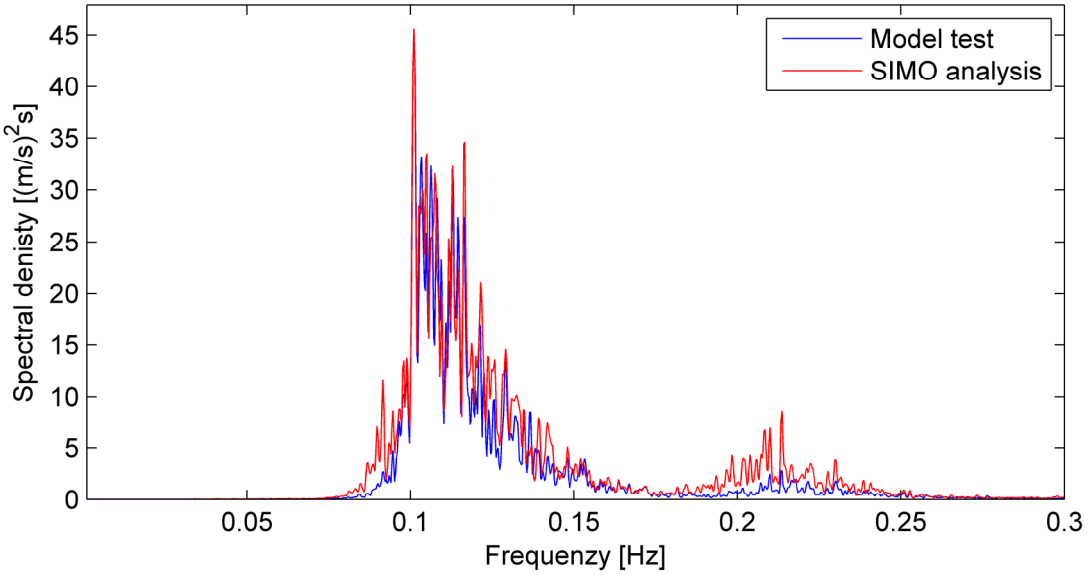

Figure 17.13, Velocity response spectrum, cylinders superimposed (Low VCG, Hs=2.5m,Tp=9,0s)

The replication of the velocity in the power extraction units are very good for the base case sea state.

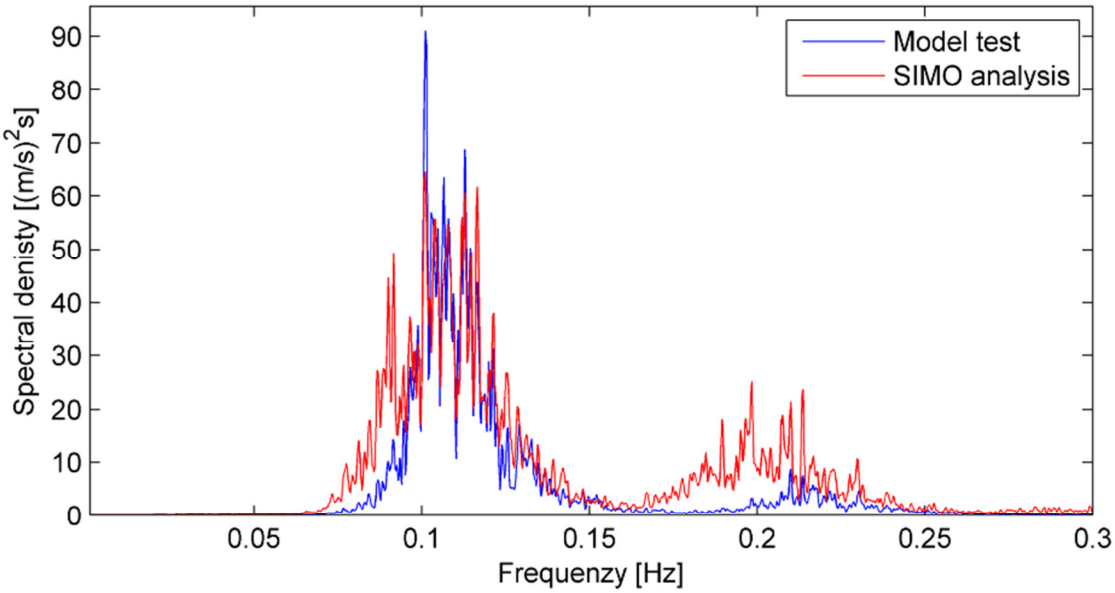

Figure 17.14, Velocity response spectrum, cylinders superimposed (Low VCG, Hs=3.5m,Tp=11.5s)

The SIMO velocity is clearly larger in the high frequency region. Decay test 20 (appendix 7.20) shows a natural period in pitch for the disc of 4.2 seconds. This equals 0.24 Hz and can be the reason for the high response at this high frequency. This contribution could be brought down with more pitch damping.

18. Conclusion

The power estimates for the typical sea states in the designated operating area of the buoy are highly satisfactory. With the most probable occurring sea state the power output is estimated to 180 kW for the best buoy configuration (low VCG, smooth bottom section, 1mm choke).

The energy lost in water flowing in to and out through the moon pool inlet was estimated to maximum of 13% by using the edged bottom section than the rounded one. Less energy was lost for smaller sea states. Decay tests proved that the quadratic drag damping associated with the water entry and exit was almost eliminated for the rounded bottom section.

High damping level of the power extraction units is desirable. Irregular sea tests showed an approximately 10% higher power output for the 1.0 mm choke than with 1.5 mm choke. This was a surprisingly small considered that the linear damping coefficient is doubled. High damping prevents unnecessary large motions and thereby reduces wear and tear of the device.

Two different vertical centers of gravity were tested. Low VCG gave a pitch natural period at the spectral peak period - the high VCG setup did not. The desire to change between them was to determine if pitch contributed to the power output. Estimated power output in low VCG was over 30% higher than for high VCG. An active ballast system, able to move the VCG, would able a controlling unit to keep the pitch natural period at Tp for a range of sea conditions. The opposite can be achieved in survival conditions.

The guide system worked very well during the model test. De disc never “jumped” out of the guides and no significant jamming were observed. The system did also perform well under the survival sea condition. The main concept of the guide system designed by the authors is recommended for further design, also in full scale.

The heave and pitch motions were too large in the survival condition. The eight meter freeboard was completely submerged at some points. The cylinders reached its end stops and large peak forces were observed in the time series. A complete locking of the disc could be desirable to change the natural periods of the system and prevent extreme motions.

As the main purpose of the thesis was to give a pointer towards the viability of the device and compare different parameters the reliability of the results has not been formally analyzed. Uncertainty and bias error could overestimate the power output. The sources of error will not significantly affect the comparison of different input parameters since the measuring devices stay the same.

The numerical analyses replicated the result for small sea states with good agreement with the model test. For the larger seas the model gave significantly larger power output. It is clear that SIMO has coupling elements very useful for representation wave energy converter. Although the effort creating the numerical model was not unconditionally successful it has been proven that SIMO is a good design tool for systems like the Dynocean buoy.

19. Recommendation for Further Work

- Perform an uncertainty study of the model test results.
- Tune body and coupling characteristics to make the numerical decay tests reproduce the decay test performed in model scale more closely.
- Investigate if higher damping levels in the power extraction units will reduce motions without reducing power output.
- Investigate the effect of passive latching from static friction in power extraction units.
- Investigate the effect of active latching in the power extraction units.
- Implement static friction in power extraction couplings in the numerical model

20. References

Amdahl, J., Fuglerud, G., Minsaas, K., Rasmussen, M. , Sillerud, B., Sortland, B., Valland H., (2005). TMR 4105 - Marinteknikk 1.

Brandsvoll, R. A. (2010). Wave Energy Driven Desalination of Seawater.

Cruz, J. (2008). Ocean Wave Energy: Current Status and Future Prespectives. Berlin, Heidelberg, Springer-Verlag.

Edwards, C. H. and D. E. Penney (2002). Calculus. Upper Saddle River, N.J., Prentice Hall.

Falnes, J. and K. Budal (1978). Wave power conversion by point absorbers.

Faltinsen, O. M. (1990). Sea loads on ships and offshore structures. Cambridge, Cambridge University Press.

Hogben, N., G. F. Olliver, et al. (1986). Global wave statistics. Old Working, Published for British Maritime Technology by Unwin Brothers Limited.

Johannessen, T. B. (2009). Patent application - Wave Power System.

Johannessen, T. B., Brandsvoll,R.A., Palmstrøm, A., Sole,S., Pedersen,E & Steen,S. (2010). "A system for wave driven desalination of seawater." OMAE2011-49419 DRAFT.

Kreyszig, E. (2006). Advanced engineering mathematics. Hoboken, N.J., Wiley.

MacCamy, R. C. and R. A. Fuchs (1954). Wave forces on piles: a diffraction theory. Washington, The Board.

Marintek (2004) "SIMO user manual, appendix A."

Myrhaug, D. (2007). TMR 4180 Uregelmessig sjø.

Newland, D. E. (1993). An introduction to random vibrations, spectral and wavelet analysis. Harlow, Longman.

Palmstrøm, A. (2010). "Wave Energy Driven Desalination of Seawater - Experimental investigation of the hydrodynamic performance."

Tipler, P. A. and G. Mosca (2004). Physics for scientists and engineers. New York, Freeman.

Pettersen, B. (2007). TMR4247: Marin Teknikk 3 - Hydrodynamikk.

Sandmark, S. (2011). Personal conversation - 31.03.2011.

Steen, S. (2010). TMR7 - Experimental Methods in Marine Hydroynamics.

Welch, P. D. (1967). "The Use of Fast Fourier Transform for the Estimation of Power Spectra: A Method Based on Time Averaging Over Short, Modified Periodograms."

21. Appendix Index

Enclosed

APPENDIX 1: Datasheet of Bosch RexRoth double acting cylinder.

APPENDIX 2: Stability Analysis.

APPENDIX 3: Pendulum test calculations.

APPENDIX 4: Calculation of spring stiffness.

APPENDIX 5: Wave calibration.

APPENDIX 6: Power estimation from Irregular wave tests.

APPENDIX 7: Decay tests.

APPENDIX 8: SIMO: Decay tests.

APPENDIX 9: SIMO: Irregular Sea.

Digital

APPENDIX 10: MATLAB scripts.

APPENDIX 11: Excel database of all tests and resulting time series.

APPENDIX 12: Test matrix document written during the test week.

APPENDIX 13: All time series recorded during test week.

APPENDIXES 1-9 are also enclosed on the digital media, as well as the present thesis.